

NCC2-374

IN-34

4/31/4744

UNIVERSITY OF CALIFORNIA

Los Angeles

Experimental Investigation Of Jet Impingement Heat Transfer
Using Thermochromic Liquid Crystals

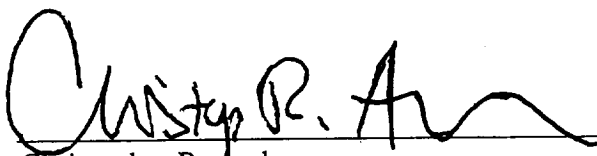
A dissertation submitted in partial satisfaction of the
requirements for the degree of Doctor of Philosophy
in Mechanical Engineering

by

Brian Paul Dempsey

1997

The dissertation of Brian Paul Dempsey is approved.



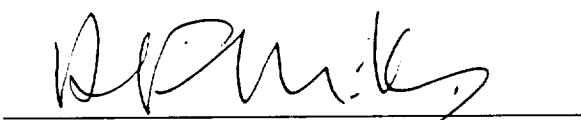
Christopher R. Anderson



Nasr M. Ghoniem



Adrienne G. Lavine



Anthony F. Mills, Committee Chair

University of California, Los Angeles

1997

DEDICATION

To my parents for their encouragement and help with all my educational goals,
and to Sheri for her patience, understanding, and support.

TABLE OF CONTENTS

Dedication	iii
Table of Contents	iv
List of Figures	vii
List of Tables	xi
Nomenclature	xii
Acknowledgments	xvi
Vita	xvii
Abstract	xviii
1. Introduction	1
1.1 Background	1
1.2 Objectives	1
1.3 Previous Work	2
1.3.1 Analytical Studies	2
1.3.2 Numerical Studies	3
1.3.3 Experimental Studies	7
1.3.4 Liquid Crystal Methods	10
2. Analysis	18
2.1 Preliminary Design Considerations	18
2.1.1 Cooling System Design	19
2.2 Heat Transfer Analysis	24

2.2.1 Conduction Analysis	26
2.2.2 Convection Analysis	30
2.2.3 Computational Method	31
3. Error Analysis	34
3.1 Introduction	34
3.2 Error Assessment Due to All Numerical Methods Considered Together . .	34
3.3 Error Assessment Due to Each Numerical Method Considered	
Separately	38
3.3.1 Smoothing and derivatives	38
3.3.2 Integrations	39
3.3.3 Step Size	41
3.4 Systematic Errors	42
3.4.1 Transient Temperature Measurement Lag	42
3.4.2 Crystal Transition Temperature	43
3.4.3 Backing Paint Thickness	46
3.4.4 One-dimensional Assumption	47
3.5 Temperature Changes in the Air	48
3.6 Error Due to the Simultaneous Solution for the Heat Transfer	
Coefficient and the Recovery Temperature	50
3.7 Summary	54
4. Experimental Details	55

4.1 Air Delivery System	55
4.2 Instrumentation	56
4.3 Leading Edge Model	57
4.4 Liquid Crystals	58
5. Results	60
5.1 Introduction	60
5.2 Validation of the Results	61
5.3 Data trends	65
5.4 Recovery Temperature Data	74
6. Summary and Recommendations for Further Research	79
6.1 Concluding Comments	79
6.2 Suggestions for Further Research	80
Appendix A Solution to Time Varying Convection Equation	85
Appendix B Design Drawings	90
Appendix C Airfoil Temperature Calculation	97
Appendix D Heat Transfer Coefficients and Recovery Temperature Data	99
References	132

LIST OF FIGURES

Figure 1: Control volume used for an energy balance on the leading edge cooling system	20
Figure 2: Jet temperature vs. time for two different heating rates	28
Figure 3: Actual air temperature data and approximating function	35
Figure 4: Typical noise in air temperature measurement	36
Figure 5: Error due to the presence of noise in the inlet air temperature measurement	37
Figure 6: Relative errors in heat transfer coefficients caused by omitting numerical smoothing and by using a first order derivative approximation	39
Figure 7: Relative error in the heat transfer coefficient from using subintervals of 2 times and 4 times larger than the nominal subinterval in the heat transfer coefficient iteration	40
Figure 8: Relative error in the heat transfer coefficient from using subintervals of two times larger than the nominal subinterval for the wall temperature evaluation	41
Figure 9: Relative error in the heat transfer coefficient due to doubling the downstream step size	42
Figure 10: Error due to crystal transition temperature uncertainty	45
Figure 11: Typical heat transfer coefficient data very near the stagnation point	47
Figure 12: Test case to determine the maximum expected error	49
Figure 13 Relative error caused by ignoring the effect of energy loss in the air	50

Figure 14: Absolute error in the heat transfer coefficient due to $\pm 0.0275\text{s}$ transition time deviation	51
Figure 15: Absolute error in the recovery temperature due to $\pm 0.0275\text{s}$ transition time deviation	52
Figure 16: Relative error in the heat transfer coefficient due to $\pm 0.0275\text{s}$ transition time error	53
Figure 17: Relative error in recovery temperature due to $\pm 0.0275\text{s}$ transition time error	53
Figure 18. Comparison of the present stagnation line Nusselt numbers to literature results for $\text{Re}=4200$	63
Figure 19. Comparison of the present stagnation line Nusselt numbers to literature results for $\text{Re}=8300$	63
Figure 20. Comparison of the present Nusselt numbers to literature results for $\text{Re}=8300$ from the stagnation line to 8 nozzle widths down-stream	64
Figure 21. Nusselt number vs. distance from the stagnation line for $\text{Re}=8,300$ and slot width 0.127cm	66
Figure 22. Nusselt number vs. distance from the stagnation line for $\text{Re}=4,200$ and slot width 0.127cm	68
Figure 23. Nusselt number vs. distance from the stagnation line for $\text{Re}=8300$ and slot width 0.287cm	70

Figure 24. Comparison of Nusselt numbers for Re=4,200 and Re=8,300 at z/W = 4 and W=0.127cm	71
Figure 25. Comparison of Nusselt numbers for Re=4,200 and Re=8,300 at z/W = 8 and W=0.127cm	71
Figure 26. Comparison of Nusselt numbers for Re=4,200 and Re=8,300 at z/W = 10 and W=0.127cm	71
Figure 27. Comparison of Nusselt numbers for Re=4,200 and Re=8,300 at z/W = 14 and W=0.127cm	71
Figure 28. Comparison of Nusselt numbers for Re=8,300 at z/W = 4 and slot widths 0.127cm and 0.287cm	72
Figure 29. Comparison of Nusselt numbers for Re=8,300 at z/W = 6 and slot widths 0.127cm and 0.287cm	72
Figure 30. Comparison of Nusselt numbers for Re=8,300 at z/W = 8 and slot widths 0.127cm and 0.287cm	73
Figure 31. Comparison of Nusselt numbers for Re=8,300 at z/W = 10 and slot widths 0.127cm and 0.287cm	73
Figure 32. Nusselt number for Re=8,300 with z=0.762cm and W=0.127cm and 0.287cm	74
Figure 33. Recovery temperature difference for a high velocity case (Test 3) and a low velocity case (Test 17)	78
Figure A1 Comparison between Eq. (A1) and an exponential function	86

Figure B1 Schematic of jet impingement experimental rig	91
Figure B2 Leading edge model	92
Figure B3 Nozzle design	93
Figure B4a Entry plate and center section for the high pressure drop manifold	94
Figure B4b Side view of the high pressure drop manifold	95
Figure B4c Exit plate for the high pressure drop manifold	96
Figure C1 Temperatures of the leading edge and the leading edge coolant	98

LIST OF TABLES

Table 1 Jet impingement design program output part 1	22
Table 2 Jet impingement design program output, part 2	23
Table 3 Calibration data for TLC paint, product BM/R35C1W/C17-10, batch 40909-1	44
Table 4 Jet impingement heat transfer test matrix	61
Table 5 Comparison of experimentally determined stagnation line recovery temperature differences with predicted stagnation line recovery temperature differences	76
Table A1 Dimensionless parameter range for Eq. (A3)	87
Table D1a Heat transfer coefficient data from tests 1-5	99
Table D1b Heat transfer coefficient data from tests 6-10	103
Table D1c Heat transfer coefficient data from tests 11-15	107
Table D1d Heat transfer coefficient data from tests 16-19	111
Table D1e Recovery temperature difference data from tests 1-5	115
Table D1f Recovery temperature difference data from tests 6-11	119
Table D1g Recovery temperature difference data from tests 11-15	122
Table D1h Recovery temperature difference data from tests 16-19	127

NOMENCLATURE

A	area (m^2)
a	arbitrary constant
b	arbitrary constant
c	arbitrary constant
c_p	specific heat at constant pressure (J/kg K)
D	width of the exhaust duct (m)
F	transformed arbitrary function
f	arbitrary function
g	arbitrary function
H	Heavyside step function
h	heat transfer coefficient ($\text{W/m}^2 \text{K}$)
k	thermal conductivity (W/m K), turbulence modeling parameter
L	height of the duct (m)
\mathcal{L}	Laplace transform operator
M	mass (kg)
\dot{m}	mass flow rate (kg/s)
q	heat flux (W/m^2)
R	gas constant (J/kg K)
r	recovery factor

s	Laplace transform variable
T	temperature (K)
t	time (s)
u	velocity (m/s)
V	average velocity of the fluid (m/s)
W	slot nozzle width, turbulence modeling parameter (m)
w	arbitrary function
x	rectangular coordinate representing the direction of conduction into the plate
y	rectangular coordinate representing the direction of flow along the plate
z	rectangular coordinate parameter representing the distance from the nozzle to the plate

Dimensionless Groups

Bi	Biot number
M	Mach number
Nu	Nusselt number
Pr	Prandtl number
Re	Reynolds number
St	Stanton number

Greek Symbols

α	thermal diffusivity (m^2/s)
ϵ	turbulence modeling parameter, surface emissivity
σ	Stefan-Boltzmann constant
ρ	density (kg/m^3)
τ	dummy time variable of integration
μ	dynamic viscosity ($kg/m\ s$)
ν	kinematic viscosity (m^2/s)

Subscripts

aw	adiabatic wall
e	one component of the dependent variable in a linear differential equation
f	fluid
i	x component of a vector quantity, initial
j	y component of a vector quantity
k	spatial index
r	recovery
s	surface
tc	thermocouple

u	one component of the dependent variable in a linear differential equation
w	wall
0	initial
∞	great distance or time

Superscripts

m	exterior iterative step for finding the fluid temperature
n	interior (nested) iterative step for finding the fluid temperature
'	time varying component
*	dimensionless quantity

Overscores

—	average, or transformed variable
---	----------------------------------

ACKNOWLEDGMENTS

I would like to thank Professor Mills for his technical guidance, careful review, and encouragement towards the completion of this dissertation, and Professors Christopher Anderson, C. J. Kim, Nasr M. Ghoniem and Adrienne Lavine for their review and helpful suggestions. The financial support of the NASA Dryden Flight Research Center for this experimental research is gratefully acknowledged: the technical monitor was Robert Quinn, and his encouragement is also gratefully acknowledged. I would also like to thank Wes Prochino, and Murray Durham from TRW for their useful suggestions in the design of this experiment.

VITA

May 7, 1958

Born, Canton, New York

1981

B.S. Mechanical Engineering
Colorado State University
Ft. Collins, Colorado

1981-1982

Nuclear Construction Engineer
Daniel International Corp.
Newport, Michigan

1986

M.S. Mechanical Engineering
University of Arizona
Tucson, Arizona

1986-1996

Member of the Technical Staff
TRW
Redondo Beach, California

1996

Staff Engineer
Lockheed Martin
Denver, Colorado

ABSTRACT OF THE DISSERTATION

Experimental Investigation Of Jet Impingement Heat Transfer Using Thermochromic Liquid Crystals

by

Brian Paul Dempsey

Doctor of Philosophy in Mechanical Engineering

University of California, Los Angeles, 1997

Professor Anthony F. Mills, Committee Chair

Jet impingement cooling of a hypersonic airfoil leading edge is experimentally investigated using thermochromic liquid crystals (TLCs) to measure surface temperature. The experiment uses computer data acquisition with digital imaging of the TLCs to determine heat transfer coefficients during a transient experiment. The data reduction relies on analysis of a coupled transient conduction - convection heat transfer problem that characterizes the experiment. The recovery temperature of the jet is accounted for by running two experiments with different heating rates, thereby generating a second equation that is used to solve for the recovery temperature. The resulting solution requires a complicated numerical iteration that is handled by a computer. Because the

computational data reduction method is complex, special attention is paid to error assessment. The error analysis considers random and systematic errors generated by the instrumentation along with error generated by the approximate nature of the numerical methods. Results of the error analysis show that the experimentally determined heat transfer coefficients are accurate to within 15%. The error analysis also shows that the recovery temperature data may be in error by more than 50%. The results show that the recovery temperature data is only reliable when the recovery temperature of the jet is greater than 5° C, i.e. the jet velocity is in excess of 100 m/s. Parameters that were investigated include nozzle width, distance from the nozzle exit to the airfoil surface, and jet velocity. Heat transfer data is presented in graphical and tabular forms. An engineering analysis of hypersonic airfoil leading edge cooling is performed using the results from these experiments. Several suggestions for the improvement of the experimental technique are discussed.

Chapter 1

INTRODUCTION

1.1 Background

Impinging fluid jets as a means of cooling have been widely used in industry for over 100 years. The characterization of jet impingement heat transfer for engineering purposes has taken place largely over the last 40 years. Recently, new high heat flux technologies have accelerated the interest in jet impingement cooling. Hypersonic airfoils, gas turbine blades, VLSI electronic circuitry, and diode lasers are a few of the new technologies that require high heat flux rates. Progress in this area of heat transfer has been relatively slow due to the complicated fluid dynamics of jets, and because of the importance of the surface geometry to the problem. These two factors make theoretical analysis impossible for all but the simplest cases. Numerical analysis has also been of little help in this area of heat transfer because of difficulties in modeling of turbulence in these flow configurations. Therefore, most engineering data has come from experiments.

1.2 Objectives

In past experimental heat transfer studies a very direct method of determining heat transfer coefficients was used. Using Newton's law of cooling,

$$q = h(T_w - T_f) \quad (1)$$

the heat transfer coefficient can be determined by measuring two temperatures and a heat flux. The advantages of using this method are that the data reduction and error estimation are extremely simple. Unfortunately, there are also several disadvantages to this method. For each spatial point on a surface that the heat transfer coefficient is needed, sensors must be installed. When the heat transfer coefficient varies greatly over the surface (as is the case in jet impingement heat transfer) a large number of sensors are needed to characterize the heat transfer. This leads to a long setup time, which makes it difficult to investigate many configurations.

The goal of this work is to add to the body of knowledge in the area of jet impingement heat transfer, specifically as it relates to the cooling of the leading edge of a hypersonic vehicle. It will be shown that use of currently available low-cost, high-speed computer resources makes the process of obtaining data more efficient. A more efficient experimental method can be used to try several cooling arrangements quickly in order to obtain the optimal design in a short period of time.

1.3 Previous Work

1.3.1 *Analytical Studies*

Due to the complicated fluid dynamics involved in jet impingement heat transfer, analytical techniques have not been very effective in characterizing the flow and predicting heat transfer. Still, a few researchers have generated results for some simple cases. The fluid dynamics of a wall jet are discussed by Glauert [1] for both the laminar

and turbulent case. A similarity solution for the laminar case is discussed, however he was unable to obtain a solution for the turbulent case and only draws some general conclusions. Meyer et al. [2] tried to model a turbulent wall jet using the 1/7 power law for both the temperature and velocity profiles with poor results. Good heat transfer results for laminar jets have been obtained by some researchers by solving a potential flow problem, and then coupling the solution to the plate with boundary layer equations and solving these numerically [3,4]. Finally some success was achieved for both laminar and turbulent jets using a potential flow solution and coupling it to heat transfer at the plate using experimentally determined parameters [5-8].

1.3.2 *Numerical Studies*

There have been many attempts to model turbulent jet impingement fluid dynamics and heat transfer using numerical methods. Generally, turbulent fluid dynamics problems are solved numerically by first modifying the Navier-Stokes and continuity equations by replacing the flow variables with time averaged plus fluctuating variables. This substitution yields the turbulent forms of the momentum and energy equations. When the turbulent forms of the momentum and energy equations are compared to their laminar counterparts additional terms are noticed. In the momentum equation the ordinary viscous stress term is modified by $\rho \overline{u'_i u'_j}$, which is known as the apparent turbulent stress, or Reynolds stress. Similarly in the energy equation the

conduction term is modified by $\rho c_p \overline{T'_i u'_j}$, which is known as the apparent turbulent heat flux, or Reynolds heat flux. The details of this analysis can be found in a number of books on the subject e.g. [9]. The turbulent forms of the conservation equations cannot be solved directly because the additional terms must be regarded as new unknowns. The closure problem is handled by writing additional "turbulence modeling" equations. Turbulence modeling can be accomplished in several ways. The simplest (and very successful for simple flow geometries) method is the mixing length model suggested by Prandtl. This is one example of a "zero-equation" model, the "zero" refers to the number of partial differential equations used to describe one of the turbulent flow parameters. There do not appear to be any successful jet impingement studies, which use this type of turbulence model. A one-equation model has been used by Wolfshtein [10] with some success to model the fluid dynamics problem. Currently one of the most popular methods for solving turbulent problems numerically is the two-equation model. Examples of this type of model are the well known $k - \varepsilon$ and $k - W$ models. Several researchers have used this type of analysis to get good results for the fluid dynamics problem [11-15]. The $k - \varepsilon$ model has also been used to model more complicated fluid dynamics of jets. Chuang et al. [16] modeled the fluid dynamics of twin jets impinging on a flat surface in a cross flow. In each of these studies the results compare favorably with experiments except near the stagnation point where errors in the velocity were 30%-50%.

The numerical heat transfer problem has proven to be even more difficult than simply solving for fluid dynamic quantities. Nearly all of the numerical analyses of the heat transfer problem use the $k - \varepsilon$ two-equation turbulence model. The difference in the analyses is how the problem is solved near the wall and near the stagnation point. Several researchers have used wall functions to couple the $k - \varepsilon$ model to the near wall region. A plane turbulent jet impinging at a 70° angle was solved using a wall function by Hwang and Tsou [17]. The fluid dynamic results compared favorably with experiments, however the heat transfer at the stagnation point is over predicted by about 30%. A normally impinging turbulent jet was explored by Looney and Walsh [18]. Again the wall function yielded good fluid dynamics results but poor heat transfer results at the stagnation point. The normally impinging jet was also explored by Polat et al. [19]. They solved the problem with several different wall functions and found that when a particular wall function gave good results at the stagnation point the results were poor downstream. Yuan and Liburdy [20] used a wall function model and found that by varying some of the parameters good agreement between the numerical solution and experimental results could be achieved.

The other common way of solving the jet impingement heat transfer problem is to use a two-layer model. The flow away from the plate is solved using a standard $k - \varepsilon$ turbulence model and the flow near the plate is solved using a low Reynolds number $k - \varepsilon$ model. Rodi and Scheuerer [21] used the low Reynolds number turbulence model of

Lam and Bremhorst [22] to solve the heat transfer problem around a gas turbine blade. No results were obtained for the stagnation point, and poor results were obtained for the laminar to turbulent transition region. Satisfactory results were obtained for points in between the two regions. The low Reynolds number model was used by Chang and Mills [23] to study turbulent jet impingement heat transfer. Key parameters in the model were varied in an effort to obtain improved jet impingement heat transfer predictions. They found that the best results were obtained by using the low-Reynolds number model of Yap [24] as modified by Jones and Launder [25]. The results showed good agreement with experiments except at the stagnation point where the heat transfer was over-predicted by up to 50%. Finally, it should also be mentioned that there have been attempts to solve the heat transfer problem for supersonic impinging jets [26]. This is an even more difficult problem to solve and, as expected, the heat transfer results do not compare well with experiment.

The fact that the numerical results do not compare very well with experimental data might have been predicted. Turbulence models contain constants that are determined by comparing numerical solutions to experimental results. Therefore, it may be unreasonable to expect that a single set of constants in a turbulence model could accurately predict heat transfer results for all types of flows. In addition, a particular turbulence model may not even contain the mathematical terms that characterize the

physics of the fluid flow under consideration. In particular, the k - ϵ turbulence model is known to have trouble modeling flows in which streamlines are highly curved.

1.3.3 *Experimental Studies*

During the last 40 years, experiments have provided the majority of data for jet impingement heat transfer. The heat transfer coefficient for a high speed impinging jet is not only a function of the usual Reynolds number and Prandtl number, but it is also a function of the Mach number, geometry, and the difference between the jet and the ambient temperature. With this many parameters it would take much experimental work to characterize the heat transfer for all the common engineering applications. In fact, since many applications have a unique geometry, it may not be realistic to assume that a general data base of heat transfer coefficients can be developed that would meet the needs of all designs. Much of the significant data on jet impingement heat transfer has been assembled and discussed in three major review articles [27-29]. The investigations discussed in these reviews cover several important parameters including: Reynolds number, Prandtl number, nozzle shape, nozzle to plate spacing, jet exit turbulence, flow confinement, recovery factor, entrainment effects, and impingement angle. One parameter, which has not been covered as extensively is the effect of a curved impingement surface. There have been three basic methods used to study jet impingement heat transfer; heated plate/ heat flux meter, sublimation of naphthalene,

and a relatively new method involving temperature sensitive coatings that undergo a color change at a specific temperature.

Jet impingement heat transfer of curved surfaces was first investigated primarily as a means of cooling gas turbine blades. One of the early studies was done by Metzger et al. [30]. Average Stanton number data for a row of jets impinging on a semi-cylindrical surface as a function of several geometrical parameters, as well as Reynolds number were obtained. A study by Tabakoff and Clevenger [31] investigated a slot jet, a row of round jets, and an array of round jets impinging on a semi-cylinder. Average and local Nusselt number data were presented as a function of several geometric parameters and Reynolds number. Hrycak [32] added to the data of jets impinging on a semi-cylindrical surface and develops a empirical correlation for the average and local Nusselt number. A series of papers by Livingood and Gauntner [33-35] presents data and correlations for a row of jets impinging on a semi-cylindrical surface, and for a single jet impinging on a hemispherical surface. Heat transfer of a slot jet impinging on both the interior and exterior of a cylinder was investigated by Chung [36]. In this study flow visualization techniques are used to gain insight into the nature of jet impingement heat transfer. More experimental data for jets impinging on concave surfaces is presented by Chupp et al. [37] and Jusionis [38]. All of the preceding experimental studies were done using a constant temperature or constant heat flux surface instrumented with thermocouples and heat flux meters.

Another important aspect of jet impingement heat transfer is the effect of ambient fluid entrainment into the jet. This issue was addressed by Hollworth et al. [39,40], and it was found that the local heat transfer coefficient does not depend explicitly on the temperature difference between the jet and the ambient fluid if the heat transfer coefficient is defined in terms of a local recovery temperature that includes the effect of the ambient fluid. A study of the recovery factor for an impinging jet was done by Goldstein et al. [41]: a significant minimum in the recovery factor was found at the stagnation point. Also presented is a correlation for the jet impingement heat transfer coefficient in terms of the adiabatic wall temperature. Similar use of the recovery factor and adiabatic wall temperature by Goldstein and Seol [42] has yielded heat transfer data and a correlation for a row of impinging jets. A similar study was done by Baughn et al. [43]; however, Baughn used Plexiglas coated with temperature sensitive liquid crystals to reduce the error caused by lateral conduction in the thin foil heater used by Goldstein and Soel.

Flow visualization has been used in the area of jet impingement heat transfer to provide a basic understanding of the fluid dynamics involved. One such flow visualization study for an impinging jet was done by Popiel and Trass [44]. Using a smoke wire technique the interactions between the large scale toroidal vortex structure and the impingement surface are shown. More useful for heat transfer applications is a flow visualization study done by Stevens et al. [45]. Velocities were measured using

laser Doppler velocimetry. Mean velocities and turbulence levels were presented and discussed in terms of local heat transfer coefficients.

1.3.4 *Liquid Crystal Methods*

For decades there have been two major ways of experimentally determining heat transfer coefficients. The most popular method is to subject a constant temperature (or constant heat flux) surface to a flow and measure the heat transfer with a heat flux meter. The other useful method is to make a model of the heat transfer surface out of a subliming material and expose it to the flow. By using the heat and mass transfer analogy the rate of recession of the surface is related to the heat transfer coefficient. During the last 20 years, a third method that uses temperature sensitive liquid crystal to determine heat transfer coefficients has been developed. Liquid crystals were first observed in 1888 by an Austrian botanist, Friedrich Reinitzer. He found that certain organic compounds appeared to have two melting points, an initial melting point that turned the opaque solid phase to a cloudy liquid, and a second melting point, which turned the cloudy liquid clear. Further research showed that indeed an intermediate phase did exist, which Reinitzer termed the "liquid crystal phase". Since Reinitzer's original work several other researchers have written papers on the physics, chemistry, and technology of liquid crystals [46-48]. Of interest to the heat transfer field are papers by Castellano and Brown [49,50], in which the chemistry and physics of thermotropic liquid crystals are discussed.

Temperature sensitive liquid crystals display all the colors of the visible spectrum at a specific "transition temperature". The transition temperature is both selectable and repeatable. A process of micro-encapsulating the liquid crystals was developed, which protects the crystals from ultraviolet light and extends their life from only a few hours to a few years. In the microencapsulated form, the crystals can be suspended in a binder and applied (painted on) to a surface. Once done, the surface has essentially been instrumented with millions of temperature sensors, which can be read by observing color. Temperature sensitive liquid crystals were first used as a simple qualitative indication of hot regions and cold regions. Woodmansee [51] used liquid crystals to find flow blockages in heat exchangers, indicated by hot spots. Temperature sensitive liquid crystals have also been used to determine the location of transition to turbulence in wind tunnels (Klein [52,53].) In the field of optics, liquid crystals have been used to characterize infrared laser interference patterns (Keilmann [54].) Studies were done using liquid crystals to observe nucleation sites in boiling experiments by Raad and Myers [55]. More recently it has been shown that micro-encapsulated liquid crystals can be suspended in a fluid and used as a flow visualization method for fluid flows with temperature gradients [56].

Quantitative heat transfer studies began when it was found that temperature sensitive liquid crystals could be calibrated to within 1° C. One of the first quantitative heat transfer studies was done by Cooper et al. [57]. The crystals were used to find the circumferential variation of Nusselt number on a cylinder placed in a cross flow. The

crystals were calibrated to eight different temperatures and applied in paint form to a heated cylinder. Thus, a single steady state run yielded at least eight Nusselt number data points. An excellent history on the use of liquid crystals is also presented in this paper. A similar technique was used by Hippenstein et al. [58] to find heat transfer coefficients on gas turbine blades. A single transition temperature liquid crystal paint was used on the airfoil. By observing the location of the transition line while supplying a known heat flux from a thin metal film heater the heat transfer coefficient could be ascertained. Results are presented for various Reynolds number and turbulence levels. The effect of local leading-edge sand grain roughness was also explored. A transient liquid crystal technique was used to examine film cooling of a gas turbine airfoil by Byerley [59]. The transient technique involves suddenly exposing the liquid crystal coated model to heated air; the time that it takes for the liquid crystal to reach the known transition temperature is used in the solution of a one dimensional conduction problem to determine the heat transfer coefficient. The transient, 1-D, conduction equation with associated convection and semi-infinite boundary conditions is

$$\frac{\partial T_w}{\partial t} = \alpha \frac{\partial^2 T_w}{\partial x^2} \quad (2a)$$

$$-k \frac{\partial T_w(0,t)}{\partial x} = h [T_f - T_w(0,t)] \quad (2b)$$

$$T_w(\infty, t) = T_0 \quad (2c)$$

The initial condition is

$$T_w(x, 0) = T_0 \quad (2d)$$

The solution to this system is

$$\frac{T_w - T_0}{T_f - T_0} = \operatorname{erfc} \left[\frac{x}{(4\alpha t)^{1/2}} \right] - e^{\frac{hx}{k} + (\frac{h}{k})^2 \alpha t} \operatorname{erfc} \left[\frac{x}{(4\alpha t)^{1/2}} + \frac{h}{k} (\alpha t)^{1/2} \right] \quad (3)$$

It can be seen from Eq. (3) that the heat transfer coefficient, h , can be evaluated if the initial temperature T_0 , the fluid temperature T_f , the transition time, and the properties of the materials are known.

It was recognized by many researchers that liquid crystals would be very useful in determining local heat transfer coefficients for complicated flow or complicated surface structure. Transverse ribs are often used in ducts to enhance heat transfer but the local heat transfer coefficients are hard to characterize because of the discontinuous nature of the wall. The transient liquid crystal technique was used by Baughn and Yan [60] to study this type of duct flow. For their experiment it was decided to heat the test section, and then suddenly move it into the flow in order to achieve a step function cooling. Again the heat transfer coefficient is determined from the 1-D transient conduction solution. Results for various Reynolds number and rib pitch are presented. The issue of the breakdown of the one dimensional conduction model near the corner of the rib is also addressed. A similar study on a ribbed duct was done by Wang et al. [61]. A charge coupled device (CCD) camera and computer were used to monitor the phase

change of the crystals. The intensity vs. time of various points (pixels) was used to decide the precise time of transition. In an excellent paper by Saabas [62] it was pointed out that in order to use the transient liquid crystal method in small ducts it is necessary to account for the temperature change of the fluid. This was done by coupling the energy equation for the fluid to the 1-D transient conduction equation. The coupled system is then solved using a combination of analytical and numerical techniques. Other researchers have used variations of these ideas to explore heat transfer inside ducts [63-65].

Jet impingement heat transfer research is another area that has benefited from liquid crystal technology. Given the number of parameters involved in jet impingement heat transfer, liquid crystals are particularly well suited to this area of research. One of the first jet impingement heat transfer studies to use liquid crystals was done by Goldstein and Franchett [66]. Their study gives results for Reynolds number between 10,000 and 35,000, jet orifice-to-plate spacing of 4, 6, and 10, and various angles between the jet center line and the plate. A heat transfer study by Lucas et al. [67] explores the effect of a heated top plate, which constrains the flow of the jet radially outward. The transient method was used by Metzger and Kim [68] to investigate jet impingement heat transfer on a rotating surface. The effect of an air jet issuing from an elliptic nozzle impinging on a flat plate was investigated, using liquid crystals, by Lee, Lee, and Lee [69]. Huber and Viskanta [70] used liquid crystals to investigate the heat transfer characteristics of an array of jets. It was found that the geometry of the spent

air exit played a significant role in the results. In their study, Huber and Viskanta (and many other researchers) used a thin foil stainless steel or gold heater to supply the constant heat flux for the steady state method. The effect of radial conduction in the surface is almost always neglected, however in cases where the heat transfer coefficient is changing rapidly in the radial direction (which can be the case in jet impingement heat transfer), it can be shown that the negligible conduction assumption causes significant error.

Many researchers have looked into the basic problems of using liquid crystals for heat transfer research. An early paper by Herold and Wiegel [71] explains some of the problems encountered with lighting and the collection of photographic data from liquid crystals. The effect of off-axis lighting, color filters, and polarizers are discussed. A more thorough investigation on how to improve liquid crystal thermometry through the proper use of lighting and filters is presented by Akino et al. [72]. These researchers performed experiments with 18 different narrow band pass optical filters and a gray scale video camera to resolve isothermal lines. The gray scale images were digitized so that a computer could be used to define the isothermal contours, thus removing human uncertainty from the process. A few researchers have attempted to use color videos of the liquid crystals during transition to improve accuracy and increase the amount of data available per frame. Camci et al. [63] show how a color image can be used to get three isotherms per image using the three base video colors, red, green, and blue. The method is then demonstrated by finding heat transfer coefficients on the

bottom of a duct in a decelerating flow. In a second paper, Camci et al. [73] improve the method to get 40 isotherms per frame using a hue system. The method is then demonstrated for a round jet impinging on a flat plate; unfortunately, the Nusselt number data that is presented appears to be incorrect. The error is probably caused by using the transient method to solve for the heat transfer coefficients. It can be shown that the error in the heat transfer coefficient increases as the time to transition for the liquid crystals increases. The data given in this paper shows a very long time to transition. It is also not explained why more than one isotherm per frame is desirable since all transient liquid crystal heat transfer experiments take place over a period of a few seconds and standard video equipment records at a rate of 30 frames per second. In order to increase accuracy, other researchers have developed calibration methods based on a hue system. Chan et al. [74] show a calibration method for liquid crystals, but by far the most complete study on this subject is done by Farina et al. [75]. This study includes nearly every parameter involved in doing an accurate calibration of liquid crystals based on a hue system. A study by Kimoto et al. [76] deviates from most of the other researchers by attempting to use a scanning photo sensor to measure the location of the crystal transition. The method was used to determine the heat transfer coefficient for a circular impinging jet and yielded good results. Another potentially useful method for finding heat transfer coefficients is presented by Wolfersdorf et al. [77]. The method involves using a film heater like the steady state method then suddenly changing the heater power and measuring the time to transition as in the

transient case. The advantage in using this method is that nonuniformities in the heating pattern are allowed (ensuring a uniform heat flux using electrical heating with a thin metallic film is often difficult) and the crystals need not be calibrated. Finally, it should be noted that infrared imaging radiometry and melting point surface coatings can be used to determine heat transfer coefficients in a manner similar to that of liquid crystal methods: Pan et al. [78], Lytle and Webb [79], and Metzger and Larson [80] discuss these methods.

Chapter 2

ANALYSIS

2.1 Preliminary Design Considerations

It is proposed that jet impingement heat transfer be used to cool the leading edge of a hypersonic vehicle. Prior to designing an experiment to obtain the required heat transfer coefficient data, the important parameters of the problem must be established. These parameters are:

1. Expected heat flux profiles for the leading edge.
2. Aerodynamic design of the leading edge.
3. Operating temperature of the leading edge.
4. The type of coolant and flow rate available.
5. Approximate heat transfer data from previous experiments.

Once this information has been obtained, a preliminary design of the cooling system for the leading edge can be done. The preliminary design then establishes the parameter space to be covered in order for the experiment to give pertinent results.

Over the past several years, studies have been done by various aerospace contractors on the feasibility of flying a hypersonic transport airplane, commonly referred to as National Aerospace Plane (NASP). A document by Friestad et al. [81] gives preliminary design parameters for the NASP leading edge. Included in this document is information on the leading edge geometry, leading edge material characteristics, aerodynamic heating, trajectory characteristics and structural

requirements. The aerodynamic heating was predicted using the Fay and Riddell theory for laminar boundary layers [81]. A parametric study was conducted in which the wall temperature and leading edge radius of curvature were varied. Heat flux curves are presented for both the upper and lower surfaces, at all times during ascent and descent. It was decided to investigate the worst case heat flux, which occurs on the lower surface during ascent at a Mach number of 18. The baseline leading edge radius of 0.508 cm is selected together with a wall temperature of 810 K, which is approximately the upper limit for use of titanium alloys. Other materials are also available, such as molybdenum-rhenium alloys, which allow the leading edge temperature to reach a temperature of 2400 K and thus allow a smaller load on the cooling system.

2.1.1 *Cooling System Design*

The method of determining the design of the jet impingement cooling system is illustrated below, starting with Fig. 1.

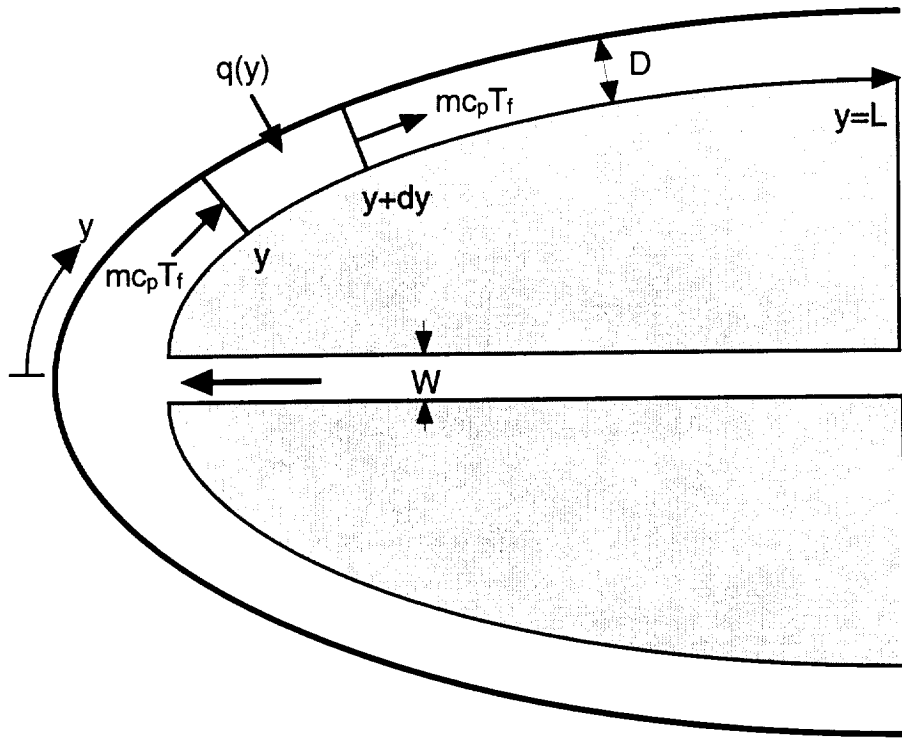


Figure 1. Control volume used for an energy balance on the leading edge cooling system.

A steady state energy balance on an element of cooling passage dy long is

$$\dot{m}c_p T_f \Big|_{y+dy} - \dot{m}c_p T_f \Big|_y = q(y) dy \quad (4)$$

where T_f is the bulk fluid temperature, and \dot{m} is the mass flow rate per unit depth of the cooling passage. A Taylor series expansion about y and a rearrangement of terms yields,

$$\dot{m}c_p \frac{dT_f}{dy} = q(y) \quad (5)$$

Expressing $q(y)$ in terms of a heat transfer coefficient $h(y)$,

$$q(y) = h(y)[T_w(y) - T_f(y)] \quad (6)$$

The bulk fluid temperature is obtained by solving Eq. (5) as an ordinary differential equation and gives,

$$T_f(y) = T_{f0} + \frac{1}{\dot{m}c_p} \int_0^y q(y) dy \quad (7)$$

where T_{f0} is the temperature at the entrance to the duct. Equation (7) can also be expressed in terms of the jet Reynolds number based on the width of the slot.

$$T_f(y) = T_{f0} + \frac{2}{\mu c_p Re} \int_0^y q(y) dy \quad (8)$$

where,

$$Re = \frac{VW}{v} \quad (9)$$

and W is the width of the slot.

A preliminary design for the leading edge cooling system can now be generated using Eqs. (6) and (8). Using Eq. (8) and the q vs. y data from [81], T_b vs. y data can be obtained for various Reynolds numbers and slot geometries. Then using the approximate h vs. Re and y data available in [36] and [82] and the T_b vs. y data from Eq. (8), T_w vs. y can be obtained from Eq. (6). It is assumed that some sort of enhanced surface can be provided (such as transverse ribs or pin fins) such that h does

not drop below 1,000 W/m²K regardless of the distance from the stagnation line. In order for this solution to be valid, the wall temperature must be the same as the wall temperature used to generate the q vs. y data in [80], that is 810 K for all y . This suggests that an iterative method must be used where the Reynolds number and the slot geometry are varied until a nearly constant wall temperature of 810 K is obtained. Obviously it will not be possible to find an h vs. y profile that matches perfectly the q vs. y profile to give a constant 810 K wall temperature. However, this computation is useful as an approximate means of bounding the important parameters for the experimental study. A computer program was written to handle the numerical integration in Eq. (8) and to speed up the iterative process. Tables 1 and 2 show sample output from a single iteration.

Table 1. Jet impingement design program output part 1.

Re	14502.6
Nu.....	101.8
JET STAGNATION h	12877.1 W/m ² K
SLOT HEIGHT	0.12 cm
SLOT LENGTH	10.0 cm
VOLUMETRIC FLOW RATE	0.04075 m ³ /s
MASS FLOW RATE	0.00500 kg/s
NOZZLE EXIT VELOCITY	339.6 m/s

NOZZLE EXIT MACH NUMBER 0.316

NOZZLE HYDRAULIC DIAMETER / DISTANCE TO PLATE 20.0

Table 2. Jet impingement design program output, part 2.

x [cm]	q [W/m ²]	h [W/m ² K]	T WALL [K]	T BULK [K]
0.000	7.090E+06	12877.1	750.6	200.0
0.254	6.390E+06	11756.6	792.4	248.9
0.508	4.260E+06	10733.5	684.4	287.6
0.762	1.770E+06	9799.5	490.1	309.4
1.270	1.560E+06	8168.3	524.6	333.6
2.540	1.340E+06	5181.4	644.8	386.2
5.080	9.200E+05	2084.8	909.5	468.2
7.620	7.100E+05	1000.0	1237.4	527.4
15.240	5.000E+05	1000.0	1159.1	659.1
30.480	3.500E+05	1000.0	1194.1	844.1
50.800	2.100E+05	1000.0	1216.7	1006.7

Table 2 shows that this design is capable of keeping the wall temperature below 810 K for a distance of about 4 cm from the stagnation point. At the 4 cm point additional coolant must be injected to reduce the bulk temperature and maintain a wall temperature below 810 K. Note a sharp drop in wall temperature occurs at about

7 cm from the stagnation point, which is due to a sharp drop in wall heat flux at about the same location. In general, the results show that sufficient cooling can be achieved with a wide range of Reynolds numbers. As the coolant moves away from the stagnation line the bulk temperature rises and additional coolant must be injected in order to maintain an acceptable wall temperature. For a Reynolds number of 10,000, the additional coolant must be injected at about 3.0 cm from the stagnation point; however, for a Reynolds number of 46,000 the injection is not necessary until about 11 cm.

2.2 Heat Transfer Analysis

The principle behind the experiment is that a heat transfer coefficient can be determined if we know the bulk temperature of the fluid, the initial temperature of the wall, and how long it takes the wall surface to reach a specific temperature. Thermocouples are used to obtain the initial temperature of the wall and the time-varying temperature of the jet. The imaging system and the liquid crystals are used to determine the time for the surface to reach a specific temperature. Initially the wall and the fluid above the wall are at the same temperature. The time-varying temperature of the fluid at $y=0$ is $f(t)$. The time it takes for the surface of the wall to reach a particular temperature is obtained from the experiment. It is assumed that there is no conduction in the streamwise direction in either the fluid or the wall. The

differential equation that describes the temperature variation in the wall is the familiar one-dimensional transient heat conduction equation,

$$\frac{\partial^2 T_w}{\partial x^2} = \frac{1}{\alpha} \frac{\partial T_w}{\partial t} \quad (10a)$$

The initial and boundary conditions are

$$T_w(x, 0) = T_\infty \quad (10b)$$

$$T_w(\infty, t) = T_\infty \quad (10c)$$

$$-k \frac{\partial T_w(0, t)}{\partial x} = h [T_{aw}(y, t) - T_w(0, t)] \quad (10d)$$

The adiabatic wall temperature is used here in place of the fluid temperature. It will be seen later that it is necessary to take into account the conversion of kinetic energy to thermal energy at the impingement surface.

The transient form of the convection equation is derived by again referring to Fig. 1. An energy balance on an element of cooling passage dy long with the energy storage term included is

$$\rho D c_p \frac{\partial T_f}{\partial t} dy = \rho D c_p T_f \Big|_y - \rho D c_p T_f \Big|_{y+dy} - q dy \quad (11)$$

Denoting the bulk fluid velocity V , and expressing q in terms of the heat transfer coefficient h , Eq. (11) becomes,

$$\rho c_p dy D \frac{\partial T_f}{\partial t} = \rho V D c_p T_f \Big|_y - \rho V D c_p T_f \Big|_{y+dy} - h dy (T_f - T_w(t)) \quad (12)$$

A Taylor series expansion about y yields the differential equation that governs the fluid temperature

$$\frac{\partial T_f}{\partial t} = -V \frac{\partial T_f}{\partial y} - \frac{h}{\rho D c_p} (T_f - T_w(t)) \quad (13a)$$

The associated initial and boundary conditions are

$$T_f(y,0) = T_i \quad (13b)$$

$$T_f(0,t) = f(t) \quad (13c)$$

2.2.1 Conduction Analysis

Equations (10a-10d) can be solved if the time varying bulk temperature at each y location is known. Equations (13a-13c) can be solved if the time varying wall temperature at each y location is known and the wall temperature is constant in y . For this purpose the channel is discretized into finite y -steps, and T_w assumed constant over each step. It should be noted that for the conduction equation $T_{aw}(t)$ must be known to find $T_w(t)$. For the convection equation $T_w(t)$ must be known to find $T_f(t)$. This suggests that an iterative procedure will be required to obtain numerical results.

With the above assumptions, the solution for Eqs. (10a-10d) with T_{aw} constant in time can be found most directly using Laplace transforms. A similarity solution can also be found after simplifying Eqs. (10a-10d) with the substitution $\theta = [T_{aw}(y,t) - T_w(0,t)] + \frac{k}{h} \frac{\partial T_w(0,t)}{\partial x}$. Details of this solution are found in Carslaw and Jaeger [83]. In either case the solution to Eqs. (10a-10d) is given in Eq. (14).

$$\frac{T - T_\infty}{T_{aw} - T_\infty} = \operatorname{erfc} \frac{x}{(4\alpha t)^{1/2}} - e^{hx/k + (h/k)^2 \alpha t} \operatorname{erfc} \left[\frac{x}{(4\alpha t)^{1/2}} + \frac{h}{k} (\alpha t)^{1/2} \right] \quad (14)$$

Duhamel's theorem can now be applied to find the wall temperature with a time varying T_{aw} . The result is

$$T - T_\infty = [T_{aw}(0) - T_\infty] \left\{ \operatorname{erfc} \frac{x}{(4\alpha t)^{1/2}} - e^{hx/k + (h/k)^2 \alpha t} \operatorname{erfc} \left[\frac{x}{(4\alpha t)^{1/2}} + \frac{h}{k} (\alpha t)^{1/2} \right] \right\} + \int_0^t \frac{dT_{aw}}{d\tau} \left\{ \operatorname{erfc} \frac{x}{(4\alpha(t-\tau))^{1/2}} - e^{hx/k + (h/k)^2 \alpha(t-\tau)} \operatorname{erfc} \left[\frac{x}{(4\alpha t)^{1/2}} + \frac{h}{k} (\alpha(t-\tau))^{1/2} \right] \right\} d\tau \quad (15)$$

In order to use Eq. (15) to determine the heat transfer coefficient it has been assumed that a thermocouple can be used to measure the air temperature. The temperature can be measured with sufficient accuracy as long as the air velocity is low. When the air velocity becomes large the thermocouple will measure a recovery

temperature, and the surface will respond to a recovery temperature. The recovery factors for the thermocouple and the surface are not the same, thus the recovery temperatures will be different. Therefore, for high speed jets there is a second unknown in Eq. (15) namely the surface recovery temperature. It is possible to overcome the problem of the second unknown quantity in Eq. (15) by introducing a second equation. The idea is illustrated in Fig. 2.

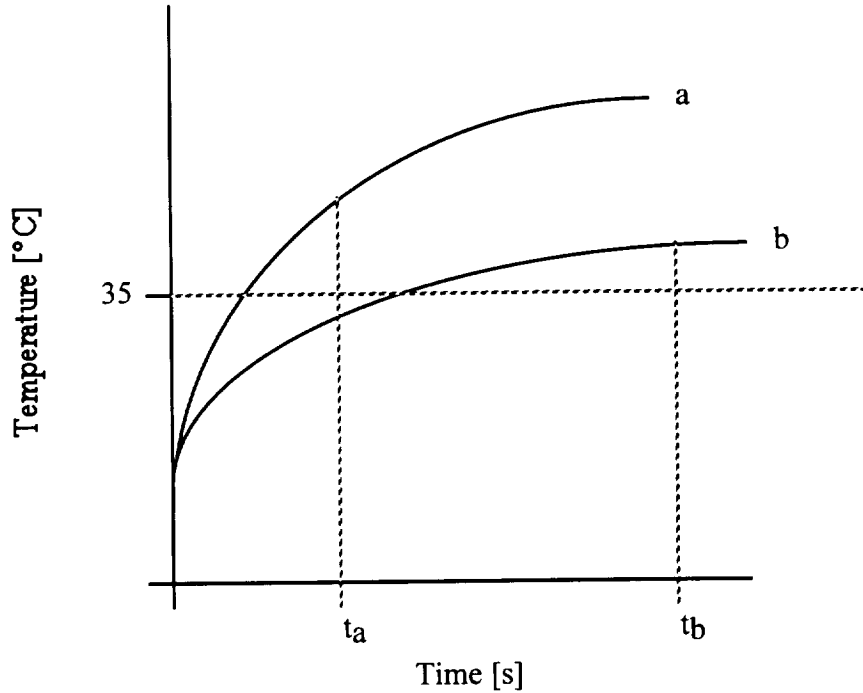


Figure 2 Jet temperature vs. time for two different heating rates.

When the jet air is heated rapidly as in curve a of Fig. 2 the crystals transition at time t_a . Curve a and the transition time t_a can be used in Eq. (15) to find the heat transfer coefficient. Likewise when the jet is heated more slowly (curve b) the

transition time is t_b . This information can also be used to determine the heat transfer coefficient. If all other parameters are constant the two heat transfer coefficients should be equal. It has been found that when the jet velocity is small the two heat transfer coefficients are the same, however when the jet velocity is large the heat transfer coefficients are different.

Since the crystal coated surface responds to the surface recovery temperature, the fluid temperature T_{aw} in Eq. (15) is expressed in terms of the measured thermocouple temperature, the thermocouple recovery temperature, and the surface recovery temperature as shown in Eq. (16).

$$T_{aw}(t) = T_{tc}(t) - T_{rc} + T_{rs} \quad (16)$$

The temperatures T_{rc} and T_{rs} can also be expressed as $r_{tc} \frac{V^2}{2C_p}$ and $r_s \frac{V^2}{2C_p}$ respectively.

Substitution into Eq. (15) produces Eq. (17) for heating rate a and Eq. (18) for heating rate b.

$$\begin{aligned} T - T_{\infty a} = & [T_{tca}(0) - T_{rc} + T_{rs} - T_{\infty a}] \times \\ & \left\{ \operatorname{erfc} \frac{x}{(4\alpha t_a)^{1/2}} - e^{hx/k + (h/k)^2 \alpha t_a} \operatorname{erfc} \left[\frac{x}{(4\alpha t_a)^{1/2}} + \frac{h}{k} (\alpha t_a)^{1/2} \right] \right\} + \\ & \int_0^a \frac{dT_{tca}}{d\tau} \left\{ \operatorname{erfc} \frac{x}{(4\alpha(t_a - \tau))^{1/2}} - e^{hx/k + (h/k)^2 \alpha(t_a - \tau)} \operatorname{erfc} \left[\frac{x}{(4\alpha t_a)^{1/2}} + \frac{h}{k} (\alpha(t_a - \tau))^{1/2} \right] \right\} d\tau \end{aligned} \quad (17)$$

$$T - T_{\infty b} = [T_{tcb}(0) - T_{rc} + T_{rs} - T_{\infty b}] \times$$

$$\left\{ \operatorname{erfc} \frac{x}{(4\alpha t_b)^{1/2}} - e^{hx/k + (h/k)^2 \alpha t_b} \operatorname{erfc} \left[\frac{x}{(4\alpha t_b)^{1/2}} + \frac{h}{k} (\alpha t_b)^{1/2} \right] \right\} +$$

$$\int_0^b \frac{dT_{tcb}}{d\tau} \left\{ \operatorname{erfc} \frac{x}{(4\alpha(t_b - \tau))^{1/2}} - e^{hx/k + (h/k)^2 \alpha(t_b - \tau)} \operatorname{erfc} \left[\frac{x}{(4\alpha t_b)^{1/2}} + \frac{h}{k} (\alpha(t_b - \tau))^{1/2} \right] \right\} d\tau \quad (18)$$

Eliminating the variable ($T_{rs} - T_{rc}$), and setting x to 0 i.e. the surface, yields Eq. (19).

$$0 = \left\{ T_{tca}(0) - T(0)_{tcb} + T_{\infty b} - T_{\infty a} + \right.$$

$$\left. \frac{T - T_{\infty b} - \int_0^b \frac{dT_{tcb}}{d\tau} \left\{ 1 - e^{(h/k)^2 \alpha(t_b - \tau)} \operatorname{erfc} \left[\frac{h}{k} (\alpha(t_b - \tau))^{1/2} \right] \right\} d\tau}{1 - e^{(h/k)^2 \alpha t_b} \operatorname{erfc} \left[\frac{h}{k} (\alpha t_b)^{1/2} \right]} \right\} \times$$

$$\left\{ 1 - e^{(h/k)^2 \alpha t_a} \operatorname{erfc} \left[\frac{h}{k} (\alpha t_a)^{1/2} \right] \right\} +$$

$$\int_0^a \frac{dT_{tca}}{d\tau} \left\{ 1 - e^{(h/k)^2 \alpha(t_a - \tau)} \operatorname{erfc} \left[\frac{h}{k} (\alpha(t_a - \tau))^{1/2} \right] \right\} d\tau - T + T_{\infty a} \quad (19)$$

Equation (19) can be solved iteratively for the heat transfer coefficient using the nozzle exit temperature curves a and b , and the transition times t_a and t_b . The difference between the surface recovery temperature T_{rs} and the thermocouple recovery temperature T_{rc} can then be obtained using Eq. (17) or (18).

2.2.2 Convection Analysis

An expression for T_f is now derived from Eqs. (13a-c). An order of magnitude analysis for Eq. (13a) shows that under most test conditions the time derivative term can

be neglected. The resulting ordinary differential equation is much simpler to solve and the solution easier to implement in the data reduction software. The solution to Eqs. (13a-c) with the time dependent term is presented in appendix A. The error caused by the exclusion of this term is analyzed in the error analysis chapter. With the time dependent term dropped from Eq. (13a), and the substitution $y=Ly^*$, made Eqs. (13a-c) become,

$$\frac{dT_f}{dy^*} + St \frac{L}{D} T_f = St \frac{L}{D} T_w(t) \quad (20a)$$

$$T_f(0,t) = f(t) \quad (20b)$$

Where St is the Stanton number defined as $St = \frac{h}{\rho c_p V}$

The solution to Eqs. (13a-b) is

$$T_f(t) = T_w(t) + (f(t) - T_w(t)) e^{-\frac{St_y}{D}} \quad (21)$$

2.2.3 Computational Method

Ultimately the goal is to obtain heat transfer coefficients. To accomplish this objective a computer program is used to implement a series of complicated but well established numerical techniques. The computation proceeds as follows. First, using the time it takes various y locations on the surface to reach the transition temperature, h is calculated iteratively from Eq. (19). If we let the function g represent Eq. (19), then h can be found using the secant method for root finding,

$$h_k^{n+1,m} = \frac{g(h_k^n, T_{fk}^n; t_k) h_k^{n-1} - g(h_k^{n-1}, T_{fk}^{n-1}; t_k) h_k^n}{g(h_k^n, T_{fk}^n; t_k) - g(h_k^{n-1}, T_{fk}^{n-1}; t_k)} \quad (22)$$

where an iterative step is represented by a superscript m or n and a step in y is represented by a subscript k. Having found h from Eq. (22) the recovery temperature difference between the surface and the thermocouple, ($T_{rs} - T_{rtc}$), can be found directly from either Eq. (17) or Eq. (18). Once h and ($T_{rs} - T_{rtc}$) have been evaluated, T_f can be evaluated explicitly using Eq. (21), starting from y=0. The explicit nature of the calculation is illustrated by Eq. (23),

$$T_{fk+1}^{m+n} = w(T_{fk}^m, h_k^m, T_{wk}^m, T_{bk+1}^m, h_{k+1}^m, T_{wk+1}^m) \quad (23)$$

where the function w represents Eq. (21). The dual superscripts m and n indicate a double iterative scheme. The n iteration is required at each y step to find h from Eq. (19). Once h is updated for each y, a new T_f can be generated without iteration since T_f is given explicitly from Eq. (23). A new T_f necessitates the evaluation of a new value of h and the calculation is returned to Eq. (21), thus the m iteration.

There are several numerical side issues involved in the iteration. Eq. (23) shows that T_{fk+1}^{m+n} is a function of both k and k+1. Since initially we do not have a value for T_{fk+1}^m the calculation is started by using only values at k. This idea is similar to some implicit finite difference solution methods for parabolic partial differential equations, which are started by an explicit method. Also, because of the way the data acquisition system

works, it will not always be possible to get the time it takes for the crystals to transition at the stagnation point. Therefore a polynomial extrapolation is done at the end of each iteration to estimate h at the stagnation point. The estimate for h at the stagnation point also helps improve the accuracy of all the other h values by allowing more accurate T_f calculations to be made. Fortunately the data acquisition system can be set up such that the extrapolation is only over a small distance.

It has been mentioned that it is necessary to evaluate h using Eq. (19) whenever high speed flow is present. For this experiment the flow slows significantly away from the stagnation line, therefore Eq. (19) is used only near the stagnation line. Away from the stagnation line the same value of h will be calculated from Eq. (15) using either curve a or curve b from Fig. 2 because the recovery temperature of the air at the surface becomes insignificant. Equation (19) can be used away from the stagnation point, however the h data becomes slightly scattered and the recovery temperature difference becomes useless. An example of this effect will be given in the error analysis section.

Chapter 3

ERROR ANALYSIS

3.1 Introduction

Error assessment is always important to experimental work: for the case of the jet impingement-TLC experiment, error assessment is of particular importance. The data reduction method relies on solving an inverse heat transfer problem involving two coupled partial differential equations. In addition, data is gathered using a relatively new method involving TLCs and digital video cameras. These factors make error assessment a complicated matter. The error assessment is done by considering the error in two parts, the error due to the numerical methods used to reduce the data, and the error generated by the instrumentation.

3.2 Error Assessment Due to All Numerical Methods Considered Together

The numerical error is the error in the result generated by the data reduction method even if the instrumentation produces error-free data. The data reduction method involves numerical filtering, derivatives, integration, interpolation, extrapolation, and root finding. Considered separately, each of the aforementioned methods has well understood error characteristics, however when used in an iterative or stepping fashion the error can be amplified. To examine the numerical error, results are first generated using a simple mathematical function representative of actual data, then subsequently results are generated using the same function with errors

representative of the actual experiment superimposed onto the simple function. The data reduction requires only 2 inputs, namely, position vs. transition time data for the impingement surface, and temperature vs. time data for air inlet.

The inlet air temperature data is well represented by the function $T = a(1 - e^{-bt}) + c$ as can be seen from Fig. 3. A typical representation of the “noise” portion of the data can be found by curve fitting actual data then subtracting the curve fit from the data: The result is shown in Fig. 4. A statistical analysis of the noise data in Fig. 4 yields a standard deviation is 0.1°C .

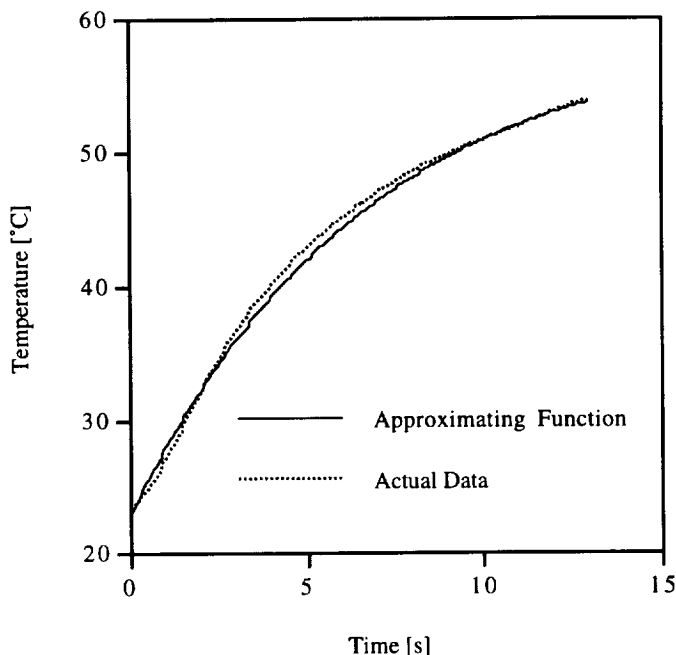


Figure 3 Actual air temperature data and approximating function.

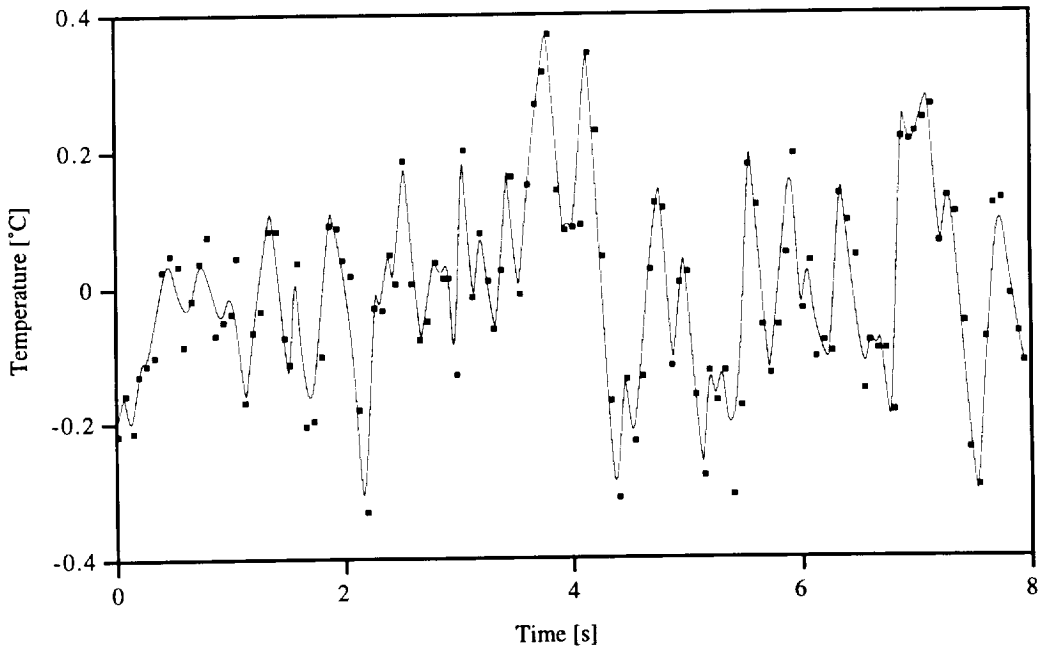


Figure 4 Typical noise in air temperature measurement.

First, heat transfer coefficients are determined using the data reduction program with the exponential representation for the inlet air temperature, then the data reduction program is run a second time with the noise function from Fig. 4 added to the exponential function. A third run is made similar to the second, but with the noise amplified by a factor of 5. The relative error between the first and second run, and the first and third run are shown in Fig. 5.

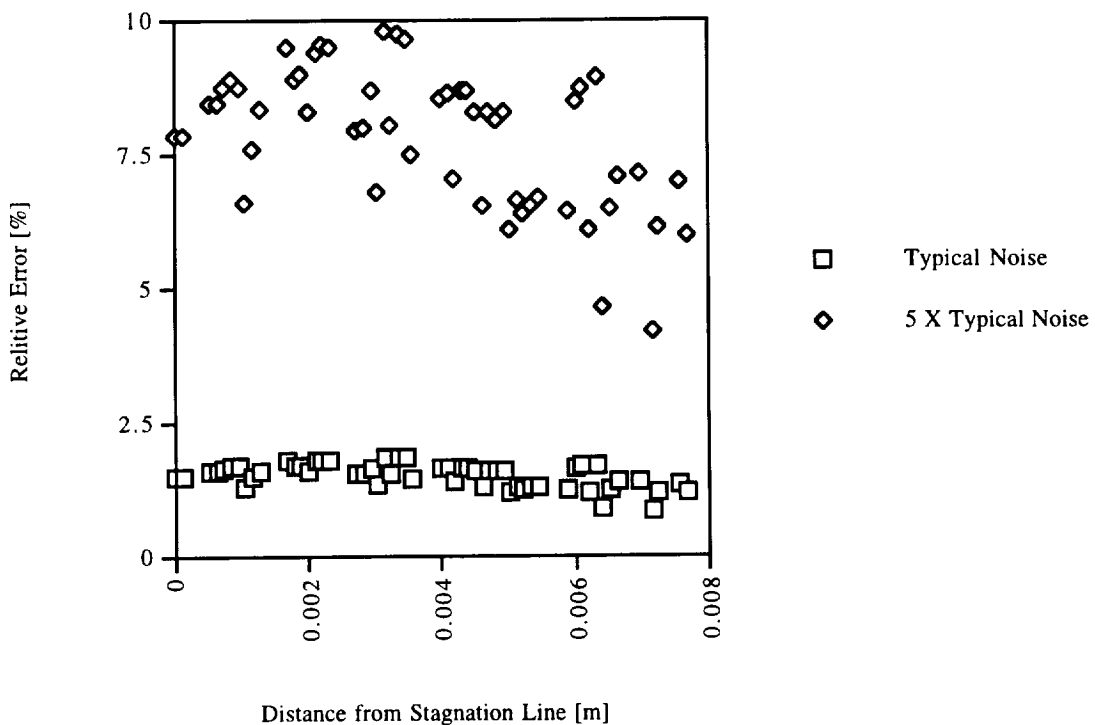


Figure 5 Error due to the presence of noise in the inlet air temperature measurement

Figure 5 shows that the typical noise from Fig. 4 causes an error of 1-2%, and the error from the 5X amplified noise is less than 10%. This result illustrates that the random element of the temperature measurement error does not cause excessive error in the final result. Figure 5 also shows that the data reduction method is stable in the sense that errors in the temperature data are not excessively amplified by the numerical data reduction. It is interesting to note that the introduction of the random noise from Fig. 4 causes the bias error shown in Fig. 5. About 10%-20% of the bias error is caused by the average value of the function in Fig. 4 being slightly less than zero. The rest of the bias error is caused by the use of the Savitzky-Golay smoothing filter on the inlet

air temperature data. The Savitzky-Golay filter assumes that relatively distant data points have some significant redundancy that can be used to reduce the level of noise. At the start and end of a data series only data from later or earlier respectively can be used to determine the filtered value of the data. In the middle of the data series data from both earlier and later can be used to derive the filtered value, and this produces a better approximation. Since the derivative of the inlet air temperature is used in later calculations, the error caused by the lower order approximation used at the beginning of the data series is amplified into a significant bias error.

3.3 Error Assessment Due to Each Numerical Method Considered Separately

3.3.1 *Smoothing and derivatives*

Figure 5 shows how all of the numerical methods in the data reduction program respond together to the inlet air temperature data and the transition time data. The numerical data reduction can be better understood if each of the several numerical methods are tested individually. Since the smoothing is done so that a better first derivative of the inlet air temperature is available for use in Eq. (15), the numerical smoothing and derivative are tested together. The effect of the smoothing can be shown by determining heat transfer coefficients from actual data with and without the filter. The error involved in the numerical derivative is also investigated by comparing results of a first order approximation of the derivative to the results of a second order approximation of the derivative. Figure 6 shows that there is a difference of between

1% and 3% in the heat transfer coefficient when the filter is not used. When the filter is used together with a first order approximation for the derivative, a difference in the heat transfer coefficient of about 0.3% exists. When smoothing is not in use and the first order derivative is used, the error is actually less than in the case of no smoothing with a second order derivative because the sign of the error is different.

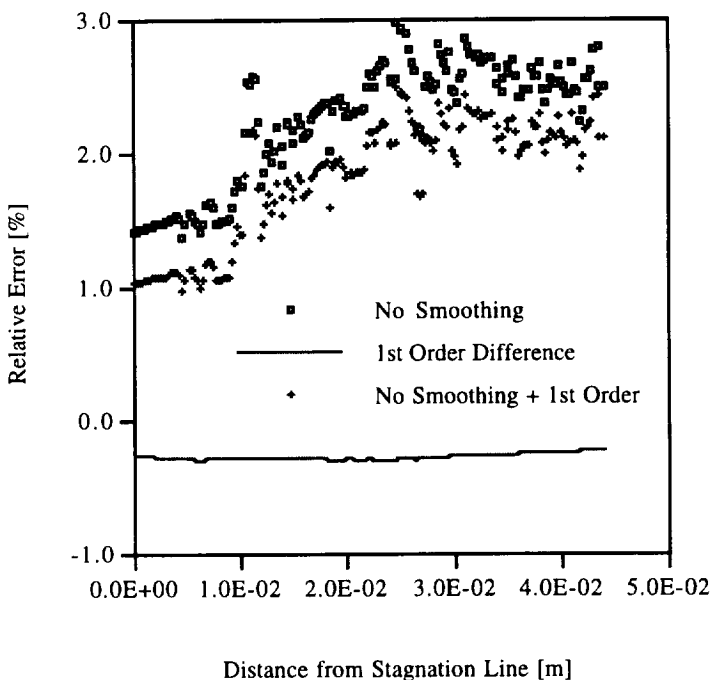


Figure 6 Relative errors in heat transfer coefficients caused by omitting numerical smoothing, and by using a first order derivative approximation.

3.3.2 Integrations

When determining the heat transfer coefficient at a point on the surface it is necessary to numerically evaluate the integral of Eq. (15). The integration is done with Simpson's rule using a minimum subinterval length of 0.01 second. Figure 7 shows the

effect of using subinterval lengths of 0.04 seconds and 0.02 seconds. A relative error of less than 0.2% for twice the minimum subinterval indicates that the integration of Eq. (15) contributes very little error to the data reduction.

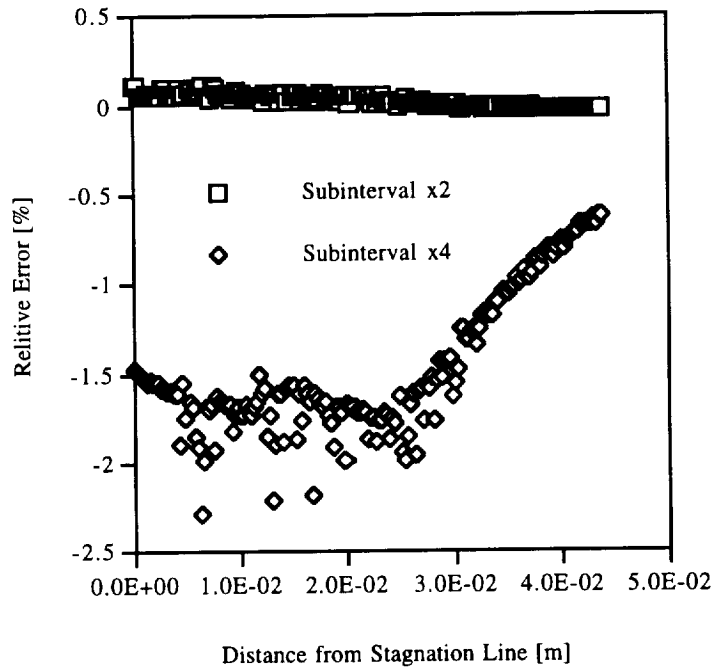


Figure 7 Relative error in the heat transfer coefficient from using subintervals of 2 times and 4 times larger than the nominal subinterval in the heat transfer coefficient iteration.

After the heat transfer coefficient has been determined it is necessary to find the wall temperature as a function of time and again this is done by numerically evaluating the integral in Eq. (15). Figure 8 shows the downstream effect of using a subinterval of twice the minimum. The relative error of less than 0.1% indicates that the integration to determine the wall temperature as a function of time again contributes very little error to the data reduction.

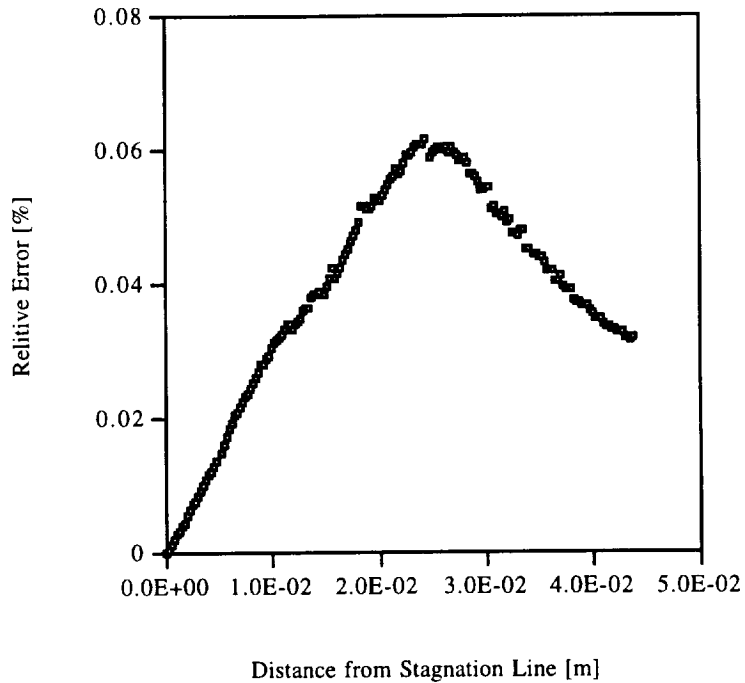


Figure 8 Relative error in the heat transfer coefficient from using subintervals of two times larger than the nominal subinterval for the wall temperature evaluation.

3.3.3 Step Size

After the heat transfer coefficient has been determined at the stagnation line the air temperature is evaluated for the next downstream location using Eq. (17). To evaluate the error due to different step sizes in marching down-stream, heat transfer coefficients are generated using the minimum step size and twice the minimum step size. The minimum step size is imposed by the maximum speed of the frame grabber computer card. The two results are compared in Fig. 9. The relative error of less than 0.1% shown in Fig. 9 indicates that the use of the minimum step size is sufficiently accurate.

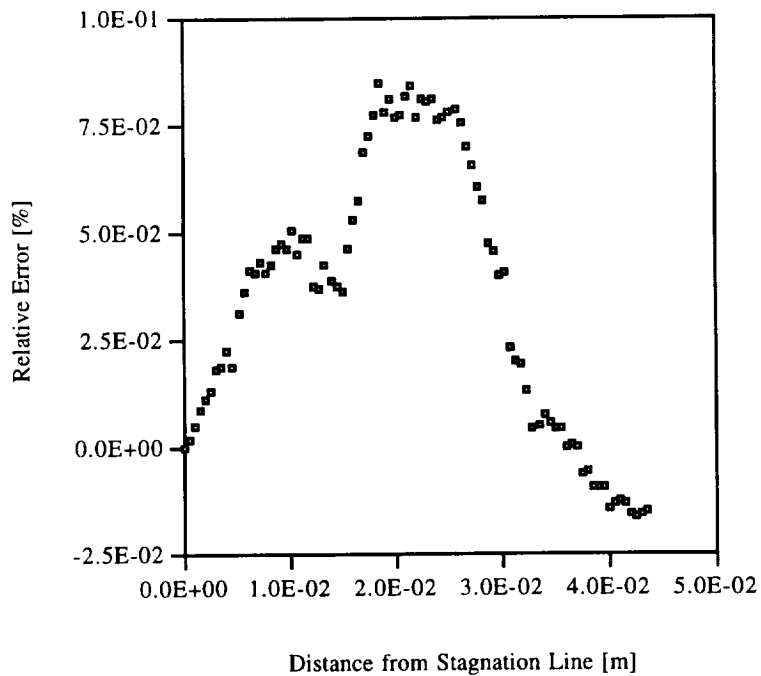


Figure 9 Relative error in the heat transfer coefficient due to doubling the downstream step size .

3.4 Systematic Errors

3.4.1 Transient Temperature Measurement Lag

A second error in the inlet temperature measurement is also expected, namely the temperature lag encountered when doing a transient temperature measurement with a thermocouple. Fortunately a correction can be made for this. An energy balance on the thermocouple bead results in Eq. (24),

$$q_{\text{convection}} - q_{\text{conduction}} - q_{\text{radiation}} = M c_p \frac{dT}{dt} \quad (24)$$

Assuming that the heat conducted up the leads of the thermocouple is negligible,

$$hA(T_{\text{air}} - T) - \sigma\epsilon A(T^4 - T_{\infty}^4) = Mc_p \frac{dT}{dt} \quad (25)$$

Solving for the air temperature gives

$$T_{\text{air}}(t) = \frac{\rho R c_p}{3h} \frac{dT}{dt} + \frac{\sigma\epsilon}{h} (T^4 - T_{\infty}^4) + T \quad (26)$$

Since $h \propto R^{1/2}$, Eq. (26) shows that the lag can be reduced by decreasing the size of the thermocouple, and thus 40 gage thermocouples are used in this experiment. When numbers typical of this experiment are substituted into Eq. (26) one finds that the temperature correction is at most 0.8°C , and that the contribution of radiation is at most 1/10 that of convection. Equation (26) together with the relationship for the heat transfer coefficient for forced convection on a sphere are used with the data reduction program to reduce the error caused by the temperature lag.

3.4.2 Crystal Transition Temperature

The accuracy and repeatability of the crystal transition temperature is critical to an accurate determination of the heat transfer coefficient. The supplier of the TLCs, Hallcrest, reports that calibration of each lot of crystals meets or exceeds the requirements of ASTM E 1061 - 85 (standard specification for direct-reading liquid crystal forehead thermometers). The calibration procedure is to place a sample of the crystal lot in a constant temperature water bath with a thermocouple traceable to NBS

reference standards and accurate to $\pm 0.1^\circ\text{C}$. The temperature is read when the crystals first become visible, at red start, at green start, and at blue start. Hallcrest reports that the overall accuracy of the crystals at transition is $\pm 0.2^\circ\text{C}$. In order to verify the Hallcrest results a similar test was performed. A sample of the crystal paint was sprayed onto a 3 x 2 x 0.16 cm copper plate. The plate was placed in a thin clear plastic bag with a 36 gage thermocouple and immersed in a water-bath that was allowed to cool from 37° C at a rate of 0.2°C per minute. The thermocouple is read with the Strawberry Tree data acquisition system when the crystals transition from one color to the next. The same experiment was then performed with the water bath heating at a rate of 0.2° C per minute in order to determine the range of temperatures for which the crystals remain at each reported color. The results of the calibration are shown in table 3.

Table 3 Calibration data for TLC paint, product BM/R35C1W/C17-10, batch 40909-1

	Hallcrest heating	Verification heating	Verification cooling
Visible Start	34.9°C	Not recorded	34.9
Red Start	35.2°C	35.1	35.3
Green Start	35.5°C	35.4	35.7
Blue Start	36.1°C	35.9	Not recorded

Two important observations can be made from the data in Table 3. First, Hallcrest's calibration data is verified to within the accuracy of the current experiment.

Second, the temperature width of the red and green color can be determined by subtracting the temperature values from the heating and cooling verification experiment. The green and red temperature widths are 0.3°C and 0.2°C respectively.

Figure 10 shows the effect of transition temperature uncertainty on the heat transfer coefficient. It can be seen that a 0.5°C uncertainty causes a 10% error in the heat transfer coefficient that is not amplified away from the stagnation line. From the calibration results in table 3 it is reasonable to assume that error due to transition temperature uncertainty is less than 5% as shown in Fig. 10.

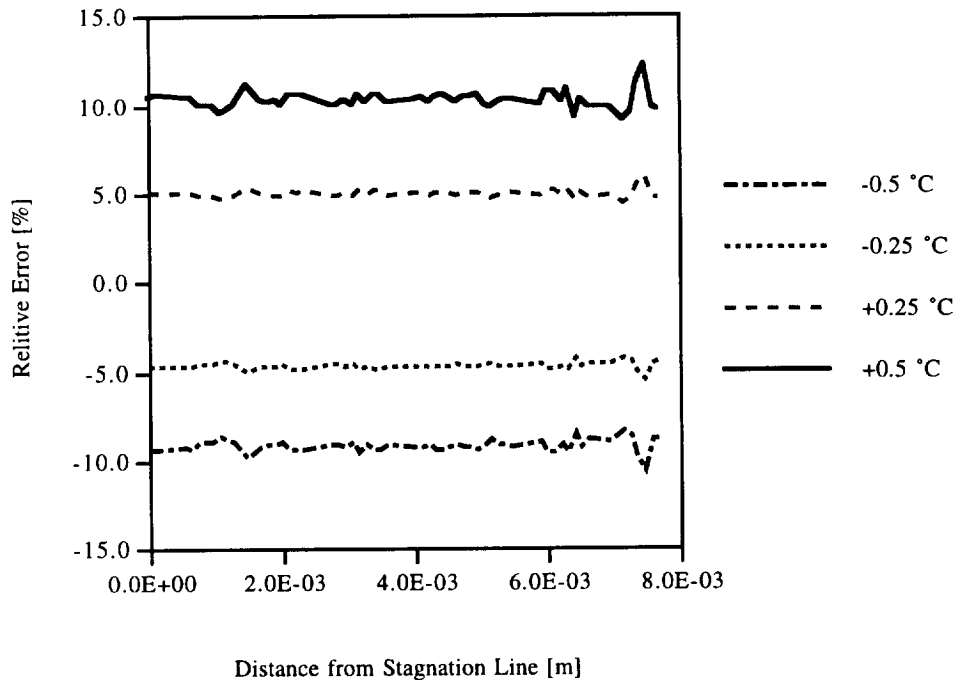


Figure 10 Error due to crystal transition temperature uncertainty.

3.4.3 Backing Paint Thickness

Another error related to transition temperature uncertainty is the effect of the black backing paint thickness. A microscopic evaluation of the painted surface reveals an uneven surface with peak to valley thickness of up to 50 μm . Given a typical heating rate at the stagnation line and assuming a uniform paint thickness of 50 μm a transition temperature error of about 0.6 $^{\circ}\text{C}$ can be expected. Referring again to Fig. 10 this translates into approximately 11% bias error in the heat transfer coefficient. Since the microscopic evaluation revealed an uneven surface, the uniform layer of paint is a poor model. It is more likely that the paint causes the data scatter characteristic of these experiments, as illustrated by Fig. 11. If the painting technique is improved such that a uniform layer of black paint can be provided a correction for the bias error can be made using a one dimensional conduction analysis. If a smooth surface cannot be provided, the problem of noisy data can be handled by curve fitting the data also shown in Fig. 11.

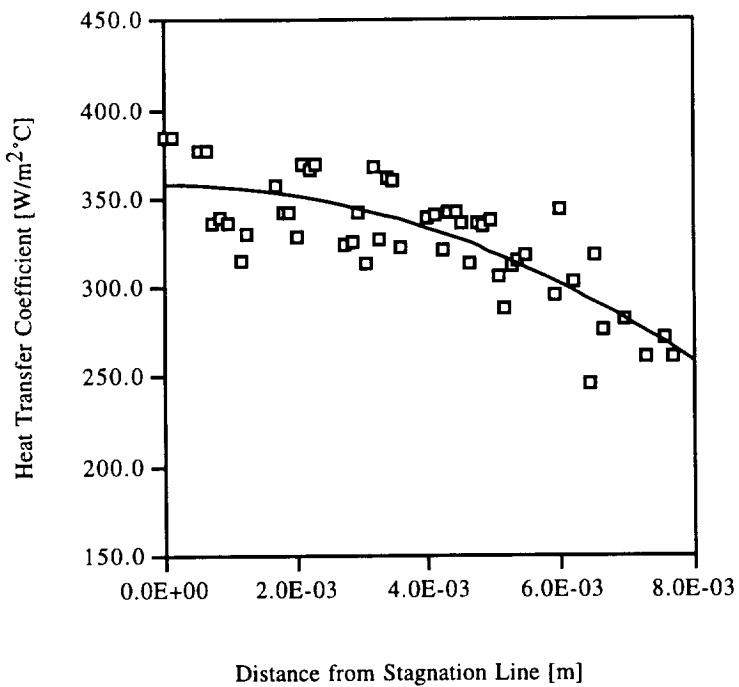


Figure 11 Typical heat transfer coefficient data very near the stagnation point.

3.4.4 One-dimensional Assumption

One important assumption in the development of this experiment is the one dimensional nature of the conduction in the plexiglas. This assumption has been discussed at length by other researchers. Baughn [60] used a transient method with TLCs to evaluate the heat transfer in a duct with transverse ribs. The one dimensional conduction model was used to determine local Nusselt numbers. To evaluate the validity of this assumption a series of 2-dimensional transient numerical conduction calculations were done. It was found that the 2-dimensional effects were negligible except very near the corners of the ribs.

Tan [84] conducted a jet impingement heat transfer study using a transient TLC method. In the error analysis it was shown that the radial conduction in the plexiglas was at most 2% of the conduction into the plexiglas. Likewise it is shown that radiative heat flux from the surface of the plexiglas was negligible because it was less than 3% of the local heat flux due to convection. The radiation heat flux was calculated by assuming a uniform surroundings temperature of 22°C. For the current work the radial conduction is expected to be similarly insignificant because the heat transfer coefficient profile is similar. The radiation correction for the current research would be even less since the surroundings are the interior of a heated duct rather than a large room as in [84]. Other instruments used in the experiment include a turbine flow meter, a pressure transducer and the internal timing circuit of the computer. The uncertainty in each of these instruments has been discussed by Tan [84] and shown to cause negligible error in the final result.

3.5 Temperature Changes in the Air

Finally, it is useful to show the effect of allowing for the air temperature change along the channel when determining the heat transfer coefficients. Data from the experiment was reduced in two ways; 1, the inlet air temperature can be used at all points along the channel to evaluate the heat transfer coefficients, or 2, the temperature of the air was adjusted for energy loss as it flows along the channel. Use of a 1.0 mm wide slot with a relatively small mass flow rate produces high heat transfer coefficients

at the stagnation line because of the high velocity. The small mass flow rate means that the air temperature change is relatively large, thus representing a worst case. Figure 12 shows the effect of reducing the data using the inlet temperature at each point along the channel, and using the actual air temperature at each point along the channel. The relative error between the two results is shown in Fig. 13. The maximum error of 35% indicates the importance of including the air temperature change in this analysis.

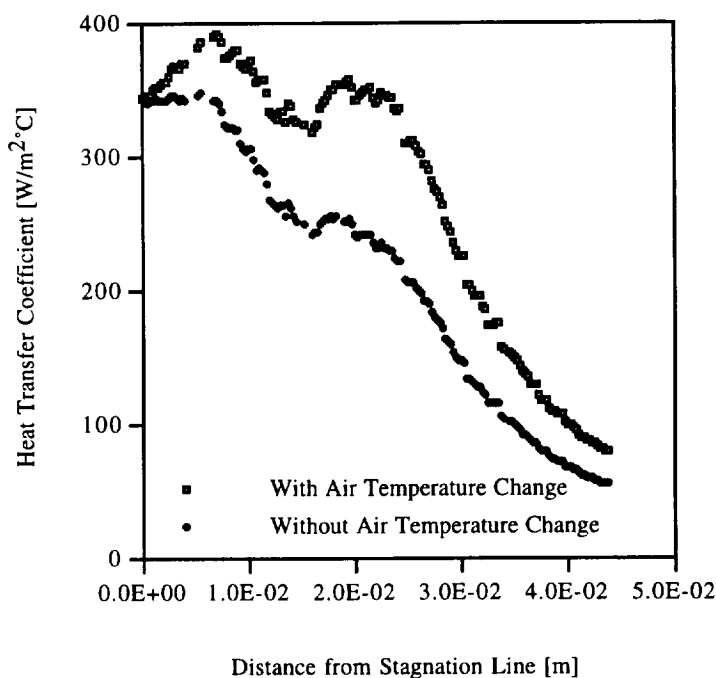


Figure 12 Test case to determine the maximum expected error.

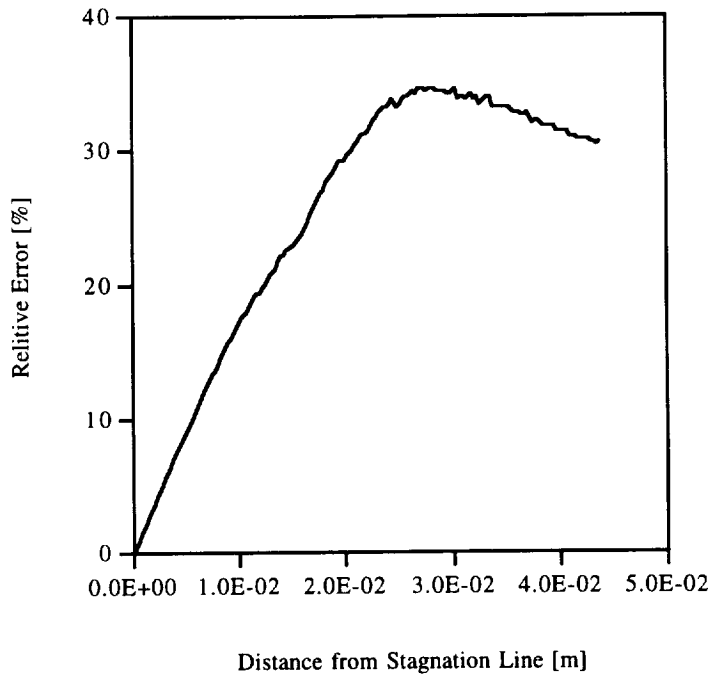


Figure 13 Relative error caused by ignoring the effect of energy loss in the air.

3.6 Error Due to the Simultaneous Solution for the Heat Transfer Coefficient and the Recovery Temperature

The experiment to determine the heat transfer coefficient is started with air at room temperature (22°C) that is then heated to above the transition temperature of the crystals (35°C). Even a moderate nozzle exit velocity of 45m/s causes a recovery temperature of 1°C , which is significant when dealing with a 13°C temperature difference. The method developed in the theory section represented by Eq. (19) is used to correct for this error. The error is only noticeable near the stagnation line since the flow immediately splits and enters a larger duct thus the velocity drops rapidly and the recovery temperature drops as the square of the velocity. Equation (19) requires data

from two experiments to be iterated on in order to determine the heat transfer coefficient. When reducing data in this manner data scatter can become a problem. In order to determine the magnitude of the problem a transition time error is added to representative experimental data. A transition time error representative of the actual computer clock error of $\pm 0.0275\text{s}$ is added to the transition time data. Figures 14 and 15 show the absolute error in the heat transfer coefficient and the recovery temperature as a function of distance from the stagnation line. An error in the transition time causes substantial error at the stagnation line that diminishes down-stream as the recovery temperature drops.

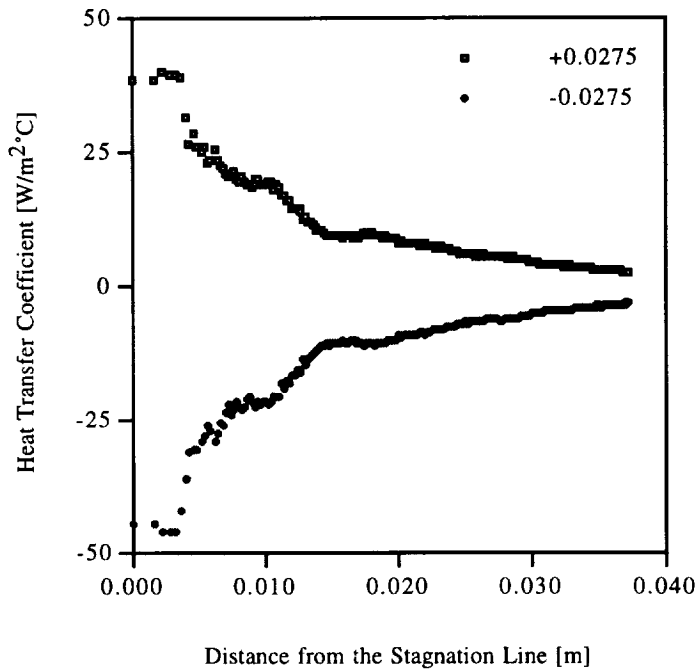


Figure 14 Absolute error in the heat transfer coefficient due to $\pm 0.0275\text{s}$ transition time deviation

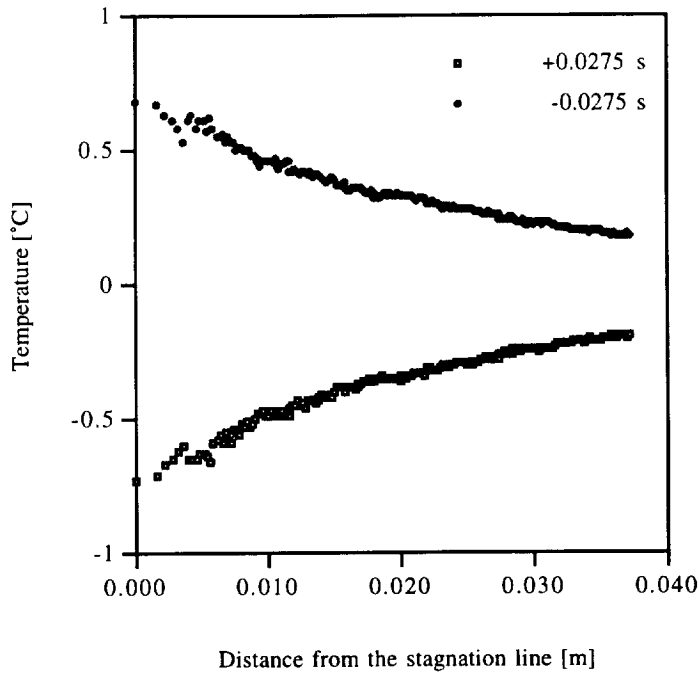


Figure 15 Absolute error in the recovery temperature due to $\pm 0.0275\text{s}$ transition time deviation

Figures 16 and 17 show the relative error in the heat transfer coefficient and the recovery temperature difference respectively. The important difference between Figs. 16 and 17 is that relative error in the heat transfer starts at about 10% and approaches 0% whereas the relative error in the recovery temperature remains at about 30% up to 2.5 cm from the stagnation line. Since the recovery temperature approaches zero away from the stagnation line the relative error becomes very large at distances greater than 2.5 cm from the stagnation line. Figures 16-17 show why the recovery temperature data can only be used to infer qualitative results while the heat transfer coefficient data is still useful in a quantitative sense.

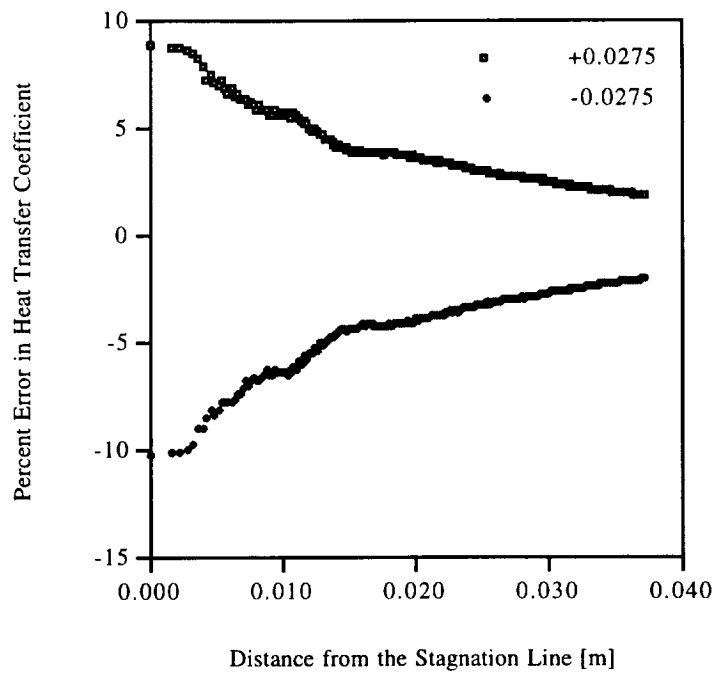


Figure 16 Relative error in the heat transfer coefficient due to $\pm 0.0275\text{s}$ transition time error

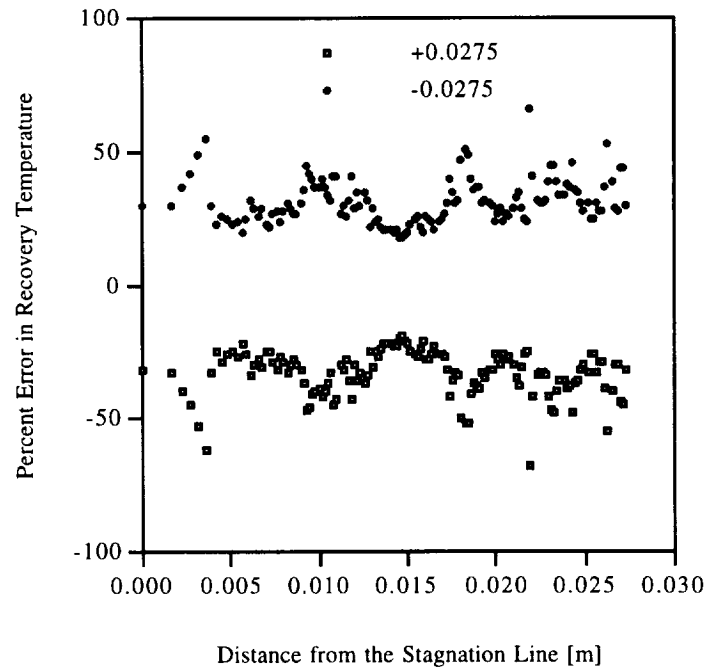


Figure 17 Relative error in recovery temperature due to $\pm 0.0275\text{s}$ transition time error

3.7 Summary

The error analysis has shown that, based on Figs. 3-5, the numerical data reduction can be expected to contribute 1-2% to the overall error in the heat transfer coefficients. When considering each of the numerical methods separately one finds that the nature of the noise in the air temperature signal and the smoothing technique are the main sources of the numerical error. All other numerical errors contribute less than 0.2% to the overall error. The errors in each instrument have been studied, and it was found that the crystal transition temperature causes the only significant error, less than 5% in the heat transfer coefficients. Two areas of concern in systematic error are the thickness of the black backing paint, and the temperature lag in the air temperature measurement. Analysis is given that explains how to reduce these errors. The analysis also shows that in some cases errors of up to 35% would be expected without a correction for the change in the air temperature along the channel. Finally analysis shows that the single largest source of error is due to the simultaneous solution for the heat transfer coefficient and the recovery temperature. When the jet velocity is greater than 50m/s, error in the heat transfer coefficient may approach 10% at the stagnation line.

Chapter 4

EXPERIMENTAL DETAILS

4.1 Air Delivery System

The goal in the design of the jet impingement heat transfer experiment is to provide an experimental rig that allows the investigation of the important parameters involved in the design of the airfoil leading edge cooling system. Since a simple and flexible design implies an indirect method of data reduction, careful attention is paid to minimizing experimental error. It is recognized that the actual cooling fluid for a hypersonic vehicle is likely to be hydrogen, however, given the difficulty in working with this fluid, air is chosen as the test fluid. Fortunately, it is possible to match the important dimensionless parameters that govern this problem with air. The air for the experiment comes from the building compressed air supply. The compressed air supply is connected to the test nozzle by 1 inch schedule 40 PVC piping. On the way to the nozzle the air passes through a pair of centrifugal separators to remove water, and a pressure regulator is used to decrease the pressure of the building air from 100 psig to 25 psig. The flow rate of the air is controlled by a precision adjustment valve. The air is heated by a computer controlled 1600 W electrical resistance heater that is located just upstream of the nozzle. A schematic drawing of the air delivery system is shown in appendix B, Fig. B1.

4.2 Instrumentation

The jet impingement experiment requires various computer controlled data acquisition equipment and instruments. The central part of the system is a 80486-33 MHz PC with a Data Translations DT-3851 frame grabber card and a 16 bit data acquisition card manufactured by StrawberryTree. Flow rate instrumentation consists of a turbine flow meter, pressure transducer, and a 40 gage copper-constantan (type T) thermocouple, all read by the computer data acquisition system. The temperature of the air at the exit of the nozzle is measured by a 40 gage type T thermocouple. The correction factor for the transient temperature lag in the thermocouple is added during the reading process. The transition of the TLCs is digitally recorded by the computer frame grabbing card using a CCD camera with a 35 - 135 mm macro lens. A schematic representation of the instrumentation is shown in Fig. B1.

Since it only takes a few seconds for the crystals to reach the transition temperature once the air heater is turned on, it is necessary to write software to automate the experiment. When the command is given, the software turns on the heater and begins timing the experiment. All of the instruments are read and the image of the crystals is digitally recorded. This cycle is repeated every 20 ms until all the crystals have reached the transition temperature (about 15 s). After the data has been recorded, image analyzing software examines the images of the crystals and outputs the time and location of the transition. The data reduction software uses the time vs. location data, along with the air temperature and flow rate data, to determine heat transfer

coefficients over the entire imaged surface. The format of the heat transfer coefficient data allows it to be quickly displayed using a standard graphing package. After observing the data, adjustments to the system can be made so as to optimize the cooling. The parameters that can be varied to optimize cooling are: slot width, nozzle to surface spacing, jet velocity, and the shape of the nozzle exit.

4.3 Leading Edge Model

Using the design information contained in reference [81] along with the analysis from Section 2.1, a model of the leading edge and the leading edge cooling system has been built. These two sources were used to estimate minimum and maximum jet Reynolds numbers, slot width, and nozzle to surface distance needed to accomplish the required leading edge cooling. The latest NASP leading edge design calls for a 7.62 mm nose radius and a 7.5° wedge angle. The aerodynamic heat flux peaks at the stagnation point and decreases to 10% of that value within 8 cm of the nose. It is therefore possible to use a full scale model of the leading edge in this experiment. The leading edge is machined out of plexiglas so that the TLCs are visible from the outside. It was also decided to machine the jet nozzle out of plexiglas because plexiglas has relatively low thermal conductivity, and thus the jet temperature responds more rapidly to the heater. A diagram of the leading edge is shown in Appendix B Fig. B2. Figure B3 shows the design of the nozzle for the cooling jet. The slot nozzle is 17.8 cm long and the width can be varied from 1.5 mm to 6.5 mm. The air is delivered to the

nozzle by a 2.54 cm pipe, therefore a method of providing an even flow to the nozzle is needed. Figures B4a-c show a high pressure drop manifold, which provides an even velocity distribution to the nozzle. The flow from the pipe enters the manifold through a 2.54 cm by 0.635 cm slot. The flow then enters the center section, which is a rectangular duct 17.8 cm by 0.635 cm, and 5.1 cm long. The center section is packed with air filter foam to provide a pressure drop sufficient to cause an even velocity distribution at the exit to the manifold. The exit of the manifold is a slot 17.8 cm by 0.318 cm in the exit plate. The flow becomes fully developed after it exits from the manifold and passes through the 10.2 cm long jet nozzle.

4.4 Liquid Crystals

After a leading edge model has been completed, the liquid crystals are applied to the surface. The liquid crystal paint is applied as evenly and thinly as possible on to the plexiglas using a standard artists air brush. A thick or uneven application will result in sporadic or blurred transition points. After the temperature sensitive crystals have been applied, they are then covered with a thin layer of black paint that provides the necessary backing to maximize the contrast of the transition.

The CCD camera and digitizing card converts the color image into 256 intensities, or gray levels. When a color image is transferred to a gray scale, two different colors can be perceived as the same intensity. This effect is minimized by using an optical filter that eliminates all colors except the one of interest. The

manufacturer of the crystals provides a calibration point at red; therefore a red filter is used to isolate the corresponding temperature.

In addition to optical filters, the method of illumination is an important factor in determining the transition location. The wavelength of the scattered light depends on the type of light source, the angle of incidence of the source, and the angle of the observation. The camera and light source are aligned coaxially to eliminate the effect of angle. The light source used to illuminate the crystals should be broad band and intense. In addition to the problem of how the crystals scatter light, the heat generated by intense incandescent light source may cause the liquid crystals to transition prematurely; therefore, a cooler halogen tungsten lamp is used to illuminate the crystals.

Chapter 5

RESULTS

5.1 Introduction

Data has been gathered in this experiment with two goals in mind. One goal is to demonstrate the speed and flexibility of the experimental method for finding heat transfer coefficients. The other goal is to use the experimental rig to show that heat transfer coefficients for impinging jets are high enough for use in cooling the leading edge of a hypersonic airfoil. To satisfy these goals, 3 sets of experiments have been run; a low mass flow rate case with a narrow nozzle, a high mass flow rate case with a narrow nozzle, and a high mass flow rate case with a wide nozzle. For each of these configurations the nozzle to surface spacing was varied. A final test was run with the wide nozzle at the maximum air flow rate available to the experimental rig. The data from that test is used to calculate the leading edge temperatures shown in appendix C. Table 4 gives a summary of each test condition. The resulting heat transfer coefficients and recovery temperature data are given in appendix D.

Table 4. Jet impingement heat transfer test matrix

#	Mass flow rate [kg/s]	Nozzle exit velocity [m/s]	Re_0	Nozzle width [cm]	Surface to nozzle spacing [Z/W]
1	.03142	117.9	8,319	0.127	4
2	.03098	116.3	8,206	0.127	6
3	.03142	117.9	8,319	0.127	8
4	.03114	116.9	8,248	0.127	9
5	.03095	116.1	8,192	0.127	10
6	.03092	116.1	8,192	0.127	14
7	.03088	115.9	8,177	0.127	18
8	.01577	59.19	4,176	0.127	4
9	.01575	59.13	4,172	0.127	6
10	.01570	58.94	4,159	0.127	8
11	.01575	59.12	4,171	0.127	10
12	.01570	58.93	4,158	0.127	14
13	.01574	59.07	4,168	0.127	18
14	.03145	52.22	8,326	0.287	2.655
15	.03108	51.62	8,231	0.287	4
16	.03147	52.27	8,334	0.287	6
17	.03146	52.25	8,331	0.287	8
18	.03147	52.26	8,333	0.287	10
19	.03647	60.57	9,658	0.287	2.655

5.2 Validation of the Results

In order to validate the results, some of the data can be compared to similar experimental data in the literature. It has already been pointed out that data are available

for a slot jet impinging on a flat surface, but very little data are available for a slot jet impinging on a highly curved surface or in a confined space, which is the case here. Nevertheless it seems reasonable to expect that stagnation line data from this experiment will be similar to data from slot jets impinging on a flat surface. Stagnation line Nusselt number data for Reynolds numbers 4,200 and 8,300 from this study, and two other studies are presented in Figs. 18 and 19, respectively. It can be seen in both graphs that magnitude and trends in each of the data are similar. One factor often cited in the literature that substantially affects the stagnation line Nusselt number is the turbulence level of the jet. Turbulence levels measured by Akfirat and Gardon [82] indicate that for Reynolds number of 11,000 the jet turbulence level for their 1.59mm slot is 0.6%, and for their 3.175mm slot is 2.5%. The stagnation point Nusselt number for the low turbulence case is up to 14% less than the Nusselt number corresponding to the high turbulence case. Saad et al. [85] found that for a Reynolds number of 5,400 a 30% decrease in Nusselt number is caused by reducing the turbulence level from 8.313% to 2.06%. A second factor affecting the stagnation line Nusselt number is the geometry of the enclosure that the jet is confined to after exit from the nozzle. Shoukri et al. [86] found that a confined round jet impinging on a flat surface has an average Nusselt number that is 21% less than a similar free jet. In a study of parallel arrays of multiple interacting slot jets Saad et al. [85] found that stagnation line Nusselt numbers decreased as the jet spacing was reduced, the maximum reduction being 27%.

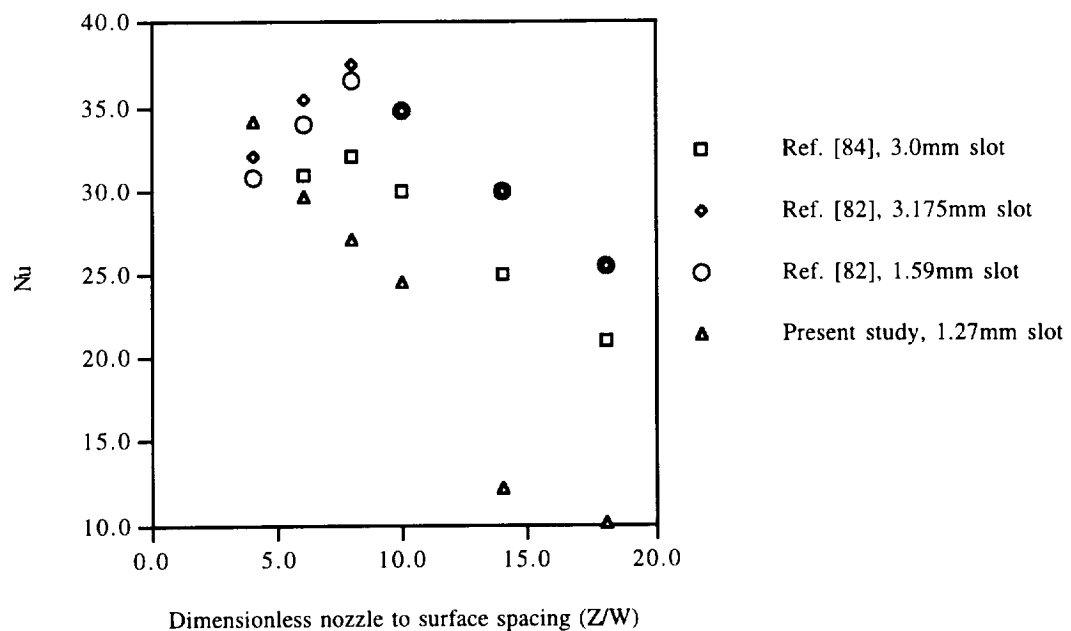


Figure 18. Comparison of the present stagnation line Nusselt numbers to literature results for $Re=4200$.

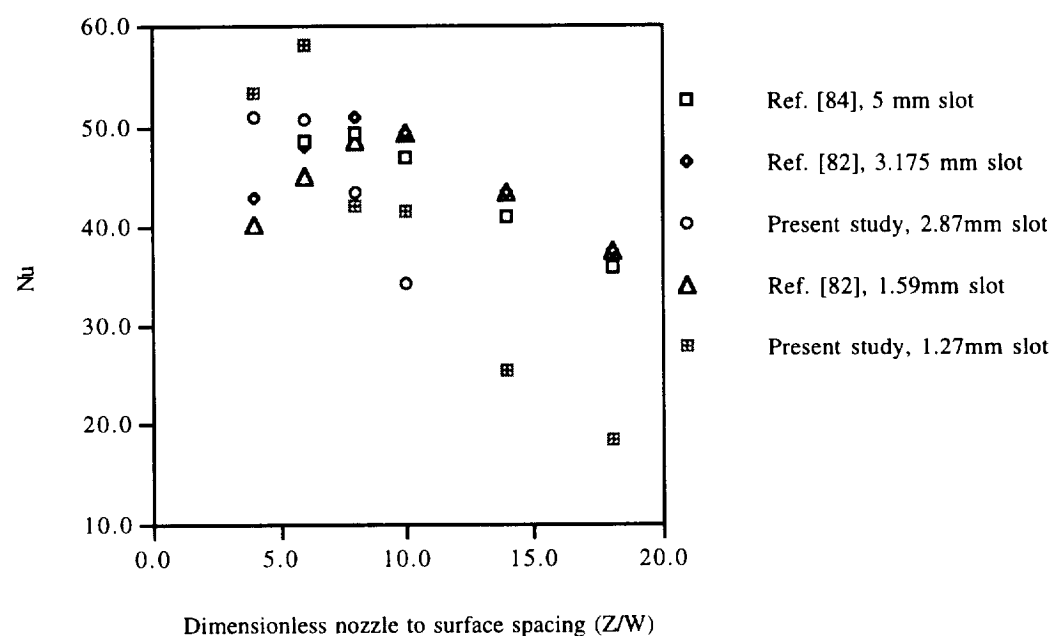


Figure 19. Comparison of the present stagnation line Nusselt numbers to literature results for $Re=8300$.

Given the spread in the experimental data and the sensitivity of jet impingement heat transfer to geometry, the stagnation line data in the present study falls within acceptable limits. It is also interesting to compare the down-stream heat transfer for the present study to results in the literature. Figure 20 compares Nusselt numbers at distances of up to 8 nozzle widths down-stream from the stagnation line for a Reynolds number of 8,300. The difference in stagnation line Nusselt numbers can probably be explained by the relatively high jet turbulence level (6.25%) for the data from Saad et al. [85]. The confinement of the jet in the present study is also a factor in the lower stagnation line Nusselt number. Between 1 and 5 nozzle widths away from the stagnation line the results are very similar.

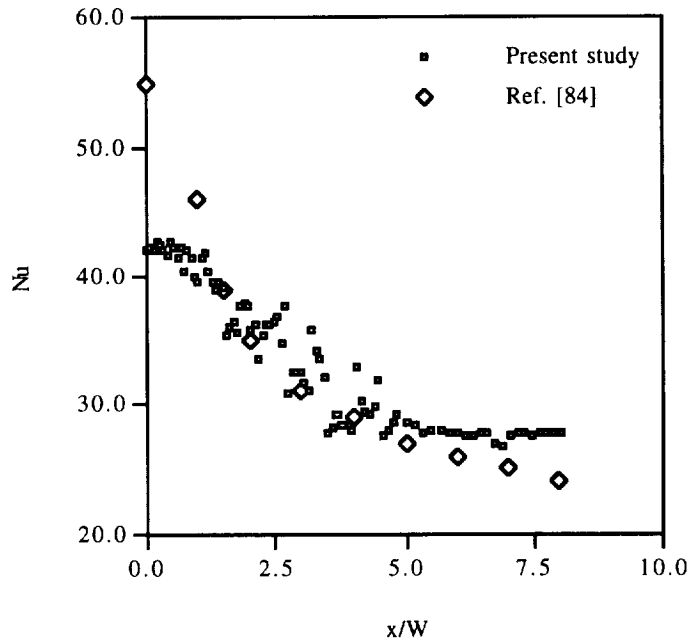


Figure 20. Comparison of the present Nusselt numbers to literature results for $Re=8300$ from the stagnation line to 8 nozzle widths down-stream.

5.3 Data Trends

Having established that the data from the current experiment is reasonably similar to data in the literature, the current data can be examined. The data from 14 of the 19 experiments performed are presented in Figs. 21-23. Some of the data are excluded from these figures because of overlap. Figure 21 shows Nusselt number data from the small slot (0.127cm) with a high flow rate ($v=117\text{m/s}$, $Re=8,300$). The maximum Nusselt number occurs at the stagnation line for a nozzle to surface spacing of 6 slot widths. Other studies have found that the maximum occurs at nozzle to surface spacing of 8 slot widths. It has been pointed out several times in the literature that the maximum usually occurs at $8W$ due to the increase in turbulence in the jet after it leaves the nozzle. The stagnation line Nusselt number begins to drop at larger nozzle to surface spacings because drop in velocity of the free jet outweighs the effect of increased turbulence. The difference in this case is probably due to entrainment of cooler air from the cavity into the jet. It can be seen from Fig. 21 that the maximum Nusselt occurs away from the stagnation line for $z/W=14$ and 18 . This phenomenon has been observed many times in past studies, e.g. [85]; the local maximum occurs where the wall jet transitions from laminar to turbulent. In flat surface and free jet studies, local maxima are observed for nozzle to surface spacings of $z/W \leq 8$, with the local maximum occurring at $4 \leq x/W \leq 10$.

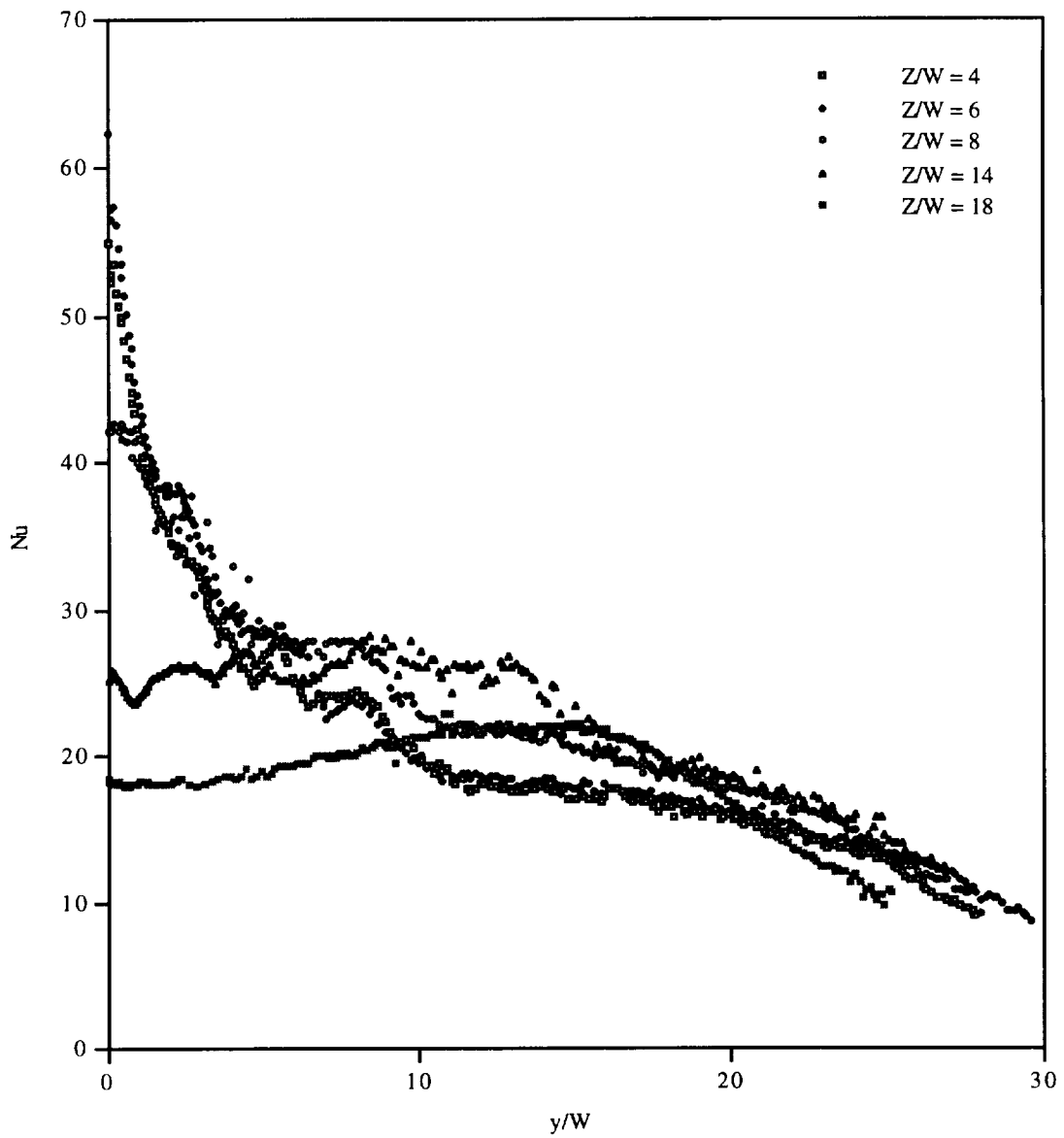


Figure 21. Nusselt number vs. distance from the stagnation line for $\text{Re}=8,300$ and slot width 0.127cm.

Figure 22 shows Nusselt number data from the 0.127cm slot with a low flow rate ($V=59\text{m/s}$, $\text{Re}=4,200$). Nozzle to surface spacings $z/W=6$ and 10 are not shown in Fig. 22 because the data falls essentially on top of $z/W=8$ data, except at the stagnation line where the Nusselt numbers for $z/W=6$ are a little higher ($\text{Nu}=29$) and $z/W=10$ are a little lower ($\text{Nu}=25$). Under these test conditions the maximum stagnation line Nusselt number occurs at $z/W=4$, not 6 as in Fig 21. A possible explanation for the maximum occurring at a smaller nozzle to surface spacing for the $\text{Re}=4,200$ case is that since the jet has less momentum, the increased shear on the jet inside the cavity reduces the centerline velocity over a short distance. For these test conditions the secondary maximum is more pronounced for all nozzle to surface spacings.

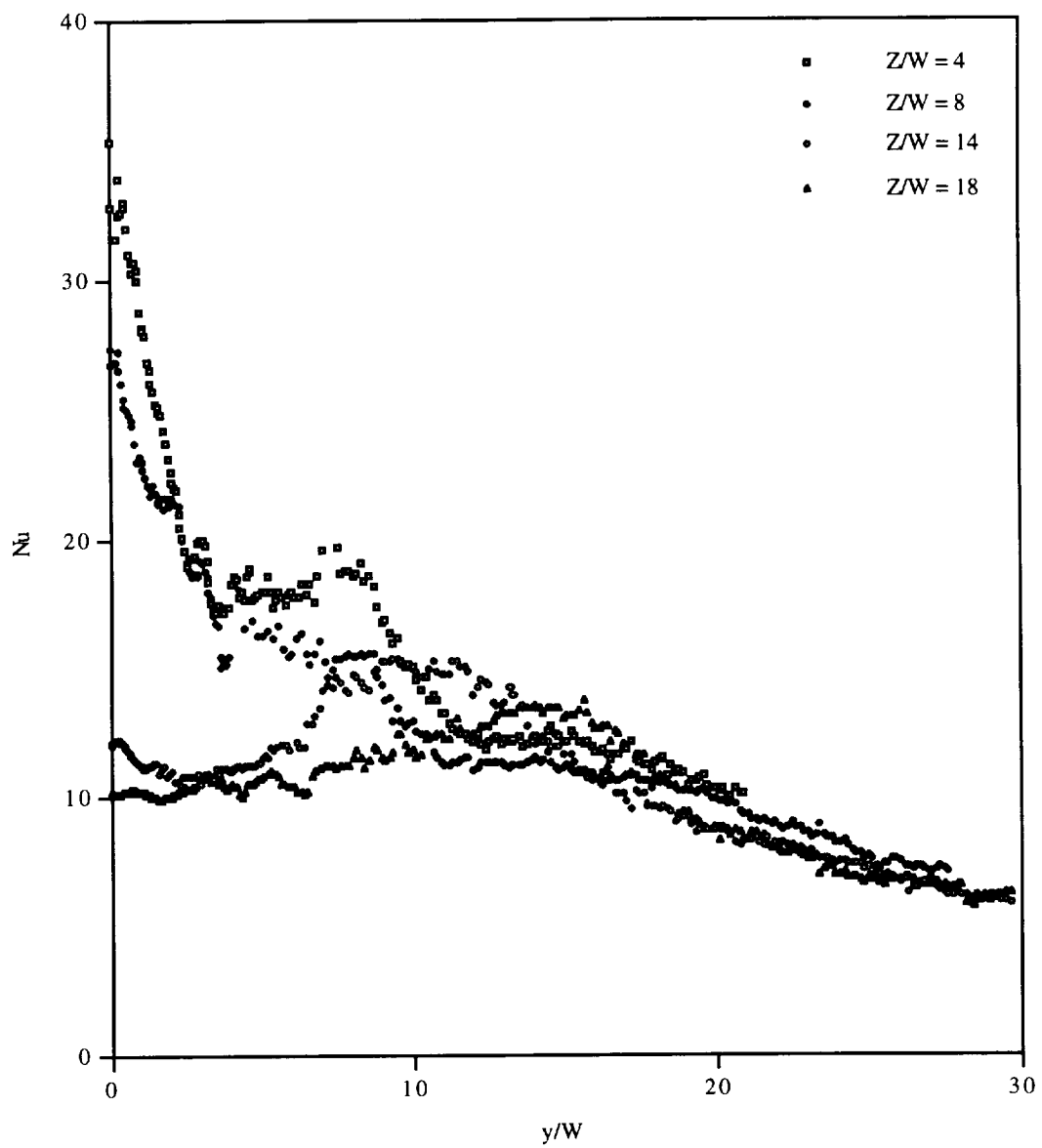


Figure 22. Nusselt number vs. distance from the stagnation line for $Re=4,200$ and slot width 0.127cm .

For the third set of experiments the nozzle was widened to 0.287cm and the velocity chosen such that Reynolds number matches that of the first set of experiments. The highest Nusselt number occurs at a nozzle to surface spacing of $z/W=2.655$, or 0.762cm. Since the wider nozzle covers a larger percentage of the cavity cross-section, the air must exit at a greater velocity thus causing greater shear in the mixing region of the jet. The greater shear causes the jet centerline velocity to drop over a shorter distance thus reducing the heat transfer when the nozzle to surface spacing is large. The nozzle to surface spacing of $z/W=2.655$ was chosen so that results could be compared with the same Reynolds number and the same absolute nozzle to surface spacing. Under these test conditions the local maxima are very pronounced for $z/W \geq 4$. This set of experiments also yielded the highest overall Nusselt numbers.

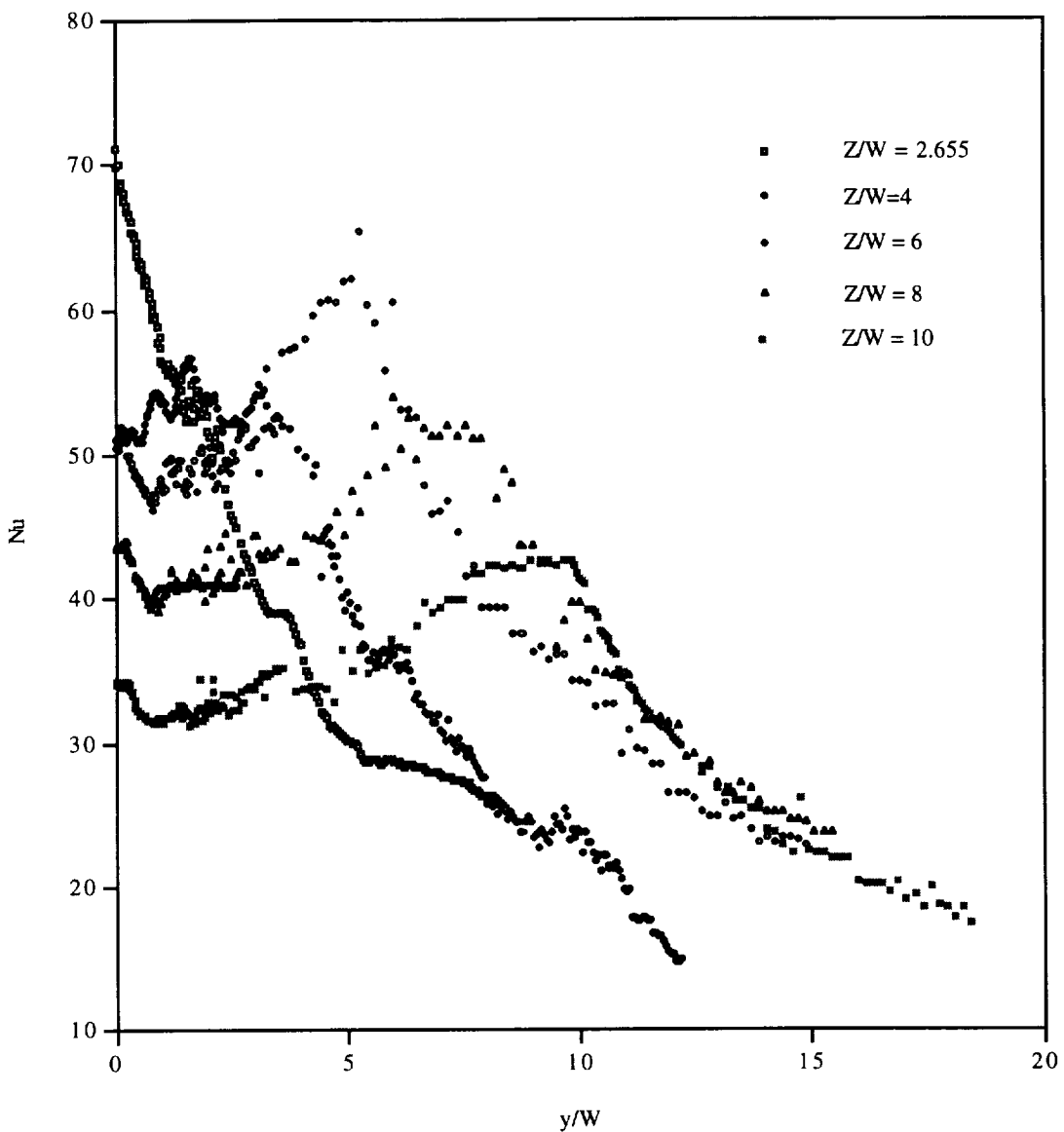


Figure 23. Nusselt number vs. distance from the stagnation line for $Re=8300$ and slot width 0.287cm .

Figures 24-27 illustrate the effect of changing the Reynolds number by varying the velocity for 4 different dimensionless nozzle to plate spacings. Figures 24-26 show that the Nusselt number for $Re=4,200$ is nearly uniformly 65% less than the Nusselt

number for the $Re=8,300$ case. In Fig. 27 it can be seen that one Nusselt number curve is not a scalar multiple of the other. This indicates that, for nozzle to surface spacings of $z/W \geq 14$, an additional geometric parameter is needed to characterize the heat transfer.

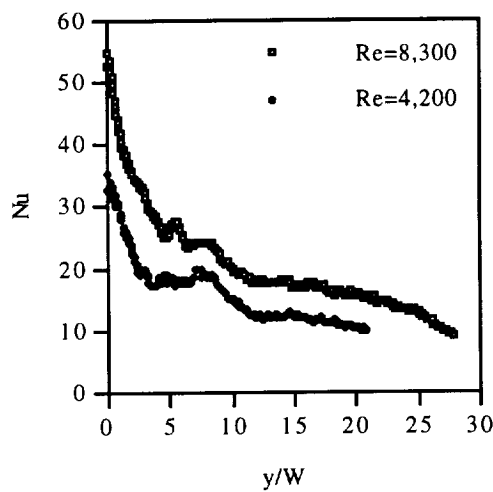


Figure 24. Comparison of Nusselt numbers for $Re=4,200$ and $Re=8,300$ at $z/W = 4$ and $W=0.127\text{cm}$.

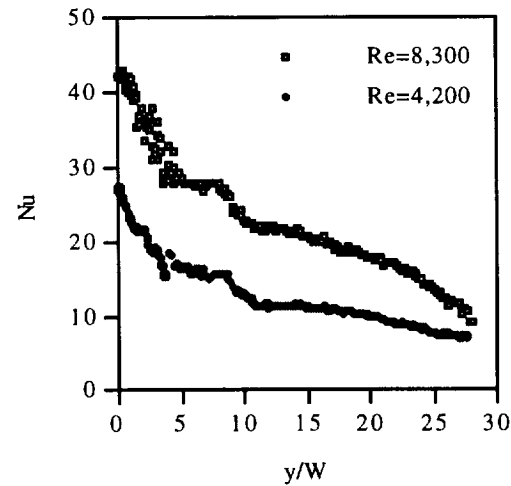


Figure 25. Comparison of Nusselt numbers for $Re=4,200$ and $Re=8,300$ at $z/W = 8$ and $W=0.127\text{cm}$.

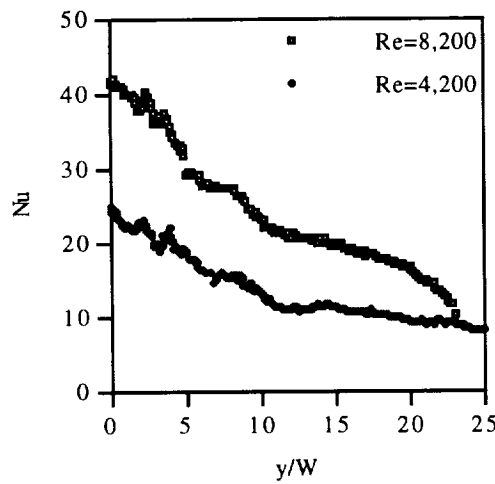


Figure 26. Comparison of Nusselt numbers for $Re=4,200$ and $Re=8,300$ at $z/W = 10$ and $W=0.127\text{cm}$.

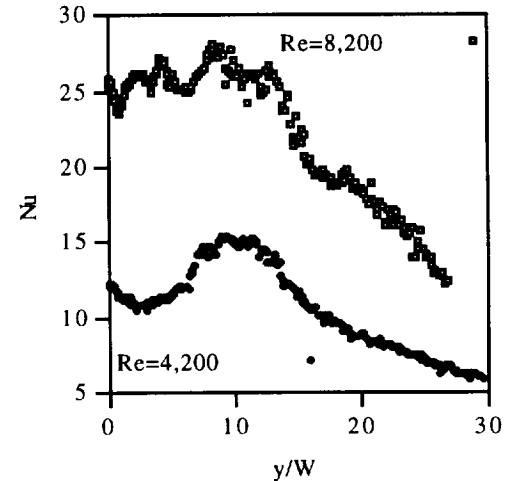


Figure 27. Comparison of Nusselt numbers for $Re=4,200$ and $Re=8,300$ at $z/W = 14$ and $W=0.127\text{cm}$.

Figures 28-31 show the effect of the nozzle width on the Nusselt number. The Reynolds number is held constant by increasing the nozzle width and decreasing the nozzle exit velocity. The dimensionless nozzle to surface spacing is the same for each figure. Figures 28-31 clearly show that the nozzle exit Reynolds number and the dimensionless nozzle to plate spacing are not sufficient to characterize the heat transfer near the stagnation line. Beyond 15 nozzle widths away from the stagnation line the two Nusselt number curves appear to approach one another. Since the mass flow rates are the same for both cases it could be expected that the heat transfer would be the same as the flow went from the impingement region, to the wall jet region, and then to duct flow.

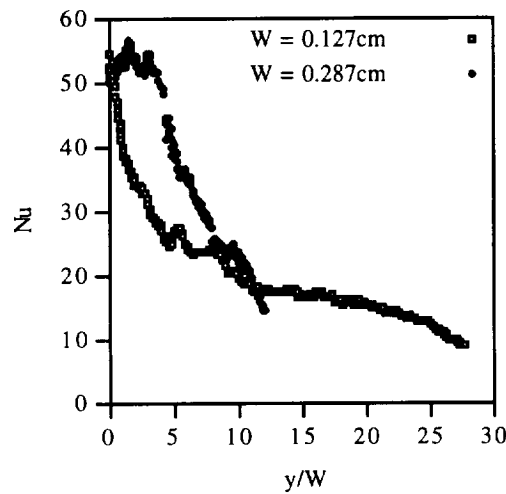


Figure 28. Comparison of Nusselt numbers for $Re=8,300$ at $z/W = 4$ and slot widths 0.127cm and 0.287cm .

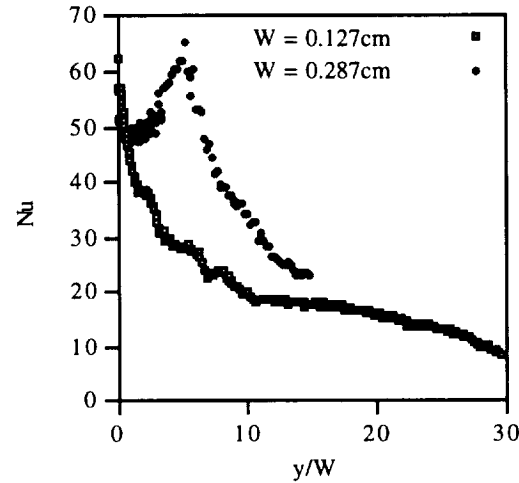


Figure 29. Comparison of Nusselt numbers for $Re=8,300$ at $z/W = 6$ and slot widths 0.127cm and 0.287cm .

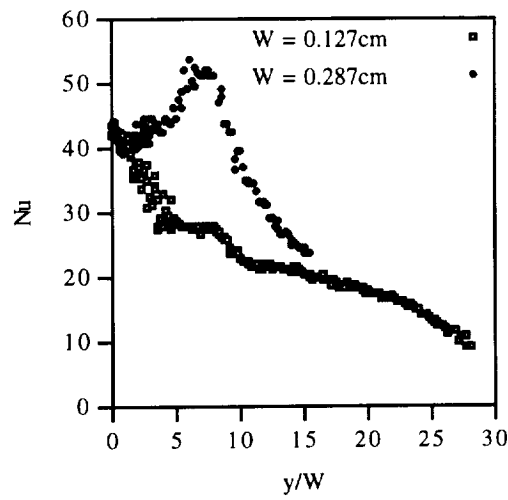


Figure 30. Comparison of Nusselt numbers for $Re=8,300$ at $z/W = 8$ and slot widths 0.127cm and 0.287cm .

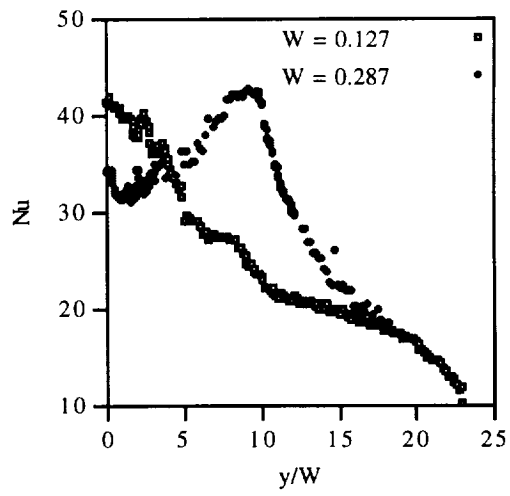


Figure 31. Comparison of Nusselt numbers for $Re=8,300$ at $z/W = 10$ and slot widths 0.127cm and 0.287cm .

Finally Fig. 32 shows Nusselt numbers for the same Reynolds number and different nozzle widths, but the same absolute nozzle to surface spacing (0.762cm). The correlation between these two curves is much stronger than for Figs. 28-31. Figure 32 confirms that the dimensionless parameter z/W is not the only dimensionless geometric parameter of importance for this type of flow.

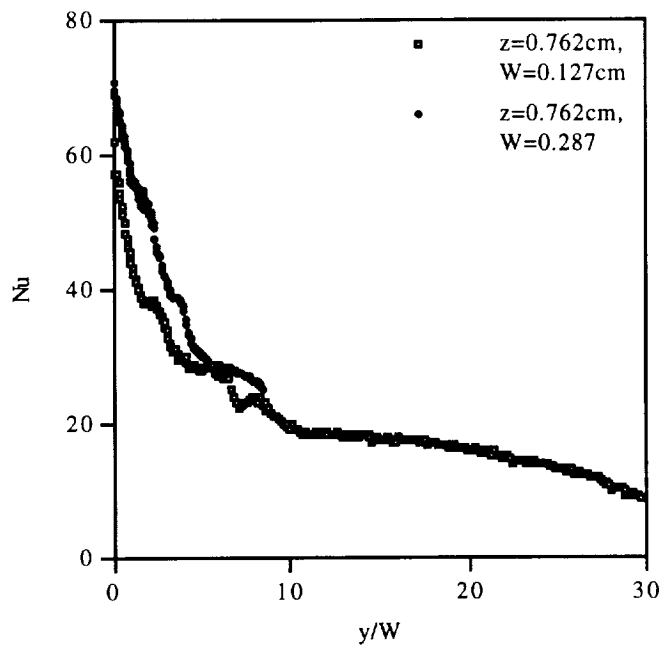


Figure 32. Nusselt number for $Re=8,300$ with $z=0.762\text{cm}$ and $W=0.127\text{cm}$ and 0.287cm .

5.4 Recovery Temperature Data

The goal of the experiment was to generate Nusselt numbers; however, the data reduction process also yields the difference between the local recovery temperature at the surface and recovery temperature for the nozzle exit thermocouple. It was shown in the section 3.6 of the error analysis chapter that significant error in the heat transfer coefficient can be caused by ignoring the recovery temperature. It was also shown in the same section that the data reduction process may yield an error in the recovery temperature difference of 50% or more. The accuracy of the experimentally determined recovery temperature difference can be evaluated by comparing the experimental value

at stagnation line to a predicted value. The recovery temperature difference at the stagnation line can be predicted using Eq. (27).

$$T_{rs} - T_{rc} = (r_s - r_{tc}) \frac{V^2}{2c_p} \quad (27)$$

The values for r_s and r_{tc} have been experimentally determined by other researchers. The value for r_s has been found to be between 1.0 and 1.2 by several researchers e.g. Goldstein et al. [41]. The recovery factor is greater than 1.0 when the jet total temperature is increased by entraining warmer ambient air. For the purposes of evaluating the current data a value of 1.0 is used in Eq. (27). The value for r_{tc} is more difficult to establish since most of the research in this area has focused on high speed flow ($\text{Mach} \geq 0.3$), and since the value for the recovery factor is dependent on the size and orientation of the thermocouple. Data from Stickley [88] and Simmons [89] suggest a recovery factor of $r=0.63$ for a thermocouple in cross flow with Mach number less than or equal to 0.3. This recovery factor is used to generate table 5, which shows the experimentally determined recovery temperature difference, the value of the recovery temperature difference predicted by Eq. (27), and the dynamic temperature at the stagnation line.

Table 5. Comparison of experimentally determined stagnation line recovery temperature differences with predicted stagnation line recovery temperature differences.

#	Re ₀	Exit velocity [m/s]	Spacing Z/D	Experimental (T _{rs} -T _{rc}) [K]	V ² /2C _p [K]	Eq. (27) (T _{rs} -T _{rc}) [K]
1	8,319	117.9	4	2.07	6.902	2.57
2	8,206	116.3	6	1.74	6.716	2.50
3	8,319	117.9	8	2.50	6.902	2.57
4	8,248	116.9	9	2.16	6.785	2.52
5	8,192	116.1	10	1.93	6.693	2.49
6	8,192	116.1	14	2.08	6.693	2.49
7	8,177	115.9	18	2.42	6.670	2.48
8	4,176	59.2	4	1.48	1.740	0.65
9	4,172	59.1	6	2.04	1.736	0.65
10	4,159	58.9	8	1.82	1.725	0.64
11	4,171	59.1	10	1.62	1.735	0.65
12	4,158	58.9	14	2.27	1.724	0.64
13	4,168	59.1	18	2.17	1.733	0.64
14	8,326	52.2	2.655	1.11	1.354	0.50
15	8,231	51.6	4	0.82	1.323	0.49
16	8,334	52.3	6	0.07	1.357	0.51
17	8,331	52.3	8	1.10	1.356	0.50
18	8,333	52.3	10	-0.03	1.356	0.50
19	9,658	60.6	2.655	0.76	1.822	0.68

It can be seen from Table 5 that the experimentally determined recovery temperature difference is quite close to the predicted value for the high velocity cases. For the low velocity cases the recovery temperature difference approaches zero and there is virtually no correlation between the experimental and theoretical values. This result was expected since the high and low heating rate experiments used to calculate each recovery temperature difference gave nearly the same heat transfer coefficients without including the effects of the recovery temperature. Since the data reduction method relies on the tests yielding different data, if the results are nearly the same then the problem reduces to 2 equations that are nearly the same with 2 unknowns. The same poor results are also seen in Fig. 33 where the down-stream recovery temperature difference is shown for high and low velocity cases. The scatter in the data for low velocity cases is so large that the experimentally determined recovery temperature difference is nearly meaningless. Other low velocity cases yield even greater scatter.

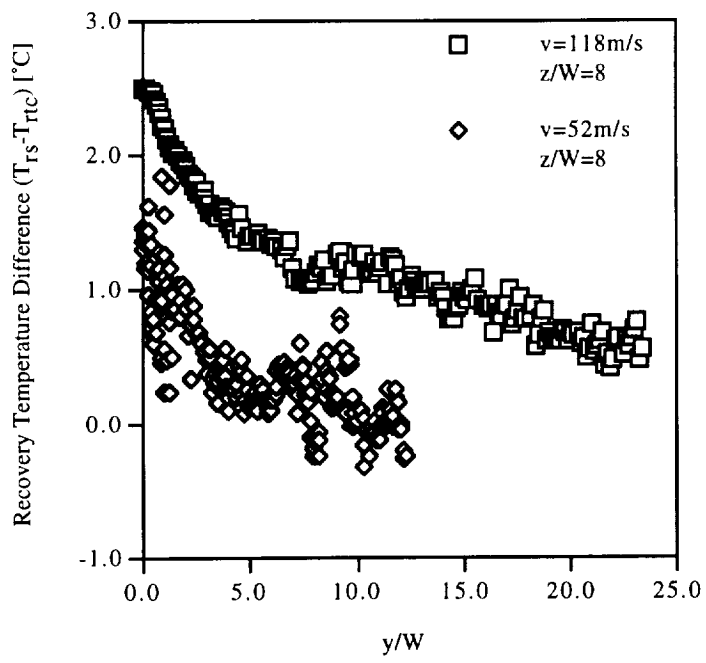


Figure 33. Recovery temperature difference for a high velocity case (Test 3) and a low velocity case (Test 17).

Chapter 6

SUMMARY AND RECOMMENDATIONS FOR FURTHER RESEARCH

6.1 Concluding Comments

A preliminary design of the leading edge cooling system was given in section 2.1.1. The results showed that, with a 0.12mm slot and a Reynolds number of 14,000, a stagnation line Nusselt number of about 101 could be expected. Under these conditions the analysis showed that the leading edge should remain below 800K. Unfortunately, the air supply for the experiment was only capable of delivering 0.0365kg/s to the nozzle, which yields a Reynolds number of 9,658, and a stagnation line Nusselt number of 77. With this cooling profile, appendix C shows that the leading edge would reach a maximum temperature of nearly 1400K. The stagnation line Nusselt number is actually a little higher than expected for a Reynolds number of 9,658, however the Nusselt number drops more rapidly away from the stagnation line than was expected. Thus the temperature of the leading edge is about 950K at the stagnation line, but it rises rapidly to 1400K then falls back to 800K as the aerodynamic heat load decreases. In order to complete an actual design of the cooling system for a leading edge, additional experiments at higher mass flow rates are necessary.

It was shown in the results section, and also pointed out by several other researchers, that there are many parameters that affect jet impingement heat transfer, among them: Reynolds number, Prandtl number, surface curvature, nozzle to surface

spacing, nozzle geometry, turbulence level of the jet, and how the gas jet is removed from the surface. Given the large number of parameters involved in jet impingement heat transfer it is not surprising that available correlations are very narrow in scope. Many researchers also noted a large amount of data scatter in the literature, which is mostly attributed to dissimilar nozzles or different turbulence levels of the jets. It is unreasonable to expect that a simple correlation can be developed that is general enough for a wide variety of actual engineering designs. The experimental method developed here has been shown to be useful for an iterative design process. Parameters can be easily changed and their effect on the heat transfer is quickly learned. Development of testing equipment based on the present technique may prove to be more useful to the design process than attempting to do a series of generalized experiments in order to develop heat transfer correlations.

6.2 Suggestions for Further Research

While building and testing the experimental rig a number of problems were encountered. In some cases the solution to the problem led to ideas for a redesign that would make the experimental rig more robust. In other cases the problems encountered pointed out areas where further research was necessary. The most serious problem encountered was dealing with the conversion of kinetic energy in the air flow to thermal energy at the impingement surface and at the nozzle exit thermocouple. The problem was resolved by grouping the two recovery temperatures as a single variable,

the recovery temperature difference, and then taking data twice while heating the air at different rates. The data from the two experiments is input to Eq. (19) and Eq. (18), in order to evaluate the heat transfer coefficient and the recovery temperature difference, respectively. Using different heating rates to generate a second equation for a second unknown is an interesting experimental technique because it provides two important pieces of engineering data using the same experiment. All other researchers in this area have designed individual experiments to collect this data. It was pointed out in the results section that this technique unfortunately causes substantial scatter in the recovery temperature difference results, and renders the data qualitative at best for all but the high velocity cases. It was also pointed out in the error analysis section that despite the error in recovery temperature difference the heat transfer coefficient error is not significantly increased.

In order to calculate the surface recovery temperature one must first know the recovery temperature of the nozzle exit thermocouple. The results shown in Table 5 rely on thermocouple recovery factor data from other researchers. While searching for thermocouple recovery factor data, it was discovered that the available data is incomplete. Neither fine gage thermocouples (36 and greater) nor low speed studies (Mach number less than 0.3) have been addressed adequately. Recovery factor data for thermocouples in Mach 0.3 flow range from 0.65-0.85, and few researchers have investigated the Reynolds number regime characterizing fine gage thermocouples.

The recovery temperature error can be reduced by providing a larger temperature difference between the surface and the air so that the recovery temperature becomes a smaller percentage of the overall temperature difference. In order to increase the surface to air temperature difference, higher temperature TLCs need to be used. The current crystal transition temperature of 35.1°C should be increased to approximately 55°C near the stagnation line. Further away from the stagnation line the high temperature crystal is not needed because the recovery temperature approaches zero, and the increased time to transition would introduce more error into the heat transfer coefficient results. One solution to this problem is to use high transition temperature crystals near the stagnation line, and lower transition temperature crystals further down stream where the heat transfer is lower. The other possibility is to mix 2 or 3 different transition temperature crystals together, and apply the mixture to the surface. This allows for the collection of 2 to 3 times more data per run, however as more crystals are mixed, it becomes more difficult to distinguish the transition point.

In addition to raising the transition temperature of the TLCs, the other step that must be taken to increase the surface to air temperature difference is to heat the nozzle exit air to a higher temperature more rapidly. Currently the air heater is upstream of the manifold: the closer the heater is moved to the nozzle exit the less heat will be lost to the manifold and duct walls; thus the exit temperature will rise more rapidly. Placing the heater downstream from the manifold also solves the problem of a

nonuniform temperature distribution at the nozzle exit. The high pressure-drop manifold gives a velocity distribution that varies less than 5% across the length of the slot, however since the air is heated prior to entering the manifold, the center of the pressure drop medium heats more than the edges thus the temperature of the air in the center of the slot is higher than the air at the edges. Higher air temperatures can be achieved simply by using a larger power supply.

Originally, a single camera looking at the front of the leading edge was used to gather crystal transition line data. Since the angle of the leading edge is only 7.5° it is difficult to see the crystal transition line as it moves away from the stagnation line. It became necessary to do two identical experiments, one with the camera facing the front of the model and one facing the side. Substantial error can be introduced unless care is taken to exactly duplicate the flow, heat, and initial temperature of the surface for the two separate experiments. Proper alignment of the camera for the side and front view experiments is difficult and can be a significant source of error. Since the data acquisition card DT-3851 supports multiple cameras the accuracy and speed of the experiment would be improved with the addition of a second camera.

One goal not achieved was a level of automation such that the Nusselt number results could be displayed in near real time. The primary reason for failure to reach this goal was the surface recovery temperature problem. Since two experiments are required in order to gather enough data to solve for the heat transfer coefficient and surface recovery temperature, near real time display is not possible. Even if the surface

recovery temperature problem is solved by implementing the changes suggested above, the current computer being used to control the experiment does not have sufficient computational power to reduce the data in near real time. Currently a more powerful computer is used to reduce the data after the data has been collected. As mentioned above, a second camera would also be necessary to achieve near real time results.

Appendix A

SOLUTION TO TIME VARYING CONVECTION EQUATION

A scaling analysis can be performed on Eq. (13a) in order to determine when the time derivative term is important. Equations (13a-c) are rewritten below as Eq. (A1a-c).

$$\frac{\partial T_f}{\partial t} + V \frac{\partial T_f}{\partial y} + \frac{h}{\rho D c_p} (T_f - T_w(t)) = 0 \quad (\text{A1a})$$

The associated initial and boundary conditions are

$$T_f(y,0) = T_i \quad (\text{A1b})$$

$$T_f(0,t) = f(t) \quad (\text{A1c})$$

In order to do a scale analysis of Eq. (A1a) we seek dimensionless dependent variables that are order of magnitude unity or less. The appropriate scaling for y is $y=y^* L$. The appropriate scaling for time is determined by recognizing that the forcing function for this problem is the wall temperature. Since the wall temperature is governed by the solution to the semi-infinite conduction problem, the argument for the exponential term in Eq. (14) can be used as the time scaling. The validity of this scaling is illustrated in Fig. A1. The solution for the surface temperature of a semi-infinite wall and the

equation, $\frac{T - T_\infty}{T_f - T_\infty} = 1 - e^{-(h/k)^2 \alpha t}$ are plotted. Clearly, the characteristic time for the

surface temperature of the semi-infinite wall is larger than the characteristic time for the

exponential curve. Thus the characteristic scaling time for Eq. (A1a) must be greater

than $\frac{1}{\alpha} \left(\frac{k}{h} \right)^2$, so $t = \frac{1}{\alpha} \left(\frac{k}{h} \right)^2 t^*$

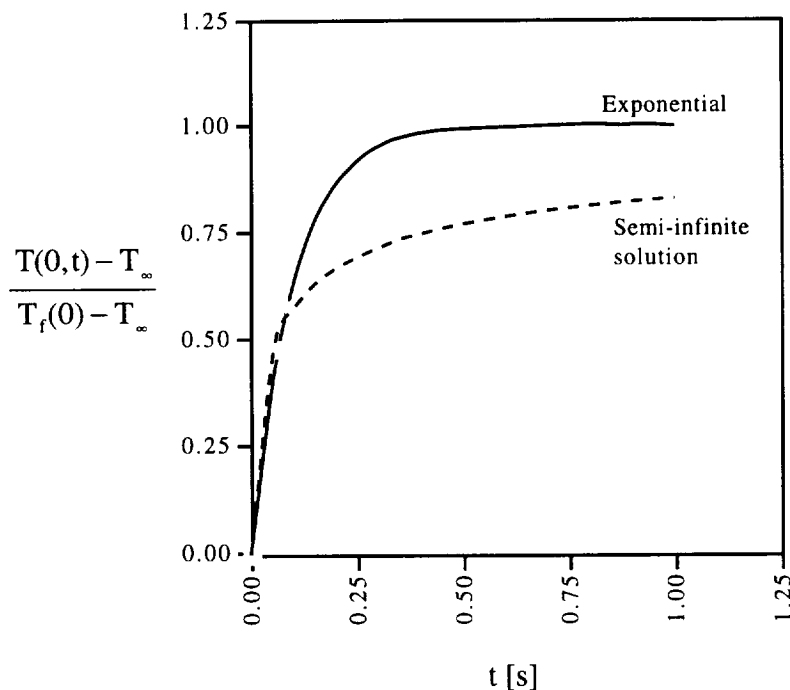


Figure A1 Comparison between Eq. (A1) and an exponential function.

Making the appropriate substitutions for t and y Eq. (A1a) becomes

$$\frac{h^2 \alpha_w}{k_w^2} \frac{\partial T_f}{\partial t^*} + \frac{V}{L} \frac{\partial T_f}{\partial y^*} + \frac{h}{\rho_f D c_p f} (T_f - T_w(t)) = 0 \quad (\text{A2})$$

Rearranging Eq. (A2) we have

$$St_w Bi_L \frac{\partial T_f}{\partial t^*} + \frac{\partial T_f}{\partial y^*} + \frac{L}{D} St_f (T_f - T_w(t)) = 0 \quad (A3)$$

Where $St = \frac{h}{V\rho c_p}$ and $Bi = \frac{hL}{k}$, the subscripts w and f refer to the properties of the wall and fluid respectively.

Table A1 gives estimated values for the four dimensionless parameters occurring in Eq. (A3).

Table A1. Dimensionless parameter range for Eq. (A3)

	St_w	St_f	Bi_L	$\frac{L}{D}$
Max	5.9×10^{-5}	8.5×10^{-2}	1.0×10^2	5.0×10^1
Min	2.4×10^{-5}	3.4×10^{-3}	1.0	1.0

It is evident from Eq. (A3) and Table A1 that the time derivative term should be at least 2 orders of magnitude less than the other two terms. It should also be noted that the time used to characterize the problem was shorter than the actual time constant of the problem, so these are conservative estimates.

Eq. (A1a-c) can be solved in closed form and used instead of Eq. (17) to quantitatively estimate the error caused by dropping the time derivative term. The solution to this system can be found by recognizing that as y goes to infinity the

solution becomes a function of time only, and therefore the solution can be decomposed into two parts.

$$T_f(y, t) = T_u(y, t) + T_e(t) \quad (A4)$$

This substitution along with letting $b = \frac{h}{\rho D c_p}$ converts Eqs. (A1a-c) into the following two sets of equations.

$$\frac{dT_e}{dt} + bT_e = bT_w(t) \quad (A5a)$$

$$T_e(0) = T_i \quad (A5b)$$

and

$$\frac{\partial T_u}{\partial t} + v \frac{\partial T_u}{\partial y} + bT_u = 0 \quad (A6a)$$

$$T_f(0, t) = f(t) - T_e(t) \quad (A6b)$$

$$T_f(y, 0) = 0 \quad (A6c)$$

The solution to Eqs. (A5a-b) is found to be

$$T_e = T_i e^{-bt} + b e^{-bt} \int T_w(t) e^{bt} dt \quad (A7)$$

Eqs. (A6a-c) can be solved using a Laplace transform. The transformed system becomes,

$$s \bar{T}_u + v \frac{d \bar{T}_u}{dy} + b \bar{T}_u = 0 \quad (A8a)$$

$$\bar{T}_u(0, s) = \mathcal{L}[f(t) - T_e(t)] \quad (A8b)$$

The boundary condition, Eq. (A8b) is not explicitly transformed. It will be shown that this will facilitate a more general solution. The solution to Eqs. (A8a-b) is,

$$\bar{T}_u = \mathcal{L}[f(t) - T_e(t)] e^{-by/v} e^{-sy/v} \quad (A9)$$

The shifting theorem for Laplace transforms states that: If $\mathcal{L}^{-1}[f(s)] = F(t)$ then,

$$\mathcal{L}^{-1}[e^{-as}f(s)] = \begin{cases} F(t-a) & t>a \\ 0 & t<a \end{cases} = F(t-a)H(t-a) \quad (A10)$$

where $H(t)$ is the Heavyside step function defined as,

$$H(t) = \begin{cases} 1 & t>0 \\ 0 & t<0 \end{cases} \quad (A11)$$

The inverse Laplace transform of Eq. (A9) is found using the shifting theorem to be

$$\bar{T}_u = e^{-by/v} \left[f\left(t - \frac{y}{v}\right) - T_e\left(t - \frac{y}{v}\right) \right] H\left(t - \frac{y}{v}\right) \quad (A12)$$

The full solution is then,

$$T_f(y,t) = e^{-by/v} \left[f\left(t - \frac{y}{v}\right) - T_e\left(t - \frac{y}{v}\right) \right] H\left(t - \frac{y}{v}\right) + T_i e^{-bt} + b e^{-bt} \int T_w(t) e^{bt} dt \quad (A13)$$

Rearranging Eq. (A13) yields a form more convenient for computation

$$T_f(y,t) = \begin{cases} f\left(t - \frac{y}{v}\right) e^{-by/v} + b \int_{t-y/v}^t T_w(\tau) e^{-b(t-\tau)} d\tau & t > \frac{y}{v} \\ T_i e^{-bt} + b \int_0^t T_w(\tau) e^{-b(t-\tau)} d\tau & t < \frac{y}{v} \end{cases} \quad (A14)$$

Appendix B

DESIGN DRAWINGS

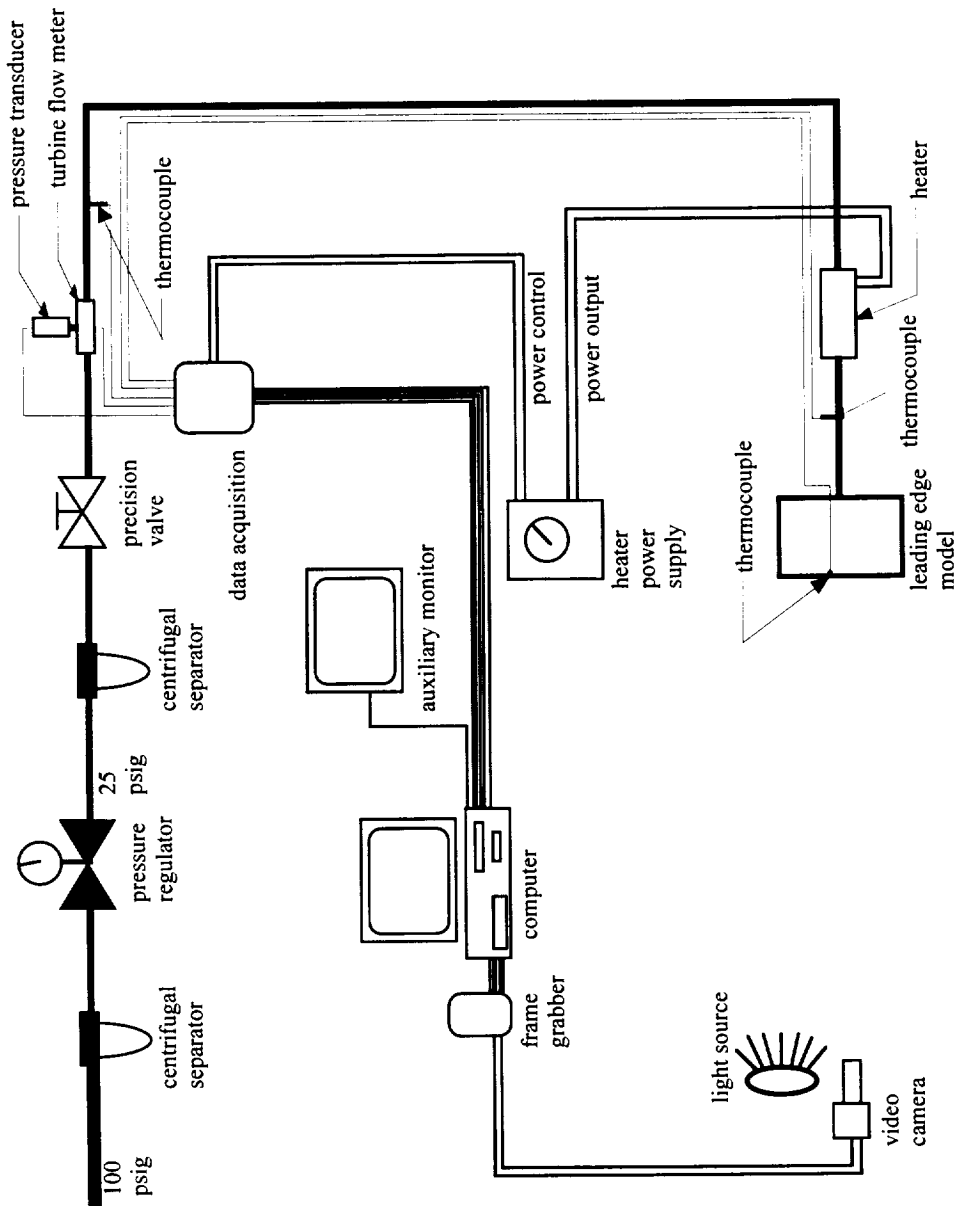


Figure B1. Schematic of jet impingement experimental rig

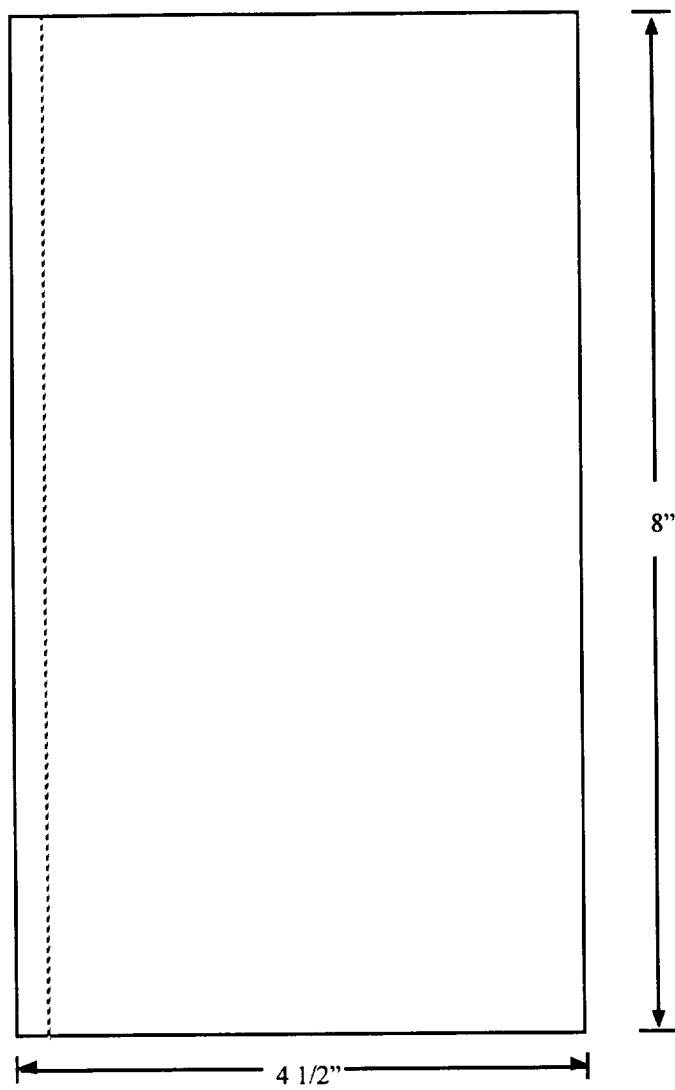
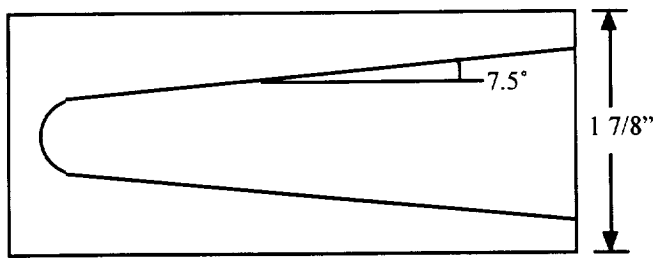


Figure B2 Leading edge model

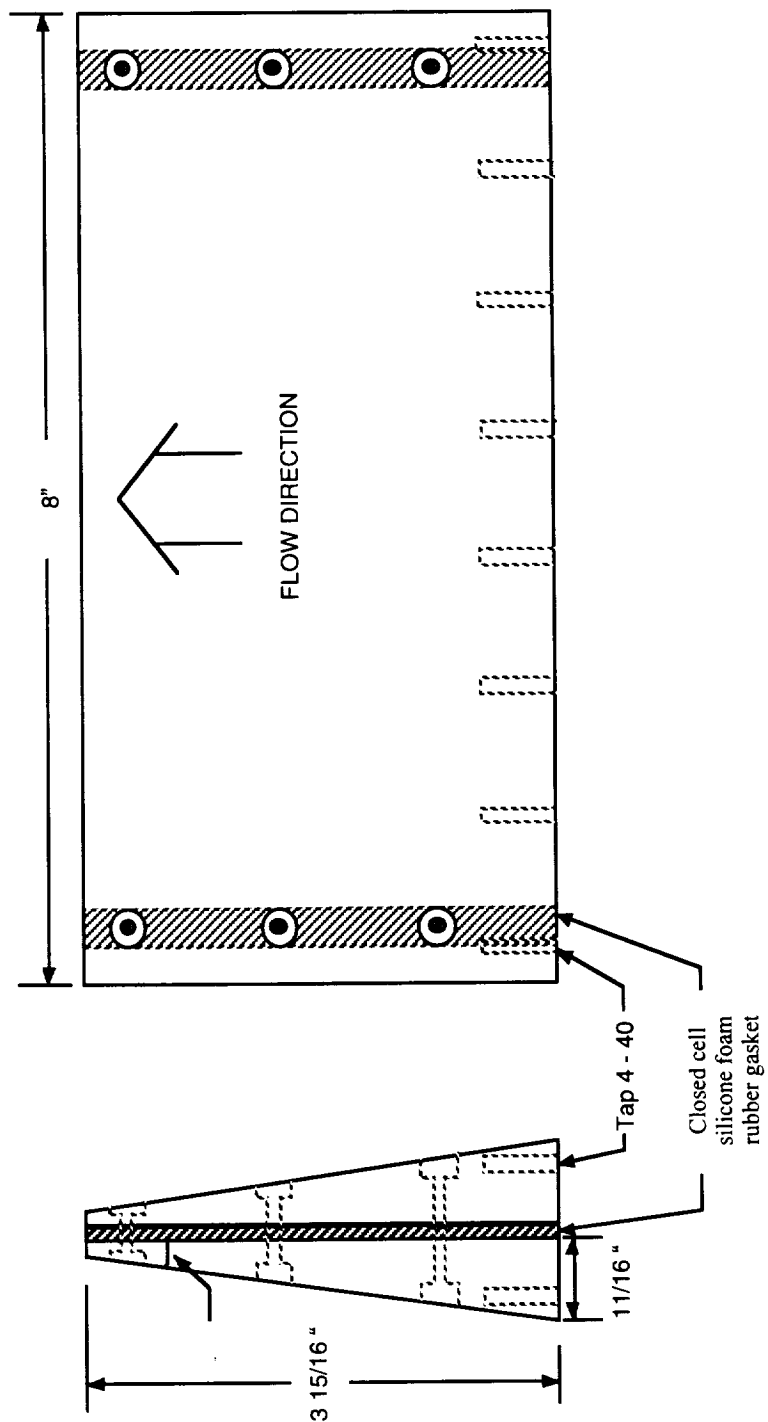


Figure B3 Nozzle design.

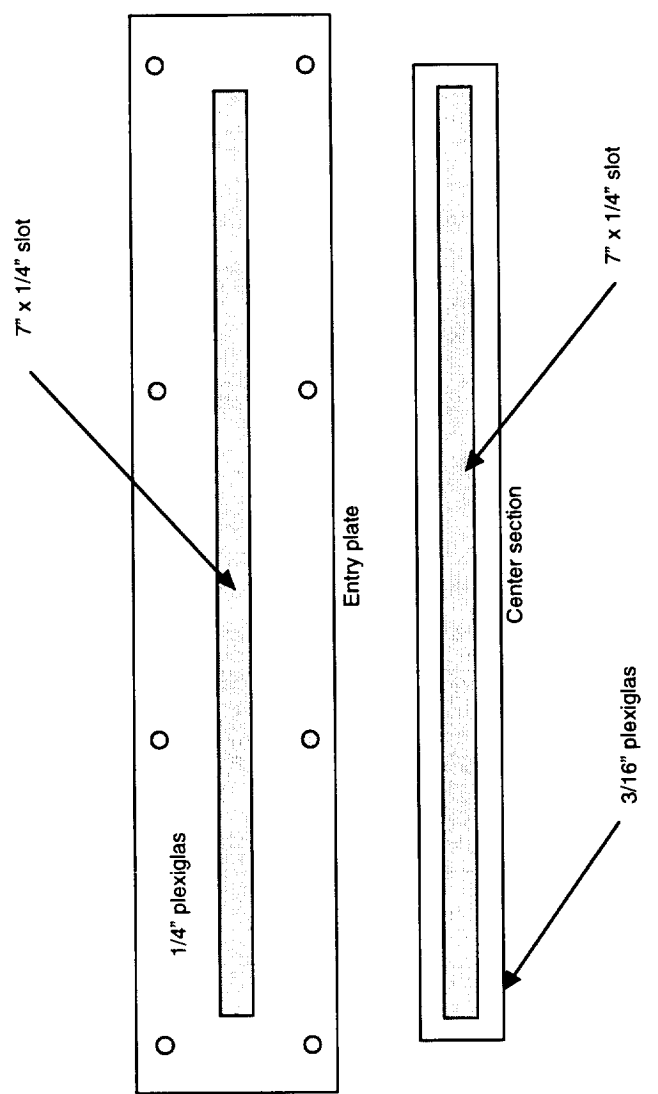


Figure B4a Entry plate and center section for the high pressure drop manifold.

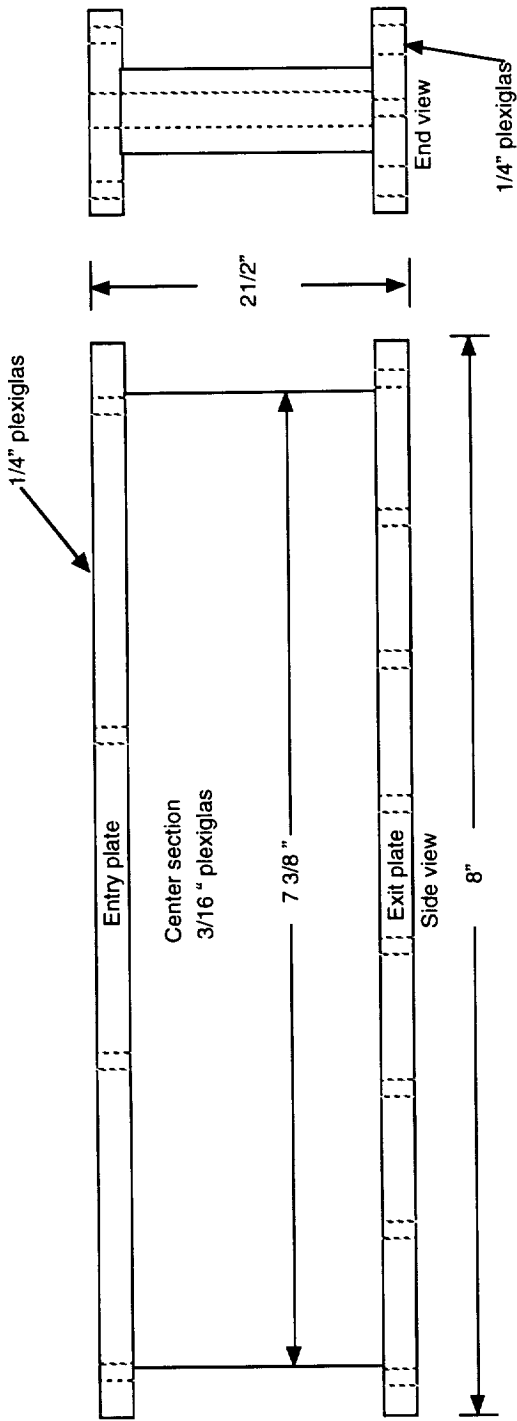


Figure B4b Side view of the high pressure drop manifold.

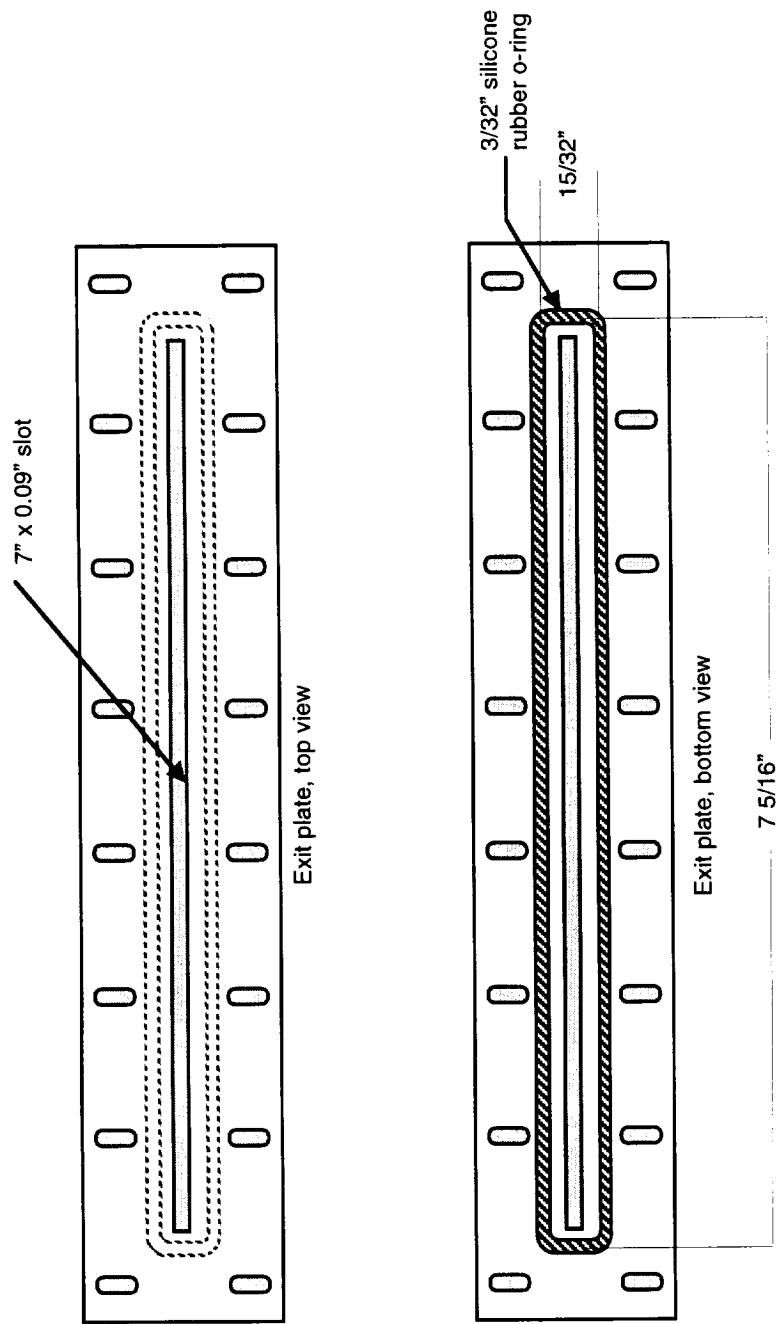


Figure B4c Exit plate for high pressure drop manifold.

Appendix C

AIRFOIL TEMPERATURE CALCULATION

Airfoil temperature calculations can be done using the analysis of chapter 2 and the results of chapter 5. Equations (6) and (7) are combined to form an expression for the wall temperature, Eq. (C1).

$$T_w(y) = \frac{q(y)}{h(y)} + T_{f0} + \frac{1}{\dot{m}c_p} \int_0^y q(y) dy \quad (C1)$$

Using this expression, the heat transfer coefficients obtained from data set 7, and the worst case wall heat flux obtained from Ref [80], the wall temperature along the airfoil is determined. Using Eq. (7) the coolant temperature is also determined. The results of this calculation are presented in Fig. C1.

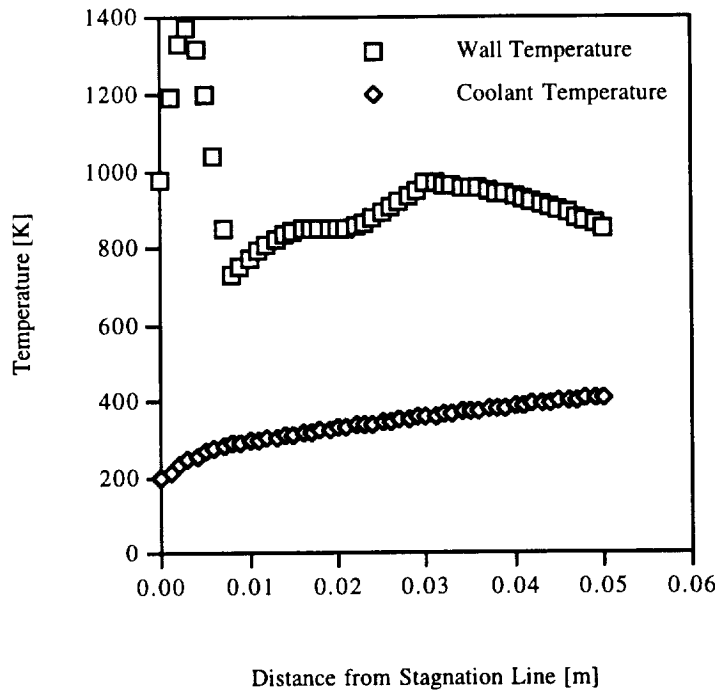


Figure C1 Temperatures of the leading edge and the leading edge coolant.

Figure C1 shows that the leading edge reaches a maximum temperature of nearly 1400K about 3mm from the stagnation line during the worst case heating. A design such as this would require the leading edge to be manufactured from a high temperature alloy such as tungsten-25 rhenium, which retains 40% of its room temperature tensile strength (242ksi) at 1600K. Past 1.0 cm the temperature of the leading edge drops significantly to 800K. At this temperature the material could be switched to a high temperature titanium alloy such as Ti-5Al-6Sn-2Zr-1Mo as a weight reduction consideration. Experiments with higher speed jets may lead to much lower temperatures and allow the entire leading edge to be constructed out of titanium alloy.

Appendix D

HEAT TRANSFER COEFFICIENTS AND RECOVERY TEMPERATURE DATA

Table D1a Heat transfer coefficient data from tests 1-5

Test 1 x [m]	h [W/mK] x [m]	Test 2 h [W/mK] x [m]	Test 3 h [W/mK] x [m]	Test 4 h [W/mK] x [m]	Test 5 h [W/mK] x [m]
0.00E+00	1187.50	0.00E+00	1348.40	0.00E+00	912.46
8.47E-05	1141.40	8.47E-05	1237.70	8.47E-05	913.32
1.70E-04	1132.00	1.70E-04	1224.10	1.70E-04	911.83
2.54E-04	1157.00	2.54E-04	1240.50	2.54E-04	922.44
3.39E-04	1114.30	3.39E-04	1213.50	3.39E-04	919.36
4.24E-04	1097.10	4.24E-04	1181.70	4.24E-04	912.79
5.09E-04	1081.80	5.09E-04	1159.20	5.09E-04	899.90
5.94E-04	1073.10	5.94E-04	1139.40	5.94E-04	923.34
6.79E-04	1045.80	6.79E-04	1111.20	6.79E-04	916.75
7.64E-04	1020.10	7.64E-04	1084.60	7.64E-04	896.89
8.49E-04	994.50	8.49E-04	1052.40	8.49E-04	913.43
9.35E-04	970.88	9.35E-04	1035.90	9.35E-04	872.92
1.02E-03	955.19	1.02E-03	1011.10	1.02E-03	911.15
1.11E-03	939.19	1.11E-03	985.63	1.11E-03	896.69
1.19E-03	917.59	1.19E-03	966.54	1.19E-03	867.13
1.28E-03	900.05	1.28E-03	951.06	1.28E-03	858.67
1.36E-03	873.76	1.36E-03	933.77	1.36E-03	896.76
1.45E-03	857.21	1.45E-03	921.88	1.45E-03	905.40
1.54E-03	846.67	1.54E-03	905.07	1.54E-03	876.68
1.62E-03	836.21	1.62E-03	890.42	1.62E-03	858.93
1.71E-03	830.41	1.71E-03	873.92	1.71E-03	842.85
1.80E-03	825.80	1.80E-03	867.27	1.80E-03	855.56
1.88E-03	814.05	1.88E-03	854.34	1.88E-03	846.27
1.97E-03	805.06	1.97E-03	842.43	1.97E-03	766.64
2.06E-03	798.89	2.06E-03	828.74	2.06E-03	779.52
2.15E-03	788.89	2.15E-03	827.31	2.15E-03	791.70
2.24E-03	782.02	2.24E-03	827.49	2.24E-03	773.49
2.32E-03	775.17	2.32E-03	832.24	2.32E-03	818.26
2.41E-03	772.47	2.41E-03	830.60	2.41E-03	819.81
2.50E-03	761.16	2.50E-03	826.24	2.50E-03	816.72
2.59E-03	747.84	2.59E-03	821.06	2.59E-03	777.07
2.68E-03	744.29	2.68E-03	820.88	2.68E-03	784.58
2.77E-03	745.11	2.77E-03	819.85	2.77E-03	727.62
2.86E-03	739.71	2.86E-03	831.80	2.86E-03	765.77
2.95E-03	741.43	2.95E-03	823.56	2.95E-03	785.63
3.05E-03	734.99	3.05E-03	814.96	3.05E-03	784.76
3.14E-03	731.01	3.14E-03	810.18	3.14E-03	789.53
3.23E-03	718.03	3.23E-03	802.17	3.23E-03	797.92
3.32E-03	719.66	3.32E-03	792.75	3.32E-03	755.16
3.42E-03	719.65	3.42E-03	783.05	3.42E-03	814.91
3.51E-03	712.84	3.51E-03	774.64	3.51E-03	669.11
3.61E-03	712.98	3.61E-03	760.00	3.61E-03	706.55
3.70E-03	698.37	3.70E-03	743.61	3.70E-03	703.52
3.80E-03	684.16	3.80E-03	734.62	3.80E-03	704.96
3.90E-03	678.56	3.90E-03	710.75	3.90E-03	686.70
3.99E-03	666.19	3.99E-03	694.04	3.99E-03	673.08
4.09E-03	657.03	4.09E-03	682.17	4.09E-03	778.29
4.19E-03	645.87	4.19E-03	667.68	4.19E-03	741.38
4.29E-03	637.74	4.29E-03	673.95	4.29E-03	728.71
4.39E-03	631.78	4.39E-03	671.36	4.39E-03	697.22
4.49E-03	624.74	4.49E-03	676.15	4.49E-03	599.58
4.60E-03	618.90	4.60E-03	659.26	4.60E-03	608.44
4.70E-03	617.66	4.70E-03	640.77	4.70E-03	631.66
4.80E-03	617.98	4.80E-03	647.79	4.80E-03	614.51
4.91E-03	610.25	4.91E-03	641.63	4.91E-03	613.15
5.02E-03	608.22	5.02E-03	644.78	5.02E-03	607.56

Table D1a Heat transfer coefficient data from tests 1-5 (cont.)

Test 1 x [m]	Test 2 h [W/mK] x [m]	Test 3 h [W/mK] x [m]	Test 4 h [W/mK] x [m]	Test 5 h [W/mK] x [m]	h [W/mK]
5.12E-03	599.08	5.12E-03 651.38	5.12E-03 712.12	5.43E-03 674.81	4.54E-03 806.71
5.23E-03	586.44	5.23E-03 634.49	5.23E-03 657.36	5.65E-03 681.92	4.63E-03 796.33
5.34E-03	576.15	5.34E-03 627.53	5.34E-03 638.48	5.86E-03 642.88	4.72E-03 791.51
5.45E-03	562.72	5.45E-03 615.20	5.45E-03 632.70	6.06E-03 686.26	4.82E-03 787.20
5.57E-03	562.30	5.57E-03 615.85	5.57E-03 644.61	6.26E-03 697.13	4.91E-03 770.30
5.68E-03	555.25	5.68E-03 620.93	5.68E-03 692.45	6.45E-03 644.59	5.01E-03 768.21
5.80E-03	544.32	5.80E-03 619.49	5.80E-03 598.08	6.64E-03 651.03	5.11E-03 754.98
5.92E-03	538.43	5.92E-03 617.37	5.92E-03 607.88	6.82E-03 643.09	5.20E-03 747.52
6.04E-03	542.92	6.04E-03 612.07	6.04E-03 617.48	7.01E-03 645.90	5.30E-03 739.85
6.16E-03	547.31	6.16E-03 607.84	6.13E-03 632.04	7.18E-03 620.06	5.40E-03 727.79
6.28E-03	575.84	6.28E-03 609.18	6.36E-03 619.17	7.36E-03 620.71	5.50E-03 726.21
6.41E-03	582.23	6.41E-03 609.00	6.58E-03 615.47	7.53E-03 618.53	5.61E-03 715.53
6.53E-03	587.43	6.53E-03 615.00	6.79E-03 601.08	7.70E-03 626.42	5.71E-03 714.60
6.67E-03	592.34	6.67E-03 613.83	7.01E-03 603.83	7.87E-03 622.64	5.82E-03 714.29
6.80E-03	597.60	6.80E-03 615.16	7.21E-03 603.67	8.03E-03 609.08	5.92E-03 709.15
6.94E-03	600.63	6.94E-03 623.81	7.42E-03 602.87	8.20E-03 609.09	6.03E-03 703.90
7.08E-03	595.25	7.08E-03 623.42	7.62E-03 602.34	8.36E-03 602.97	6.14E-03 710.48
7.22E-03	580.28	7.22E-03 608.48	7.81E-03 595.96	8.52E-03 602.62	6.25E-03 687.79
7.37E-03	571.13	7.37E-03 595.65	8.01E-03 598.18	8.68E-03 592.55	6.36E-03 632.10
7.52E-03	546.59	7.52E-03 591.97	8.20E-03 601.27	8.83E-03 591.00	6.58E-03 643.08
7.67E-03	539.06	7.67E-03 587.65	8.39E-03 601.97	8.99E-03 592.34	6.79E-03 637.74
7.83E-03	527.50	7.83E-03 581.68	8.57E-03 585.02	9.14E-03 608.58	7.01E-03 630.35
8.00E-03	518.31	8.00E-03 589.65	8.76E-03 578.77	9.29E-03 597.49	7.21E-03 631.62
8.18E-03	506.67	8.18E-03 577.35	8.94E-03 596.27	9.45E-03 616.99	7.42E-03 630.29
8.20E-03	505.77	8.36E-03 551.21	9.12E-03 601.08	9.60E-03 624.18	7.62E-03 618.71
8.39E-03	510.85	8.55E-03 525.04	9.29E-03 602.06	9.75E-03 605.52	7.81E-03 603.47
8.57E-03	515.95	8.75E-03 505.35	9.47E-03 596.93	9.90E-03 597.58	8.01E-03 599.84
8.76E-03	519.12	8.94E-03 486.77	9.65E-03 601.54	1.00E-02 597.23	8.20E-03 608.57
8.94E-03	520.60	9.12E-03 495.13	9.82E-03 602.47	1.02E-02 617.68	8.39E-03 591.04
9.12E-03	520.68	9.29E-03 499.75	9.99E-03 600.95	1.03E-02 565.04	8.57E-03 593.38
9.29E-03	520.25	9.47E-03 502.89	1.02E-02 599.52	1.05E-02 566.36	8.76E-03 603.51
9.47E-03	518.94	9.65E-03 505.31	1.03E-02 588.75	1.06E-02 622.39	8.94E-03 597.94
9.65E-03	520.71	9.82E-03 513.06	1.05E-02 580.20	1.08E-02 619.14	9.12E-03 597.75
9.82E-03	521.71	9.99E-03 517.98	1.07E-02 582.46	1.09E-02 554.26	9.29E-03 597.31
9.99E-03	524.11	1.02E-02 510.94	1.08E-02 569.43	1.11E-02 615.77	9.47E-03 595.46
1.02E-02	527.31	1.03E-02 505.99	1.10E-02 572.12	1.12E-02 520.51	9.65E-03 597.65
1.03E-02	522.50	1.05E-02 519.23	1.12E-02 562.44	1.14E-02 591.99	9.82E-03 596.43
1.05E-02	520.54	1.07E-02 493.89	1.14E-02 560.36	1.15E-02 525.59	9.99E-03 593.65
1.07E-02	515.53	1.08E-02 502.18	1.15E-02 531.61	1.16E-02 546.65	1.02E-02 592.17
1.08E-02	508.25	1.10E-02 480.75	1.17E-02 517.20	1.18E-02 543.85	1.03E-02 590.06
1.10E-02	506.46	1.12E-02 482.81	1.19E-02 520.79	1.19E-02 516.57	1.05E-02 586.49
1.12E-02	491.90	1.14E-02 468.62	1.20E-02 511.31	1.21E-02 526.83	1.07E-02 573.46
1.14E-02	483.88	1.15E-02 456.59	1.22E-02 520.81	1.22E-02 521.38	1.08E-02 570.81
1.15E-02	468.94	1.17E-02 461.86	1.24E-02 520.83	1.24E-02 522.25	1.10E-02 569.19
1.17E-02	454.47	1.19E-02 453.10	1.25E-02 510.18	1.25E-02 519.99	1.12E-02 559.27
1.19E-02	450.26	1.20E-02 444.77	1.27E-02 495.56	1.26E-02 510.36	1.14E-02 553.88
1.20E-02	452.25	1.22E-02 435.98	1.29E-02 490.77	1.28E-02 514.28	1.15E-02 533.07
1.24E-02	457.09	1.25E-02 429.96	1.32E-02 488.12	1.31E-02 501.65	1.19E-02 532.89
1.25E-02	443.34	1.27E-02 420.79	1.34E-02 485.33	1.32E-02 492.13	1.20E-02 515.55
1.27E-02	428.15	1.29E-02 433.57	1.35E-02 480.70	1.34E-02 483.60	1.22E-02 524.35
1.29E-02	424.06	1.30E-02 412.92	1.37E-02 470.36	1.35E-02 489.72	1.24E-02 508.19
1.30E-02	418.87	1.32E-02 419.75	1.39E-02 476.74	1.37E-02 490.21	1.25E-02 509.10
1.32E-02	416.99	1.34E-02 407.55	1.40E-02 474.43	1.38E-02 487.63	1.27E-02 503.53
1.34E-02	408.06	1.35E-02 403.16	1.42E-02 468.62	1.39E-02 474.17	1.29E-02 498.22
1.35E-02	420.21	1.37E-02 395.31	1.44E-02 478.41	1.41E-02 471.98	1.30E-02 480.61
1.37E-02	409.04	1.39E-02 408.50	1.45E-02 462.84	1.42E-02 465.17	1.32E-02 478.27
1.39E-02	412.70	1.40E-02 401.58	1.47E-02 464.07	1.44E-02 458.26	1.34E-02 476.82
1.40E-02	395.87	1.42E-02 399.94	1.49E-02 466.77	1.45E-02 467.54	1.35E-02 478.19
1.42E-02	392.12	1.44E-02 401.90	1.50E-02 474.21	1.47E-02 475.05	1.37E-02 468.10
1.44E-02	398.57	1.45E-02 406.34	1.52E-02 465.32	1.48E-02 466.80	1.39E-02 464.06
1.45E-02	399.74	1.47E-02 406.90	1.54E-02 471.35	1.50E-02 461.61	1.40E-02 459.88
1.47E-02	383.28	1.49E-02 400.00	1.56E-02 475.49	1.51E-02 465.90	1.42E-02 466.46
1.49E-02	380.21	1.50E-02 406.88	1.57E-02 472.38	1.52E-02 457.30	1.44E-02 471.96

Table D1a Heat transfer coefficient data from tests 1-5 (cont.)

Test 1 x [m]	h [W/mK] x [m]	Test 2 h [W/mK] x [m]	Test 3 h [W/mK] x [m]	Test 4 h [W/mK] x [m]	Test 5 h [W/mK] x [m]
1.50E-02	384.70	1.52E-02	400.74	1.59E-02	462.95
1.52E-02	391.35	1.54E-02	397.19	1.61E-02	465.35
1.54E-02	389.41	1.56E-02	397.45	1.62E-02	469.20
1.56E-02	389.51	1.57E-02	401.67	1.64E-02	471.30
1.57E-02	388.62	1.59E-02	403.82	1.66E-02	469.05
1.59E-02	386.40	1.61E-02	397.32	1.67E-02	465.62
1.61E-02	381.98	1.62E-02	390.64	1.69E-02	461.19
1.62E-02	384.72	1.64E-02	397.56	1.71E-02	460.82
1.64E-02	384.77	1.66E-02	400.02	1.72E-02	456.40
1.66E-02	380.79	1.67E-02	388.68	1.74E-02	463.42
1.67E-02	380.97	1.69E-02	389.10	1.76E-02	454.05
1.69E-02	380.39	1.71E-02	391.10	1.77E-02	455.69
1.71E-02	382.09	1.72E-02	395.04	1.79E-02	464.39
1.72E-02	386.53	1.74E-02	394.85	1.81E-02	468.96
1.74E-02	382.43	1.76E-02	396.59	1.82E-02	464.83
1.76E-02	389.19	1.77E-02	396.99	1.84E-02	457.93
1.77E-02	385.96	1.79E-02	398.39	1.86E-02	448.69
1.79E-02	382.26	1.81E-02	398.53	1.87E-02	448.05
1.81E-02	379.37	1.82E-02	389.75	1.89E-02	442.12
1.82E-02	381.29	1.84E-02	376.49	1.91E-02	444.69
1.84E-02	388.35	1.86E-02	381.65	1.93E-02	442.92
1.86E-02	382.59	1.87E-02	386.32	1.94E-02	438.27
1.87E-02	368.14	1.89E-02	382.98	1.96E-02	436.12
1.89E-02	369.23	1.91E-02	385.24	1.98E-02	428.21
1.91E-02	368.40	1.93E-02	385.83	1.99E-02	436.52
1.93E-02	374.21	1.94E-02	393.66	2.01E-02	434.31
1.94E-02	373.62	1.96E-02	390.57	2.03E-02	432.69
1.96E-02	368.16	1.98E-02	379.83	2.04E-02	433.35
1.98E-02	367.40	1.99E-02	377.57	2.06E-02	431.16
1.99E-02	370.59	2.01E-02	374.70	2.08E-02	441.99
2.01E-02	363.86	2.03E-02	389.38	2.09E-02	424.74
2.03E-02	372.64	2.04E-02	382.81	2.11E-02	426.88
2.04E-02	381.75	2.06E-02	382.62	2.13E-02	427.12
2.06E-02	382.61	2.08E-02	381.71	2.14E-02	420.30
2.08E-02	382.72	2.09E-02	380.16	2.16E-02	419.02
2.09E-02	379.58	2.11E-02	377.61	2.18E-02	407.65
2.11E-02	373.56	2.13E-02	378.03	2.19E-02	419.81
2.13E-02	366.93	2.14E-02	379.48	2.21E-02	414.35
2.14E-02	366.04	2.16E-02	380.23	2.23E-02	409.91
2.16E-02	367.33	2.18E-02	377.37	2.24E-02	400.42
2.18E-02	364.17	2.19E-02	370.90	2.26E-02	404.99
2.19E-02	363.68	2.21E-02	379.60	2.28E-02	404.61
2.21E-02	369.86	2.23E-02	367.24	2.29E-02	403.39
2.23E-02	357.64	2.24E-02	367.89	2.31E-02	397.09
2.24E-02	347.51	2.26E-02	371.27	2.33E-02	412.38
2.26E-02	357.65	2.28E-02	369.32	2.35E-02	407.63
2.28E-02	359.86	2.29E-02	371.27	2.36E-02	400.10
2.29E-02	358.18	2.31E-02	360.27	2.38E-02	395.63
2.31E-02	340.04	2.33E-02	367.44	2.40E-02	406.74
2.33E-02	359.58	2.35E-02	363.28	2.41E-02	400.86
2.35E-02	348.12	2.36E-02	363.70	2.43E-02	398.88
2.36E-02	346.80	2.38E-02	363.68	2.45E-02	394.93
2.38E-02	352.78	2.40E-02	357.33	2.46E-02	393.28
2.40E-02	348.30	2.41E-02	366.42	2.48E-02	394.59
2.41E-02	348.30	2.43E-02	361.69	2.50E-02	384.49
2.43E-02	341.10	2.45E-02	354.39	2.51E-02	383.04
2.45E-02	347.99	2.46E-02	351.78	2.53E-02	385.76
2.46E-02	350.37	2.48E-02	357.48	2.55E-02	383.00
2.48E-02	353.65	2.50E-02	352.40	2.56E-02	383.19
2.50E-02	339.41	2.51E-02	346.46	2.58E-02	379.33
2.51E-02	341.17	2.53E-02	349.14	2.60E-02	380.08
2.53E-02	344.20	2.55E-02	350.24	2.61E-02	376.75
2.55E-02	337.20	2.56E-02	345.84	2.63E-02	380.89

Table D1a Heat transfer coefficient data from tests 1-5 (cont.)

Test 1 x [m]	h [W/mK] x [m]	Test 2 h [W/mK] x [m]	Test 3 h [W/mK] x [m]	Test 4 h [W/mK] x [m]	Test 5 h [W/mK] x [m]	h [W/mK]
2.56E-02	341.93	2.58E-02	352.11	2.65E-02	375.42	2.45E-02
2.58E-02	335.54	2.60E-02	346.13	2.66E-02	358.43	2.46E-02
2.60E-02	331.07	2.61E-02	335.43	2.68E-02	370.69	2.48E-02
2.61E-02	334.90	2.63E-02	344.36	2.70E-02	370.44	2.49E-02
2.63E-02	333.12	2.65E-02	344.36	2.72E-02	367.91	2.50E-02
2.65E-02	325.35	2.66E-02	340.63	2.73E-02	365.19	2.52E-02
2.66E-02	325.68	2.68E-02	334.37	2.75E-02	371.01	2.53E-02
2.68E-02	317.87	2.70E-02	333.37	2.77E-02	364.93	2.55E-02
2.70E-02	325.10	2.72E-02	344.01	2.78E-02	367.52	2.56E-02
2.72E-02	332.86	2.73E-02	327.42	2.80E-02	362.17	2.58E-02
2.73E-02	314.40	2.75E-02	332.08	2.82E-02	353.02	2.59E-02
2.75E-02	306.79	2.77E-02	318.76	2.83E-02	351.35	2.60E-02
2.77E-02	319.23	2.78E-02	332.47	2.85E-02	354.24	2.62E-02
2.78E-02	322.50	2.80E-02	328.59	2.87E-02	348.26	2.63E-02
2.80E-02	321.99	2.82E-02	324.94	2.88E-02	349.06	2.65E-02
2.82E-02	317.14	2.83E-02	319.08	2.90E-02	343.74	2.66E-02
2.83E-02	317.97	2.85E-02	304.02	2.92E-02	339.88	2.68E-02
2.85E-02	314.40	2.87E-02	313.20	2.93E-02	335.59	2.69E-02
2.87E-02	309.35	2.88E-02	311.86	2.95E-02	345.78	2.71E-02
2.88E-02	305.75	2.90E-02	312.18	2.97E-02	338.83	2.72E-02
2.90E-02	306.05	2.92E-02	308.88	2.98E-02	333.25	2.73E-02
2.92E-02	300.27	2.93E-02	302.76	3.00E-02	329.17	2.75E-02
2.93E-02	295.23	2.95E-02	300.06	3.02E-02	323.67	2.76E-02
2.95E-02	301.69	2.97E-02	306.32	3.03E-02	323.10	2.78E-02
2.97E-02	297.58	2.98E-02	311.31	3.05E-02	320.28	2.92E-02
2.98E-02	295.30	3.00E-02	309.59	3.07E-02	308.99	
3.00E-02	293.56	3.02E-02	304.27	3.09E-02	307.53	
3.02E-02	293.79	3.03E-02	300.85	3.10E-02	306.98	
3.03E-02	292.20	3.05E-02	307.08	3.12E-02	302.73	
3.05E-02	287.86	3.07E-02	300.25	3.14E-02	301.96	
3.07E-02	285.45	3.09E-02	301.28	3.15E-02	300.72	
3.09E-02	285.80	3.10E-02	299.71	3.17E-02	289.32	
3.10E-02	287.11	3.12E-02	296.90	3.19E-02	288.59	
3.12E-02	287.12	3.14E-02	290.98	3.20E-02	283.84	
3.14E-02	281.58	3.15E-02	288.00	3.22E-02	281.46	
3.15E-02	281.13	3.17E-02	288.91	3.24E-02	274.18	
3.17E-02	281.00	3.19E-02	288.09	3.25E-02	267.23	
3.19E-02	276.56	3.20E-02	286.40	3.27E-02	267.08	
3.20E-02	267.54	3.22E-02	284.20	3.29E-02	266.85	
3.22E-02	265.58	3.24E-02	278.98	3.30E-02	260.24	
3.24E-02	259.82	3.25E-02	287.09	3.32E-02	244.27	
3.25E-02	252.53	3.27E-02	284.22	3.34E-02	255.82	
3.27E-02	249.85	3.29E-02	272.97	3.35E-02	253.37	
3.29E-02	250.78	3.30E-02	278.00	3.37E-02	249.44	
3.30E-02	248.88	3.32E-02	276.18	3.39E-02	249.25	
3.32E-02	238.55	3.34E-02	272.33	3.40E-02	250.37	
3.34E-02	234.47	3.35E-02	266.94	3.42E-02	248.99	
3.35E-02	230.36	3.37E-02	266.91	3.44E-02	218.94	
3.37E-02	223.20	3.39E-02	265.50	3.45E-02	232.87	
3.39E-02	223.40	3.40E-02	261.53	3.47E-02	232.76	
3.40E-02	221.30	3.42E-02	261.03	3.49E-02	231.94	
3.42E-02	220.27	3.44E-02	259.44	3.51E-02	231.48	
3.44E-02	215.43	3.45E-02	256.77	3.52E-02	194.11	
3.45E-02	216.92	3.47E-02	250.60	3.54E-02	195.20	
3.47E-02	211.49	3.49E-02	245.10	3.56E-02	199.39	
3.49E-02	206.05	3.51E-02	239.21			
3.51E-02	206.30	3.52E-02	236.03			
3.52E-02	202.21	3.54E-02	230.38			
		3.56E-02	219.99			
		3.57E-02	223.61			
		3.59E-02	227.30			
		3.61E-02	222.04			
		3.62E-02	223.23			

Table D1b Heat transfer coefficient data from tests 6-10

Test 6 x [m]	h [W/mK] x [m]	Test 7 h [W/mK] x [m]	Test 8 h [W/mK] x [m]	Test 9 h [W/mK] x [m]	Test 10 h [W/mK] x [m]
0.00E+00	544.12	0.00E+00	396.89	0.00E+00	766.75
7.63E-05	550.77	7.41E-05	398.81	7.69E-05	712.71
1.53E-04	560.13	1.48E-04	396.38	1.54E-04	685.14
2.29E-04	554.91	2.22E-04	392.75	2.31E-04	686.10
3.05E-04	547.86	2.96E-04	395.56	3.08E-04	736.49
3.82E-04	546.40	3.71E-04	395.43	3.85E-04	705.75
4.58E-04	543.23	4.45E-04	393.73	4.62E-04	707.41
5.35E-04	538.62	5.19E-04	392.79	5.39E-04	716.76
6.11E-04	533.49	5.93E-04	391.16	6.16E-04	711.76
6.88E-04	528.21	6.68E-04	388.76	6.93E-04	693.63
7.65E-04	520.17	7.42E-04	387.96	7.71E-04	672.98
8.41E-04	516.09	8.16E-04	388.53	8.48E-04	665.32
9.18E-04	515.82	8.91E-04	389.57	9.25E-04	656.26
9.95E-04	512.35	9.66E-04	389.63	1.00E-03	665.07
1.07E-03	509.66	1.04E-03	390.60	1.08E-03	659.75
1.15E-03	513.90	1.12E-03	391.71	1.16E-03	649.71
1.23E-03	516.81	1.19E-03	392.20	1.24E-03	624.71
1.30E-03	520.53	1.27E-03	393.65	1.31E-03	611.79
1.38E-03	524.39	1.34E-03	395.08	1.39E-03	609.20
1.46E-03	530.25	1.42E-03	395.21	1.47E-03	605.12
1.54E-03	533.67	1.49E-03	394.30	1.55E-03	582.88
1.62E-03	538.20	1.57E-03	393.12	1.63E-03	576.73
1.69E-03	542.76	1.64E-03	392.30	1.71E-03	564.97
1.77E-03	548.33	1.72E-03	390.90	1.79E-03	557.85
1.85E-03	547.85	1.79E-03	391.16	1.86E-03	546.93
1.93E-03	549.51	1.87E-03	391.18	1.94E-03	545.11
2.01E-03	550.27	1.95E-03	391.12	2.02E-03	541.72
2.09E-03	550.61	2.02E-03	390.73	2.10E-03	539.09
2.17E-03	551.61	2.10E-03	390.67	2.18E-03	525.66
2.25E-03	554.10	2.18E-03	390.80	2.26E-03	525.59
2.33E-03	555.97	2.26E-03	391.83	2.34E-03	514.75
2.41E-03	559.66	2.33E-03	392.13	2.43E-03	502.53
2.49E-03	559.64	2.41E-03	391.74	2.51E-03	490.74
2.57E-03	562.26	2.49E-03	392.35	2.59E-03	482.49
2.65E-03	562.89	2.57E-03	392.80	2.67E-03	477.36
2.73E-03	564.71	2.65E-03	393.35	2.75E-03	474.47
2.81E-03	565.37	2.72E-03	394.36	2.83E-03	454.91
2.89E-03	566.02	2.80E-03	395.57	2.92E-03	444.61
2.98E-03	562.97	2.88E-03	397.42	3.00E-03	435.21
3.06E-03	564.94	2.96E-03	399.24	3.08E-03	424.10
3.14E-03	561.40	3.33E-03	390.23	3.17E-03	414.35
3.23E-03	564.65	3.65E-03	387.72	3.25E-03	412.78
3.31E-03	561.89	3.95E-03	392.25	3.34E-03	419.21
3.39E-03	562.37	4.23E-03	395.75	3.42E-03	418.79
3.48E-03	564.15	4.49E-03	399.09	3.51E-03	419.57
3.56E-03	567.47	4.74E-03	402.81	3.59E-03	431.05
3.65E-03	564.36	4.98E-03	401.77	3.68E-03	432.11
3.74E-03	560.18	5.21E-03	399.68	3.77E-03	434.08
3.82E-03	556.92	5.43E-03	403.14	3.85E-03	433.71
3.91E-03	557.18	5.65E-03	412.35	3.94E-03	428.38
4.00E-03	553.76	5.86E-03	399.34	4.03E-03	415.57
4.09E-03	555.76	6.06E-03	402.44	4.12E-03	398.62
4.18E-03	554.25	6.26E-03	410.22	4.21E-03	382.30
4.27E-03	548.39	6.45E-03	404.07	4.30E-03	373.60
4.36E-03	539.62	6.64E-03	407.82	4.39E-03	371.83
4.45E-03	552.42	6.82E-03	412.74	4.49E-03	378.15
4.54E-03	557.19	7.01E-03	418.95	4.58E-03	375.71
4.63E-03	556.66	7.18E-03	417.65	4.67E-03	371.57
4.72E-03	564.81	7.36E-03	417.39	4.77E-03	371.66
4.82E-03	567.19	7.53E-03	419.34	4.86E-03	377.72
4.91E-03	568.20	7.70E-03	421.96	4.96E-03	375.91
5.01E-03	571.67	7.87E-03	422.65	5.06E-03	396.96

Table D1b Heat transfer coefficient data from tests 6-10 (cont.)

Test 6 x [m]	Test 7 h [W/mK] x [m]	Test 8 h [W/mK] x [m]	Test 9 h [W/mK] x [m]	Test 10 h [W/mK] x [m]
5.11E-03 578.72	8.03E-03 423.48	5.15E-03 403.51	7.81E-03 363.44	5.65E-03 359.29
5.20E-03 589.22	8.20E-03 423.55	5.25E-03 400.32	8.01E-03 360.26	5.89E-03 365.79
5.30E-03 580.59	8.36E-03 427.60	5.35E-03 385.84	8.20E-03 363.50	6.13E-03 353.48
5.40E-03 583.89	8.52E-03 432.08	5.45E-03 391.08	8.39E-03 370.89	6.36E-03 353.50
5.50E-03 586.64	8.68E-03 432.17	5.56E-03 383.66	8.57E-03 376.56	6.58E-03 356.79
5.61E-03 586.82	8.83E-03 432.36	5.66E-03 402.42	8.76E-03 378.37	6.79E-03 351.25
5.71E-03 586.00	8.99E-03 429.84	5.77E-03 408.13	8.94E-03 374.95	7.01E-03 361.38
5.82E-03 584.25	9.14E-03 431.68	5.87E-03 409.73	9.12E-03 369.49	7.21E-03 342.86
5.92E-03 572.27	9.29E-03 430.81	5.98E-03 383.96	9.29E-03 372.38	7.42E-03 335.88
6.03E-03 566.42	9.45E-03 436.59	6.09E-03 385.44	9.47E-03 378.64	7.62E-03 336.61
6.14E-03 551.46	9.60E-03 433.16	6.20E-03 388.53	9.65E-03 378.66	7.81E-03 351.22
6.25E-03 546.48	9.75E-03 436.99	6.31E-03 390.13	9.82E-03 382.46	8.01E-03 355.94
6.36E-03 558.18	9.90E-03 434.65	6.43E-03 389.42	9.99E-03 382.68	8.20E-03 337.69
6.48E-03 556.97	1.00E-02 433.23	6.54E-03 403.73	1.02E-02 385.41	8.39E-03 328.60
6.58E-03 567.34	1.02E-02 435.67	6.66E-03 389.70	1.03E-02 403.23	8.57E-03 338.42
6.79E-03 553.90	1.03E-02 443.07	6.78E-03 376.03	1.05E-02 403.64	8.76E-03 348.68
7.01E-03 544.16	1.05E-02 439.14	6.91E-03 382.76	1.07E-02 386.78	8.94E-03 331.89
7.21E-03 542.57	1.06E-02 442.56	7.03E-03 389.00	1.08E-02 373.95	9.12E-03 318.78
7.42E-03 543.02	1.08E-02 445.40	7.16E-03 384.86	1.10E-02 354.81	9.29E-03 324.41
7.62E-03 543.99	1.09E-02 450.20	7.30E-03 379.69	1.12E-02 358.16	9.47E-03 332.44
7.81E-03 541.74	1.11E-02 451.15	7.43E-03 388.16	1.14E-02 358.53	9.65E-03 333.40
8.01E-03 548.58	1.12E-02 453.83	7.57E-03 389.56	1.15E-02 340.76	9.82E-03 336.21
8.20E-03 542.11	1.14E-02 448.07	7.71E-03 385.58	1.17E-02 333.98	9.99E-03 337.44
8.39E-03 544.93	1.15E-02 445.87	7.86E-03 386.30	1.19E-02 350.46	1.02E-02 335.56
8.57E-03 546.35	1.16E-02 444.12	8.01E-03 395.54	1.20E-02 320.30	1.03E-02 334.40
8.76E-03 557.33	1.18E-02 421.04	8.17E-03 388.11	1.22E-02 284.25	1.05E-02 337.28
8.94E-03 562.92	1.19E-02 451.93	8.33E-03 395.95	1.24E-02 286.86	1.07E-02 336.23
9.12E-03 565.76	1.21E-02 453.03	8.51E-03 380.97	1.25E-02 298.92	1.08E-02 337.83
9.29E-03 566.34	1.22E-02 453.90	8.69E-03 403.72	1.27E-02 314.40	1.10E-02 337.90
9.47E-03 572.42	1.24E-02 455.40	8.87E-03 425.66	1.29E-02 299.50	1.12E-02 318.52
9.65E-03 569.27	1.25E-02 459.74	9.52E-03 427.81	1.30E-02 290.03	1.14E-02 310.54
9.82E-03 573.80	1.26E-02 458.84	9.65E-03 405.45	1.32E-02 308.42	1.15E-02 297.53
9.99E-03 586.72	1.28E-02 459.99	9.82E-03 407.05	1.34E-02 285.48	1.17E-02 300.49
1.02E-02 592.80	1.29E-02 460.37	9.99E-03 407.97	1.35E-02 274.21	1.19E-02 281.23
1.03E-02 600.51	1.31E-02 459.72	1.02E-02 403.23	1.37E-02 284.36	1.20E-02 291.69
1.05E-02 600.74	1.32E-02 463.99	1.03E-02 404.56	1.39E-02 278.97	1.22E-02 280.37
1.07E-02 609.24	1.34E-02 462.68	1.05E-02 413.23	1.40E-02 279.07	1.24E-02 275.26
1.08E-02 589.56	1.35E-02 470.07	1.07E-02 399.64	1.42E-02 281.76	1.25E-02 277.77
1.10E-02 589.68	1.37E-02 464.47	1.08E-02 404.18	1.44E-02 274.69	1.27E-02 280.75
1.12E-02 588.32	1.38E-02 495.94	1.10E-02 393.32	1.45E-02 277.96	1.29E-02 271.70
1.14E-02 604.28	1.39E-02 495.68	1.12E-02 376.20	1.47E-02 280.02	1.30E-02 268.53
1.17E-02 593.14	1.42E-02 476.59	1.15E-02 366.79	1.50E-02 263.22	1.34E-02 264.67
1.19E-02 551.62	1.44E-02 480.76	1.17E-02 356.01	1.52E-02 259.55	1.35E-02 254.74
1.20E-02 573.77	1.45E-02 477.67	1.19E-02 345.87	1.54E-02 267.58	1.37E-02 249.26
1.22E-02 571.68	1.47E-02 475.14	1.20E-02 350.68	1.56E-02 264.86	1.39E-02 246.31
1.24E-02 601.91	1.48E-02 478.30	1.22E-02 329.85	1.57E-02 266.36	1.40E-02 242.40
1.25E-02 565.52	1.50E-02 475.84	1.24E-02 326.39	1.59E-02 267.75	1.42E-02 243.65
1.27E-02 563.03	1.51E-02 462.45	1.25E-02 328.02	1.61E-02 271.69	1.44E-02 246.36
1.29E-02 584.93	1.52E-02 463.81	1.27E-02 326.71	1.62E-02 273.76	1.45E-02 246.37
1.30E-02 565.02	1.54E-02 467.89	1.29E-02 315.76	1.64E-02 274.76	1.47E-02 248.26
1.32E-02 575.76	1.55E-02 476.10	1.30E-02 307.04	1.66E-02 275.04	1.49E-02 250.30
1.34E-02 575.87	1.57E-02 474.82	1.32E-02 318.85	1.67E-02 278.44	1.50E-02 248.89
1.35E-02 556.91	1.58E-02 473.04	1.34E-02 298.54	1.69E-02 274.91	1.52E-02 238.03
1.37E-02 549.57	1.60E-02 479.00	1.35E-02 302.48	1.71E-02 272.63	1.54E-02 240.63
1.39E-02 557.96	1.61E-02 475.05	1.37E-02 297.67	1.72E-02 275.12	1.56E-02 244.55
1.40E-02 525.84	1.62E-02 475.26	1.39E-02 287.63	1.74E-02 275.99	1.57E-02 245.70
1.42E-02 566.33	1.64E-02 477.64	1.40E-02 287.00	1.76E-02 278.50	1.59E-02 245.75
1.44E-02 562.80	1.65E-02 470.64	1.42E-02 278.28	1.77E-02 285.65	1.61E-02 245.29
1.45E-02 563.90	1.67E-02 470.22	1.44E-02 274.30	1.79E-02 279.11	1.62E-02 246.26
1.47E-02 568.17	1.68E-02 473.09	1.45E-02 271.29	1.81E-02 280.31	1.64E-02 246.24
1.49E-02 561.28	1.70E-02 474.55	1.47E-02 268.56	1.82E-02 276.46	1.66E-02 244.34
1.50E-02 563.24	1.71E-02 470.43	1.49E-02 268.62	1.84E-02 267.54	1.67E-02 241.38
1.52E-02 567.25	1.73E-02 471.69	1.50E-02 264.54	1.86E-02 265.82	1.69E-02 242.63

Table D1b Heat transfer coefficient data from tests 6-10 (cont.)

Test 6 x [m]	h [W/mK] x [m]	Test 7 h [W/mK]	x [m]	Test 8 h [W/mK]	x [m]	Test 9 h [W/mK]	x [m]	Test 10 h [W/mK]	
1.54E-02	537.74	1.74E-02	473.47	1.52E-02	263.60	1.87E-02	281.97	1.71E-02	244.22
1.56E-02	549.51	1.75E-02	476.36	1.54E-02	269.59	1.89E-02	281.57	1.72E-02	243.90
1.57E-02	541.51	1.77E-02	474.59	1.56E-02	261.19	1.91E-02	277.08	1.74E-02	244.44
1.59E-02	542.99	1.78E-02	475.19	1.57E-02	255.89	1.93E-02	276.20	1.76E-02	247.28
1.61E-02	571.88	1.80E-02	472.03	1.59E-02	263.27	1.94E-02	281.92	1.77E-02	249.36
1.62E-02	562.65	1.81E-02	474.52	1.61E-02	266.17	1.96E-02	274.64	1.79E-02	245.33
1.64E-02	579.90	1.83E-02	476.15	1.62E-02	267.45	1.98E-02	275.74	1.81E-02	247.42
1.66E-02	562.57	1.84E-02	476.01	1.64E-02	261.18	1.99E-02	271.31	1.82E-02	253.98
1.67E-02	565.49	1.86E-02	471.28	1.66E-02	264.32	2.01E-02	275.60	1.84E-02	244.74
1.69E-02	561.48	1.87E-02	478.69	1.67E-02	264.09	2.03E-02	271.42	1.86E-02	240.15
1.71E-02	555.87	1.88E-02	475.31	1.69E-02	266.32	2.04E-02	272.64	1.87E-02	238.99
1.72E-02	548.09	1.90E-02	480.98	1.71E-02	267.95	2.06E-02	265.00	1.89E-02	241.64
1.74E-02	546.04	1.91E-02	480.12	1.72E-02	259.09	2.08E-02	273.75	1.91E-02	244.02
1.76E-02	520.83	1.93E-02	477.81	1.74E-02	260.20	2.09E-02	257.91	1.93E-02	239.25
1.77E-02	514.38	1.94E-02	472.28	1.76E-02	263.80	2.11E-02	275.84	1.94E-02	237.22
1.79E-02	511.71	1.96E-02	471.47	1.77E-02	266.53	2.13E-02	269.44	1.96E-02	237.31
1.81E-02	536.06	1.97E-02	468.76	1.79E-02	264.29	2.14E-02	270.37	1.98E-02	236.70
1.82E-02	531.55	1.99E-02	472.27	1.81E-02	263.20	2.16E-02	278.59	1.99E-02	237.53
1.84E-02	494.09	2.00E-02	470.64	1.82E-02	271.22	2.18E-02	276.74	2.01E-02	236.98
1.86E-02	465.55	2.01E-02	465.05	1.84E-02	277.05	2.19E-02	278.15	2.03E-02	233.49
1.87E-02	473.86	2.03E-02	471.12	1.86E-02	269.91	2.21E-02	271.13	2.04E-02	233.33
1.89E-02	474.84	2.04E-02	461.78	1.87E-02	268.28	2.23E-02	265.57	2.06E-02	237.00
1.91E-02	505.41	2.06E-02	460.86	1.89E-02	262.86	2.24E-02	265.32	2.08E-02	240.09
1.93E-02	474.94	2.07E-02	461.56	1.91E-02	262.63	2.26E-02	265.80	2.09E-02	235.46
1.94E-02	468.52	2.09E-02	456.88	1.93E-02	271.65	2.28E-02	260.58	2.11E-02	229.87
1.96E-02	485.63	2.10E-02	459.39	1.94E-02	266.39	2.29E-02	252.66	2.13E-02	230.99
1.98E-02	479.36	2.11E-02	457.36	1.96E-02	262.94	2.31E-02	256.53	2.14E-02	233.27
1.99E-02	448.68	2.13E-02	455.76	1.98E-02	260.88	2.33E-02	251.96	2.16E-02	233.94
2.01E-02	436.04	2.14E-02	452.05	1.99E-02	263.46	2.35E-02	241.61	2.18E-02	234.60
2.03E-02	439.41	2.16E-02	449.01	2.01E-02	258.92	2.36E-02	255.62	2.19E-02	235.11
2.04E-02	443.44	2.17E-02	440.19	2.03E-02	253.93	2.38E-02	249.78	2.21E-02	229.28
2.06E-02	429.48	2.19E-02	447.60	2.04E-02	253.58	2.40E-02	244.42	2.23E-02	229.43
2.08E-02	421.42	2.20E-02	442.75	2.06E-02	255.93	2.41E-02	249.07	2.24E-02	229.83
2.09E-02	422.80	2.22E-02	439.15	2.08E-02	251.88	2.43E-02	251.34	2.26E-02	222.69
2.11E-02	427.13	2.23E-02	435.96	2.09E-02	248.24	2.45E-02	231.36	2.28E-02	231.42
2.13E-02	421.05	2.24E-02	432.00	2.11E-02	251.13	2.46E-02	242.31	2.29E-02	228.51
2.14E-02	422.23	2.26E-02	427.76	2.13E-02	252.94	2.48E-02	238.95	2.31E-02	230.34
2.16E-02	417.32	2.27E-02	421.90	2.14E-02	255.83	2.50E-02	233.44	2.33E-02	228.01
2.18E-02	427.55	2.29E-02	426.44	2.16E-02	255.43	2.51E-02	232.54	2.35E-02	226.64
2.19E-02	422.01	2.30E-02	414.81	2.18E-02	263.71	2.53E-02	235.67	2.36E-02	223.72
2.21E-02	418.06	2.32E-02	410.53	2.19E-02	246.77	2.55E-02	230.75	2.38E-02	221.44
2.23E-02	415.90	2.33E-02	416.30	2.21E-02	244.51	2.56E-02	231.29	2.40E-02	220.66
2.24E-02	405.73	2.35E-02	408.83	2.23E-02	243.74	2.58E-02	240.36	2.41E-02	221.95
2.26E-02	418.75	2.36E-02	400.06	2.24E-02	244.29	2.60E-02	236.03	2.43E-02	220.84
2.28E-02	411.43	2.37E-02	397.48	2.26E-02	239.82	2.61E-02	233.24	2.45E-02	219.16
2.29E-02	408.94	2.39E-02	390.63	2.28E-02	244.77	2.63E-02	228.62	2.46E-02	221.63
2.31E-02	405.65	2.40E-02	395.92	2.29E-02	247.52	2.65E-02	229.03	2.48E-02	223.95
2.33E-02	408.86	2.42E-02	390.22	2.31E-02	249.63	2.66E-02	232.97	2.50E-02	219.37
2.35E-02	421.38	2.43E-02	390.55	2.33E-02	235.46	2.68E-02	227.69	2.51E-02	215.70
2.36E-02	409.06	2.45E-02	388.46	2.35E-02	243.03	2.70E-02	224.76	2.53E-02	214.08
2.38E-02	426.18	2.46E-02	384.60	2.36E-02	237.51	2.72E-02	222.46	2.55E-02	213.62
2.40E-02	415.58	2.48E-02	387.31	2.38E-02	238.80	2.73E-02	222.28	2.56E-02	212.40
2.41E-02	430.97	2.49E-02	375.85	2.40E-02	237.87	2.75E-02	241.76	2.58E-02	210.13
2.43E-02	412.21	2.50E-02	373.40	2.41E-02	226.27	2.77E-02	219.12	2.60E-02	212.75
2.45E-02	416.04	2.52E-02	382.84	2.43E-02	230.49	2.78E-02	221.84	2.61E-02	210.42
2.46E-02	403.05	2.53E-02	364.01	2.45E-02	230.66	2.80E-02	222.60	2.63E-02	204.28
2.48E-02	412.03	2.55E-02	360.13	2.46E-02	232.28	2.82E-02	223.85	2.65E-02	201.57
2.50E-02	403.57	2.56E-02	358.59	2.48E-02	234.25	2.83E-02	217.42	2.66E-02	202.32
2.51E-02	402.16	2.58E-02	347.41	2.50E-02	226.56	2.85E-02	209.81	2.68E-02	198.33
2.53E-02	400.42	2.59E-02	346.86	2.51E-02	224.04	2.87E-02	216.94	2.70E-02	197.70
2.55E-02	400.94	2.60E-02	345.03	2.53E-02	222.79	2.88E-02	214.79	2.72E-02	195.87
2.56E-02	399.70	2.62E-02	338.92	2.55E-02	221.22	2.90E-02	205.55	2.73E-02	196.66
2.58E-02	393.49	2.63E-02	347.39	2.56E-02	224.09	2.92E-02	201.88	2.75E-02	195.27

Table D1b Heat transfer coefficient data from tests 6-10 (cont.)

Test 6 x [m]	h [W/mK] x [m]	Test 7 h [W/mK] x [m]	Test 8 h [W/mK] x [m]	Test 9 h [W/mK] x [m]	Test 10 h [W/mK] x [m]
2.60E-02	387.81	2.65E-02	333.54	2.58E-02	216.82
2.61E-02	378.41	2.66E-02	328.66	2.60E-02	216.07
2.63E-02	379.73	2.68E-02	323.62	2.61E-02	224.16
2.65E-02	410.53	2.69E-02	314.58	2.63E-02	220.31
2.66E-02	387.29	2.71E-02	312.88	2.65E-02	219.10
2.68E-02	384.35	2.72E-02	313.87		3.02E-02
2.70E-02	373.14	2.73E-02	310.73		2.03E-02
2.72E-02	365.03	2.75E-02	309.30		3.05E-02
2.73E-02	380.74	2.76E-02	311.95		3.07E-02
2.75E-02	384.83	2.78E-02	302.60		3.09E-02
2.77E-02	374.50	2.79E-02	296.60		3.10E-02
2.78E-02	351.35	2.81E-02	292.79		3.12E-02
2.80E-02	350.49	2.82E-02	289.71		3.14E-02
2.82E-02	371.94	2.84E-02	288.87		3.15E-02
2.83E-02	363.00	2.85E-02	285.23		3.17E-02
2.85E-02	353.87	2.86E-02	284.33		3.19E-02
2.87E-02	350.07	2.88E-02	280.83		3.20E-02
2.88E-02	372.62	2.89E-02	277.44		3.22E-02
2.90E-02	367.62	2.91E-02	266.77		3.24E-02
2.92E-02	354.95	2.92E-02	268.62		3.25E-02
2.93E-02	349.78	2.94E-02	268.74		3.27E-02
2.95E-02	355.26	2.95E-02	268.96		3.29E-02
2.97E-02	344.08	2.96E-02	262.56		3.30E-02
2.98E-02	338.83	2.98E-02	263.21		3.32E-02
3.00E-02	334.76	2.99E-02	262.03		3.34E-02
3.02E-02	339.09	3.01E-02	259.28		3.35E-02
3.03E-02	338.24	3.02E-02	246.81		3.37E-02
3.05E-02	344.59	3.04E-02	253.43		3.39E-02
3.07E-02	302.20	3.05E-02	256.01		3.40E-02
3.09E-02	304.28	3.07E-02	246.43		3.42E-02
3.10E-02	313.94	3.08E-02	221.17		3.44E-02
3.12E-02	326.46	3.09E-02	232.21		3.45E-02
3.14E-02	340.32	3.11E-02	237.13		3.47E-02
3.15E-02	340.85	3.12E-02	227.96		3.49E-02
3.17E-02	314.96	3.14E-02	216.96		3.51E-02
3.19E-02	306.93	3.15E-02	225.40		3.52E-02
3.20E-02	302.19	3.17E-02	211.55		3.54E-02
3.22E-02	303.65	3.18E-02	233.32		3.56E-02
3.24E-02	301.38	3.20E-02	231.43		3.57E-02
3.25E-02	293.30				3.59E-02
3.27E-02	279.90				3.61E-02
3.29E-02	283.48				3.62E-02
3.30E-02	279.99				3.64E-02
3.32E-02	277.14				3.66E-02
3.34E-02	275.47				3.67E-02
3.35E-02	281.06				3.69E-02
3.37E-02	270.24				3.71E-02
3.39E-02	264.36				3.72E-02
3.40E-02	270.01				3.74E-02
					3.76E-02
					203.69

Table D1c Heat transfer coefficient data from tests 11-15

Test 11 x [m]	h [W/mK] x [m]	Test 12 h [W/mK] x [m]	Test 13 h [W/mK] x [m]	Test 14 h [W/mK] x [m]	Test 15 h [W/mK] x [m]
0.00E+00	522.65	0.00E+00	261.90	0.00E+00	221.05
7.63E-05	536.21	7.63E-05	262.25	7.41E-05	220.22
1.53E-04	532.60	1.53E-04	264.47	1.48E-04	219.68
2.29E-04	508.28	2.29E-04	265.91	2.22E-04	218.56
3.05E-04	521.42	3.05E-04	264.18	2.96E-04	219.72
3.82E-04	520.75	3.82E-04	263.67	3.71E-04	220.04
4.58E-04	513.08	4.58E-04	262.14	4.45E-04	220.90
5.35E-04	506.11	5.35E-04	260.89	5.19E-04	221.19
6.11E-04	502.81	6.11E-04	258.51	5.93E-04	221.71
6.88E-04	500.74	6.88E-04	257.09	6.68E-04	221.46
7.65E-04	498.94	7.65E-04	254.42	7.42E-04	221.87
8.41E-04	497.09	8.41E-04	251.35	8.16E-04	222.95
9.18E-04	492.54	9.18E-04	249.32	8.91E-04	223.37
9.95E-04	482.88	9.95E-04	247.32	9.66E-04	223.56
1.07E-03	476.74	1.07E-03	246.00	1.04E-03	223.31
1.15E-03	478.72	1.15E-03	245.48	1.12E-03	222.23
1.23E-03	482.85	1.23E-03	244.22	1.19E-03	221.81
1.30E-03	486.19	1.30E-03	243.58	1.27E-03	221.36
1.38E-03	486.39	1.38E-03	241.81	1.34E-03	221.35
1.46E-03	486.40	1.46E-03	241.80	1.42E-03	220.75
1.54E-03	480.56	1.54E-03	243.17	1.49E-03	219.16
1.62E-03	475.30	1.62E-03	243.41	1.57E-03	218.23
1.69E-03	476.90	1.69E-03	243.44	1.64E-03	218.27
1.77E-03	476.65	1.77E-03	245.26	1.72E-03	217.39
1.85E-03	476.27	1.85E-03	244.98	1.79E-03	216.93
1.93E-03	474.25	1.93E-03	245.16	1.87E-03	216.58
2.01E-03	472.09	2.01E-03	237.33	1.95E-03	215.94
2.09E-03	470.22	2.09E-03	240.22	2.02E-03	215.68
2.17E-03	472.75	2.17E-03	242.59	2.10E-03	215.94
2.25E-03	477.80	2.25E-03	244.03	2.18E-03	216.27
2.33E-03	486.69	2.33E-03	235.63	2.26E-03	217.52
2.41E-03	494.50	2.41E-03	236.73	2.33E-03	216.46
2.49E-03	492.74	2.49E-03	236.75	2.41E-03	216.63
2.57E-03	488.39	2.57E-03	238.41	2.49E-03	217.29
2.65E-03	486.07	2.65E-03	229.79	2.57E-03	218.31
2.73E-03	484.67	2.73E-03	230.12	2.65E-03	219.34
2.81E-03	497.82	2.81E-03	229.18	2.72E-03	220.26
2.89E-03	484.26	2.89E-03	227.56	2.80E-03	221.83
2.98E-03	475.76	2.98E-03	235.29	2.88E-03	222.51
3.06E-03	467.30	3.06E-03	234.43	2.96E-03	222.00
3.14E-03	460.73	3.14E-03	234.26	3.04E-03	224.49
3.23E-03	463.53	3.23E-03	233.82	3.12E-03	225.17
3.31E-03	464.00	3.31E-03	234.62	3.20E-03	224.00
3.39E-03	460.16	3.39E-03	234.84	3.29E-03	222.83
3.48E-03	456.99	3.48E-03	233.51	3.37E-03	224.26
3.56E-03	428.58	3.56E-03	233.78	3.45E-03	225.70
3.65E-03	427.28	3.65E-03	235.81	3.53E-03	225.10
3.74E-03	432.34	3.74E-03	227.20	3.62E-03	227.16
3.82E-03	435.89	3.82E-03	232.23	3.70E-03	229.77
3.91E-03	432.34	3.91E-03	236.59	3.78E-03	230.76
4.00E-03	426.24	4.00E-03	233.93	3.87E-03	234.81
4.09E-03	407.33	4.09E-03	233.02	3.95E-03	236.40
4.18E-03	427.21	4.18E-03	234.54	4.04E-03	237.16
4.27E-03	426.18	4.27E-03	232.49	4.12E-03	233.83
4.36E-03	434.39	4.36E-03	240.27	4.21E-03	230.98
4.45E-03	456.71	4.45E-03	237.06	4.30E-03	234.35
4.54E-03	445.94	4.54E-03	236.60	4.39E-03	231.06
4.63E-03	453.42	4.63E-03	240.47	4.48E-03	227.10
4.72E-03	459.98	4.72E-03	242.05	4.56E-03	231.34
4.82E-03	461.47	4.82E-03	241.90	4.65E-03	228.96
4.91E-03	475.67	4.91E-03	239.96	4.75E-03	226.33
5.01E-03	455.18	5.01E-03	238.64	4.84E-03	224.62
5.11E-03	442.57	5.11E-03	241.84	4.93E-03	226.91

Table D1c Heat transfer coefficient data from tests 11-15 (cont.)

Test 11	Test 12	Test 13	Test 14	Test 15				
x [m]	h [W/mK]							
5.20E-03	437.28	5.20E-03	242.02	5.02E-03	228.17	4.48E-03	512.58	
5.30E-03	416.36	5.30E-03	244.26	5.12E-03	224.84	4.56E-03	515.40	
5.40E-03	422.44	5.40E-03	242.40	5.21E-03	225.26	4.64E-03	525.58	
5.50E-03	414.73	5.50E-03	240.61	5.31E-03	225.92	4.73E-03	512.26	
5.61E-03	410.96	5.61E-03	243.56	5.40E-03	218.72	4.81E-03	500.88	
5.71E-03	411.54	5.71E-03	242.64	5.50E-03	217.53	4.89E-03	510.21	
5.82E-03	409.17	5.82E-03	244.09	5.60E-03	221.57	4.98E-03	516.88	
5.92E-03	404.87	5.92E-03	243.14	5.70E-03	227.44	5.06E-03	521.95	
6.03E-03	413.86	6.03E-03	244.10	5.80E-03	227.37	5.15E-03	509.30	
6.14E-03	406.05	6.14E-03	246.25	5.91E-03	227.65	5.23E-03	505.45	
6.25E-03	418.66	6.25E-03	246.02	6.01E-03	231.21	5.32E-03	506.51	
6.36E-03	411.98	6.36E-03	249.30	6.12E-03	231.51	5.41E-03	509.40	
6.48E-03	399.65	6.48E-03	252.08	6.23E-03	233.02	5.50E-03	509.44	
6.59E-03	389.20	6.59E-03	250.67	6.33E-03	235.03	5.59E-03	505.71	
6.71E-03	383.93	6.71E-03	258.75	6.56E-03	235.95	5.68E-03	494.36	
6.83E-03	384.98	6.83E-03	255.61	6.67E-03	239.16	5.77E-03	490.99	
6.96E-03	384.41	6.96E-03	258.28	6.79E-03	236.27	5.86E-03	490.74	
7.08E-03	380.80	7.08E-03	260.80	6.91E-03	237.59	5.96E-03	477.26	
7.21E-03	381.48	7.21E-03	259.87	7.03E-03	234.17	6.05E-03	487.91	
7.35E-03	366.46	7.35E-03	260.86	7.15E-03	228.88	6.15E-03	490.37	
7.48E-03	358.95	7.48E-03	256.56	7.28E-03	227.91	6.25E-03	495.54	
7.62E-03	355.78	7.76E-03	262.26	7.41E-03	226.27	6.35E-03	484.29	
7.76E-03	351.51	7.91E-03	259.49	7.54E-03	226.54	6.45E-03	481.66	
7.91E-03	349.31	8.06E-03	258.66	7.68E-03	226.48	6.55E-03	470.69	
8.06E-03	346.63	8.22E-03	277.98	7.82E-03	221.41	6.71E-03	455.95	
8.39E-03	345.15	8.39E-03	278.82	7.97E-03	221.86	6.91E-03	445.95	
8.57E-03	320.45	8.56E-03	284.29	8.12E-03	218.74	7.10E-03	439.16	
8.76E-03	322.87	8.74E-03	290.60	8.27E-03	220.97	7.29E-03	435.53	
8.94E-03	328.25	8.93E-03	305.75	8.43E-03	234.88	7.48E-03	431.26	
9.12E-03	336.60	9.14E-03	311.61	8.57E-03	237.94	7.66E-03	420.11	
9.29E-03	345.73	9.35E-03	308.56	8.76E-03	240.90	7.84E-03	413.55	
9.47E-03	343.19	9.47E-03	318.67	8.94E-03	242.63	8.02E-03	410.17	
9.65E-03	339.01	9.65E-03	313.63	9.12E-03	244.09	8.20E-03	404.62	
9.82E-03	334.74	9.82E-03	307.62	9.29E-03	243.26	8.37E-03	401.58	
9.99E-03	334.81	9.99E-03	304.62	9.47E-03	241.28	8.54E-03	394.44	
1.02E-02	340.85	1.02E-02	318.89	9.65E-03	243.16	8.71E-03	391.51	
1.03E-02	336.31	1.03E-02	317.31	9.82E-03	243.45	8.88E-03	387.11	
1.05E-02	332.26	1.05E-02	314.32	9.99E-03	243.93	9.05E-03	382.68	
1.07E-02	325.72	1.07E-02	308.25	1.02E-02	250.98	9.21E-03	379.21	
1.08E-02	336.51	1.08E-02	307.86	1.03E-02	255.94	9.38E-03	375.94	
1.12E-02	308.61	1.12E-02	325.42	1.07E-02	241.77	9.70E-03	373.24	
1.14E-02	311.10	1.14E-02	331.73	1.08E-02	247.18	9.86E-03	373.88	
1.15E-02	298.74	1.15E-02	331.20	1.10E-02	258.56	1.00E-02	373.28	
1.17E-02	307.67	1.17E-02	330.95	1.12E-02	256.67	1.02E-02	373.14	
1.19E-02	313.33	1.19E-02	333.31	1.14E-02	250.84	1.03E-02	373.14	
1.20E-02	294.11	1.20E-02	332.44	1.15E-02	247.74	1.05E-02	373.08	
1.22E-02	298.63	1.22E-02	328.13	1.17E-02	250.35	1.07E-02	372.40	
1.24E-02	291.02	1.24E-02	329.67	1.19E-02	253.37	1.08E-02	370.36	
1.25E-02	293.96	1.25E-02	326.20	1.20E-02	270.70	1.10E-02	364.34	
1.27E-02	288.31	1.27E-02	324.77	1.22E-02	270.48	1.11E-02	359.98	
1.29E-02	268.67	1.29E-02	321.19	1.24E-02	261.24	1.13E-02	353.72	
1.30E-02	278.44	1.30E-02	318.63	1.25E-02	254.12	1.14E-02	353.05	
1.32E-02	266.56	1.32E-02	317.77	1.27E-02	255.76	1.16E-02	342.37	
1.34E-02	267.25	1.34E-02	323.40	1.29E-02	250.54	1.17E-02	335.47	
1.35E-02	258.33	1.35E-02	331.02	1.30E-02	253.07	1.19E-02	332.35	
1.37E-02	251.92	1.37E-02	323.03	1.32E-02	264.83	1.20E-02	322.78	
1.39E-02	251.02	1.39E-02	320.73	1.34E-02	268.28	1.22E-02	321.35	
1.40E-02	249.16	1.40E-02	320.44	1.35E-02	268.43	1.24E-02	317.88	
1.42E-02	247.72	1.42E-02	320.02	1.37E-02	268.54	1.25E-02	314.26	
1.44E-02	246.22	1.44E-02	330.82	1.39E-02	268.78	1.27E-02	308.45	
1.45E-02	238.52	1.45E-02	331.31	1.40E-02	265.98	1.28E-02	305.71	
1.47E-02	236.59	1.47E-02	327.39	1.42E-02	265.28	1.30E-02	303.51	
1.49E-02	238.70	1.49E-02	325.44	1.44E-02	273.93	1.31E-02	299.57	
							1.45E-02	380.22

Table D1c Heat transfer coefficient data from tests 11-15 (cont.)

Test 11 x [m]	h [W/mK]	Test 12 x [m]	h [W/mK]	Test 13 x [m]	h [W/mK]	Test 14 x [m]	h [W/mK]	Test 15 x [m]	h [W/mK]
1.50E-02	237.40	1.50E-02	322.24	1.45E-02	283.58	1.33E-02	298.49	1.47E-02	372.43
1.52E-02	242.41	1.52E-02	302.96	1.47E-02	274.52	1.34E-02	296.88	1.48E-02	367.32
1.54E-02	244.24	1.54E-02	309.67	1.49E-02	268.65	1.36E-02	297.12	1.50E-02	377.67
1.56E-02	245.05	1.56E-02	315.54	1.50E-02	269.34	1.38E-02	295.50	1.52E-02	364.39
1.57E-02	238.59	1.57E-02	313.69	1.52E-02	270.69	1.39E-02	293.11	1.53E-02	353.13
1.59E-02	234.05	1.59E-02	311.27	1.54E-02	266.92	1.41E-02	291.36	1.55E-02	351.08
1.61E-02	243.23	1.61E-02	295.72	1.56E-02	275.43	1.42E-02	290.81	1.56E-02	341.58
1.62E-02	243.18	1.62E-02	294.27	1.57E-02	276.93	1.44E-02	289.21	1.58E-02	342.08
1.64E-02	240.76	1.64E-02	294.35	1.59E-02	276.21	1.45E-02	288.05	1.59E-02	347.80
1.66E-02	236.45	1.66E-02	296.19	1.61E-02	281.37	1.47E-02	287.30	1.61E-02	340.59
1.67E-02	241.00	1.67E-02	308.38	1.62E-02	284.38	1.48E-02	286.44	1.62E-02	343.28
1.69E-02	241.98	1.69E-02	303.09	1.64E-02	286.11	1.50E-02	285.08	1.64E-02	347.07
1.71E-02	243.94	1.71E-02	292.27	1.66E-02	286.23	1.52E-02	280.62	1.65E-02	349.22
1.72E-02	248.66	1.72E-02	293.42	1.67E-02	287.36	1.53E-02	276.16	1.67E-02	347.44
1.74E-02	254.48	1.74E-02	276.21	1.69E-02	287.35	1.55E-02	274.04	1.69E-02	341.78
1.76E-02	250.11	1.76E-02	267.64	1.71E-02	290.48	1.56E-02	274.47	1.70E-02	351.16
1.77E-02	246.30	1.77E-02	259.95	1.72E-02	292.20	1.58E-02	276.13	1.72E-02	346.48
1.79E-02	247.11	1.79E-02	265.75	1.74E-02	292.32	1.59E-02	276.27	1.73E-02	338.10
1.81E-02	255.13	1.81E-02	266.43	1.76E-02	291.09	1.61E-02	276.30	1.75E-02	337.01
1.82E-02	255.05	1.82E-02	263.40	1.77E-02	294.41	1.62E-02	275.04	1.76E-02	334.95
1.84E-02	254.23	1.84E-02	258.90	1.79E-02	292.38	1.64E-02	273.90	1.78E-02	339.50
1.86E-02	249.75	1.86E-02	258.18	1.81E-02	286.58	1.65E-02	274.04	1.79E-02	336.30
1.87E-02	247.97	1.87E-02	258.38	1.82E-02	290.78	1.67E-02	275.87	1.81E-02	340.39
1.89E-02	247.78	1.89E-02	253.17	1.84E-02	292.47	1.69E-02	276.58	1.83E-02	336.06
1.91E-02	248.22	1.91E-02	243.76	1.86E-02	291.83	1.70E-02	276.25	1.84E-02	327.67
1.93E-02	242.42	1.93E-02	251.44	1.87E-02	291.34	1.72E-02	275.30	1.86E-02	317.06
1.94E-02	242.94	1.94E-02	246.27	1.89E-02	283.45	1.73E-02	274.24	1.87E-02	319.67
1.96E-02	241.50	1.96E-02	239.67	1.91E-02	285.89	1.75E-02	275.51	1.89E-02	313.40
1.98E-02	239.79	1.98E-02	238.79	1.93E-02	284.13	1.76E-02	273.43	1.90E-02	313.07
1.99E-02	231.36	1.99E-02	232.25	1.94E-02	286.02	1.78E-02	272.60	1.92E-02	308.48
2.01E-02	233.66	2.01E-02	230.10	1.96E-02	289.18	1.79E-02	272.19	1.93E-02	306.30
2.03E-02	234.77	2.03E-02	231.57	1.98E-02	297.97	1.81E-02	273.03	1.95E-02	306.05
2.04E-02	228.89	2.04E-02	227.61	1.99E-02	286.16	1.83E-02	272.88	1.97E-02	300.87
2.06E-02	229.72	2.06E-02	225.47	2.01E-02	278.42	1.84E-02	272.38	1.98E-02	300.41
2.08E-02	228.35	2.08E-02	230.66	2.03E-02	274.14	1.86E-02	271.06	2.00E-02	306.15
2.09E-02	231.21	2.09E-02	230.70	2.04E-02	273.18	1.87E-02	270.58	2.01E-02	296.32
2.11E-02	233.59	2.11E-02	219.28	2.06E-02	276.48	1.89E-02	271.06	2.03E-02	294.34
2.13E-02	234.59	2.13E-02	219.93	2.08E-02	275.64	1.90E-02	270.76	2.04E-02	287.87
2.14E-02	229.15	2.14E-02	219.91	2.09E-02	262.19	1.92E-02	269.67	2.06E-02	302.12
2.16E-02	224.52	2.16E-02	212.37	2.11E-02	272.65	1.93E-02	268.80	2.07E-02	289.98
2.18E-02	222.26	2.18E-02	206.87	2.13E-02	269.43	1.95E-02	268.25	2.09E-02	286.65
2.19E-02	238.77	2.19E-02	220.52	2.14E-02	260.97	1.97E-02	267.64	2.10E-02	281.96
2.21E-02	231.41	2.21E-02	218.33	2.16E-02	258.44	1.98E-02	268.25	2.12E-02	290.68
2.23E-02	226.05	2.23E-02	219.18	2.18E-02	236.91	2.00E-02	268.09	2.14E-02	285.67
2.24E-02	224.54	2.24E-02	207.36	2.19E-02	251.02	2.01E-02	265.97	2.15E-02	283.31
2.26E-02	222.60	2.26E-02	208.31	2.21E-02	252.41	2.03E-02	265.19	2.17E-02	277.53
2.28E-02	221.89	2.28E-02	209.21	2.23E-02	251.18	2.04E-02	265.10	2.18E-02	281.53
2.29E-02	225.42	2.29E-02	206.91	2.24E-02	210.49	2.06E-02	265.13	2.20E-02	283.42
2.31E-02	226.25	2.31E-02	208.43	2.26E-02	224.90	2.07E-02	264.83	2.21E-02	278.43
2.33E-02	223.86	2.33E-02	206.72	2.28E-02	229.99	2.09E-02	263.50	2.23E-02	274.71
2.35E-02	221.13	2.35E-02	203.81	2.29E-02	234.89	2.10E-02	263.02	2.24E-02	271.40
2.36E-02	218.85	2.36E-02	195.99	2.31E-02	248.36	2.12E-02	262.30	2.26E-02	267.93
2.38E-02	217.10	2.38E-02	197.19	2.33E-02	227.75	2.14E-02	261.96	2.28E-02	263.90
2.40E-02	217.18	2.40E-02	199.09	2.35E-02	226.27	2.15E-02	261.34	2.29E-02	264.28
2.41E-02	216.34	2.41E-02	199.83	2.36E-02	226.79	2.17E-02	260.86	2.31E-02	246.98
2.43E-02	217.47	2.43E-02	192.22	2.38E-02	201.45	2.18E-02	260.72	2.32E-02	246.51
2.45E-02	212.94	2.45E-02	185.50	2.40E-02	204.81	2.20E-02	259.59	2.34E-02	245.78
2.46E-02	211.40	2.46E-02	187.77	2.41E-02	204.52	2.21E-02	258.21	2.35E-02	249.42
2.48E-02	208.16	2.48E-02	189.90	2.43E-02	198.36	2.23E-02	256.24	2.37E-02	240.59
2.50E-02	205.95	2.50E-02	188.84	2.45E-02	197.83	2.24E-02	255.40	2.38E-02	245.94
2.51E-02	206.73	2.51E-02	188.85	2.46E-02	194.55	2.26E-02	254.96	2.40E-02	245.10
2.53E-02	201.33	2.53E-02	189.60	2.48E-02	189.09	2.28E-02	252.99	2.42E-02	241.61
2.55E-02	201.04	2.55E-02	191.00	2.50E-02	187.72	2.29E-02	253.20	2.43E-02	236.38

Table D1c Heat transfer coefficient data from tests 11-15 (cont.)

Test 11 x [m]	h [W/mK] x [m]	Test 12 h [W/mK] x [m]	Test 13 h [W/mK] x [m]	Test 14 h [W/mK] x [m]	Test 15 h [W/mK]
2.56E-02	204.06	2.56E-02	191.74	2.51E-02	189.12
2.58E-02	200.84	2.58E-02	186.75	2.53E-02	190.71
2.60E-02	200.29	2.60E-02	183.55	2.55E-02	180.92
2.61E-02	204.19	2.61E-02	177.68	2.56E-02	189.11
2.63E-02	206.69	2.63E-02	176.30	2.58E-02	187.57
2.65E-02	201.61	2.65E-02	180.81	2.60E-02	183.82
2.66E-02	195.54	2.66E-02	180.15	2.61E-02	187.97
2.68E-02	195.45	2.68E-02	180.79	2.63E-02	186.23
2.70E-02	200.29	2.70E-02	182.21	2.65E-02	180.85
2.72E-02	200.35	2.72E-02	177.76	2.66E-02	181.88
2.73E-02	195.51	2.73E-02	175.84	2.68E-02	187.18
2.75E-02	203.91	2.75E-02	182.73	2.70E-02	186.19
2.77E-02	205.60	2.77E-02	174.48	2.72E-02	179.96
2.78E-02	205.88	2.78E-02	177.31	2.73E-02	184.09
2.80E-02	199.87	2.80E-02	177.09	2.75E-02	174.45
2.82E-02	197.88	2.82E-02	176.90	2.77E-02	172.32
2.83E-02	193.64	2.83E-02	175.49	2.78E-02	173.85
2.85E-02	201.25	2.85E-02	173.76	2.80E-02	170.27
2.87E-02	201.37	2.87E-02	174.23	2.82E-02	169.49
2.88E-02	204.46	2.88E-02	173.61	2.83E-02	169.86
2.90E-02	199.83	2.90E-02	171.31	2.85E-02	175.83
2.92E-02	196.07	2.92E-02	166.41	2.87E-02	171.82
2.93E-02	199.74	2.93E-02	171.46	2.88E-02	169.08
2.95E-02	195.15	2.95E-02	167.82	2.90E-02	167.79
2.97E-02	197.00	2.97E-02	165.62	2.92E-02	165.54
2.98E-02	191.07	2.98E-02	165.59	2.93E-02	163.49
3.00E-02	189.26	3.00E-02	163.58	2.95E-02	167.31
3.02E-02	185.97	3.02E-02	162.32	2.97E-02	152.46
3.03E-02	182.09	3.03E-02	161.04	2.98E-02	155.43
3.05E-02	178.05	3.05E-02	161.93	3.00E-02	157.71
3.07E-02	179.38	3.07E-02	162.17	3.02E-02	158.13
3.09E-02	178.10	3.09E-02	160.95	3.03E-02	152.15
3.10E-02	177.33	3.10E-02	159.49	3.05E-02	151.17
3.12E-02	175.60	3.12E-02	159.24	3.07E-02	153.53
3.14E-02	177.16	3.14E-02	159.54	3.09E-02	148.19
3.15E-02	178.66	3.15E-02	155.05	3.10E-02	149.33
3.17E-02	177.03	3.17E-02	157.40	3.12E-02	148.93
		3.19E-02	153.85	3.14E-02	146.50
		3.20E-02	149.85	3.15E-02	145.76
		3.22E-02	150.51	3.17E-02	148.16
		3.24E-02	149.52	3.19E-02	146.87
		3.25E-02	151.45	3.20E-02	146.72
		3.27E-02	148.62	3.22E-02	143.99
		3.29E-02	146.02	3.24E-02	143.27
		3.30E-02	145.31	3.25E-02	146.62
		3.32E-02	146.56	3.27E-02	148.03
		3.34E-02	135.83	3.29E-02	147.59
		3.35E-02	139.43	3.30E-02	146.01
		3.37E-02	140.63	3.32E-02	148.56
		3.39E-02	144.72	3.34E-02	148.24
		3.40E-02	145.28	3.35E-02	147.07
		3.42E-02	146.95	3.37E-02	140.10
		3.44E-02	145.43	3.39E-02	142.89
		3.45E-02	139.98	3.40E-02	141.63
		3.47E-02	138.99	3.42E-02	142.84
		3.49E-02	137.03	3.44E-02	146.58
		3.51E-02	134.30	3.45E-02	145.27
		3.52E-02	133.53	3.47E-02	141.49
		3.54E-02	135.03	3.49E-02	142.13
		3.56E-02	133.09	3.51E-02	141.23
		3.57E-02	134.02	3.52E-02	139.43
		3.59E-02	132.71	3.54E-02	142.81
		3.61E-02	132.18	3.56E-02	143.18

Table D1c Heat transfer coefficient data from tests 11-15 (cont.)

Test 11 x [m]	Test 12 h [W/mK] x [m]	Test 13 h [W/mK] x [m]	Test 14 h [W/mK] x [m]	Test 15 h [W/mK] x [m]	h [W/mK]
	3.62E-02	134.35	3.57E-02	128.23	3.42E-02
	3.64E-02	128.42	3.59E-02	127.20	3.44E-02
	3.66E-02	133.98	3.61E-02	126.17	3.45E-02
	3.67E-02	133.98	3.62E-02	130.23	3.47E-02
	3.69E-02	133.56	3.64E-02	132.69	3.49E-02
	3.71E-02	130.92	3.66E-02	131.18	3.50E-02
	3.72E-02	129.76	3.67E-02	130.01	
	3.74E-02	129.54	3.69E-02	131.47	
	3.76E-02	127.87	3.71E-02	133.50	
			3.72E-02	133.17	
			3.74E-02	135.71	
			3.76E-02	135.46	

Table D1d Heat transfer coefficient data from tests 16-19

Test 16 x [m]	Test 17 h [W/mK] x [m]	Test 18 h [W/mK] x [m]	Test 19 h [W/mK] x [m]	h [W/mK]
0.00E+00	484.86	0.00E+00	417.10	0.00E+00
6.54E-05	485.04	6.54E-05	417.74	6.71E-05
1.31E-04	486.75	1.31E-04	416.48	1.34E-04
1.96E-04	489.19	1.96E-04	417.07	2.01E-04
2.61E-04	493.28	2.61E-04	419.38	2.69E-04
3.27E-04	496.53	3.27E-04	421.01	3.36E-04
3.92E-04	497.34	3.92E-04	421.01	4.03E-04
4.58E-04	497.01	4.58E-04	421.21	4.70E-04
5.23E-04	496.36	5.23E-04	420.37	5.37E-04
5.89E-04	488.49	5.89E-04	421.12	6.05E-04
6.54E-04	478.76	6.54E-04	417.49	6.72E-04
7.20E-04	479.47	7.20E-04	413.12	7.39E-04
7.86E-04	478.76	7.86E-04	411.67	8.07E-04
8.51E-04	476.25	8.51E-04	410.47	8.74E-04
9.17E-04	473.80	9.17E-04	409.46	9.42E-04
9.83E-04	469.84	9.83E-04	408.25	1.01E-03
1.05E-03	468.48	1.05E-03	400.12	1.08E-03
1.12E-03	466.31	1.12E-03	398.03	1.15E-03
1.18E-03	465.88	1.18E-03	399.60	1.21E-03
1.25E-03	464.43	1.25E-03	397.86	1.28E-03
1.31E-03	463.50	1.31E-03	396.16	1.35E-03
1.38E-03	463.33	1.38E-03	393.48	1.42E-03
1.45E-03	461.53	1.45E-03	395.32	1.49E-03
1.51E-03	460.20	1.51E-03	391.60	1.55E-03
1.58E-03	457.75	1.58E-03	390.40	1.62E-03
1.65E-03	457.26	1.65E-03	390.20	1.69E-03
1.71E-03	456.61	1.71E-03	389.21	1.76E-03
1.78E-03	455.32	1.78E-03	386.96	1.83E-03
1.85E-03	452.35	1.85E-03	385.28	1.90E-03
1.92E-03	452.35	1.92E-03	380.47	1.97E-03
1.98E-03	452.35	1.98E-03	384.46	2.04E-03
2.05E-03	447.85	2.05E-03	383.32	2.06E-03
2.12E-03	448.94	2.12E-03	377.68	2.13E-03
2.19E-03	453.45	2.19E-03	379.92	2.20E-03
2.26E-03	452.35	2.26E-03	381.03	2.27E-03
2.32E-03	443.47	2.32E-03	380.47	2.34E-03
2.39E-03	448.47	2.39E-03	383.32	2.41E-03
2.46E-03	450.89	2.46E-03	389.21	2.48E-03
2.53E-03	456.32	2.53E-03	391.20	2.55E-03
2.60E-03	455.70	2.60E-03	375.52	2.62E-03
2.67E-03	459.68	2.67E-03	391.20	2.69E-03
2.74E-03	461.53	2.74E-03	380.47	2.76E-03
2.81E-03	463.19	2.81E-03	381.03	2.83E-03

Table D1d Heat transfer coefficient data from tests 16-19 (cont.)

Test 16	Test 17	Test 18	Test 19		
x [m]	h [W/mK] x [m]	h [W/mK] x [m]	h [W/mK] x [m]		
2.88E-03	457.86	2.88E-03	386.24		
2.95E-03	454.89	2.95E-03	390.70		
3.02E-03	455.94	3.02E-03	387.20		
3.09E-03	473.18	3.09E-03	391.20		
3.16E-03	475.55	3.16E-03	391.60		
3.23E-03	475.55	3.23E-03	392.27		
3.31E-03	477.92	3.31E-03	401.68		
3.38E-03	476.25	3.38E-03	393.28		
3.45E-03	466.31	3.45E-03	402.95		
3.52E-03	468.03	3.52E-03	392.70		
3.60E-03	466.31	3.60E-03	391.20		
3.67E-03	471.22	3.67E-03	389.21		
3.74E-03	459.22	3.74E-03	395.32		
3.82E-03	471.22	3.82E-03	392.27		
3.89E-03	476.25	3.89E-03	392.27		
3.97E-03	476.25	3.97E-03	391.60		
4.04E-03	476.25	4.04E-03	392.27		
4.12E-03	458.46	4.12E-03	392.88		
4.20E-03	456.96	4.20E-03	390.70		
4.27E-03	461.53	4.27E-03	391.20		
4.35E-03	458.46	4.35E-03	391.78		
4.43E-03	452.35	4.43E-03	391.45		
4.51E-03	471.22	4.51E-03	392.27		
4.59E-03	459.22	4.59E-03	395.32		
4.67E-03	466.31	4.67E-03	401.68		
4.75E-03	466.31	4.75E-03	393.28		
4.83E-03	475.02	4.83E-03	393.28		
4.91E-03	476.25	4.91E-03	393.78		
4.99E-03	454.57	4.99E-03	393.78		
5.07E-03	455.32	5.07E-03	397.44		
5.16E-03	481.43	5.16E-03	393.28		
5.24E-03	484.86	5.24E-03	392.27		
5.32E-03	481.43	5.32E-03	391.20		
5.41E-03	473.80	5.41E-03	382.20		
5.50E-03	466.31	5.50E-03	403.87		
5.58E-03	476.25	5.58E-03	417.49		
5.67E-03	471.22	5.67E-03	392.27		
5.76E-03	483.48	5.76E-03	393.28		
5.85E-03	477.92	5.85E-03	392.27		
5.94E-03	474.61	5.94E-03	393.28		
6.04E-03	464.74	6.04E-03	387.20		
6.13E-03	456.96	6.13E-03	391.20		
6.23E-03	459.22	6.23E-03	392.70		
6.32E-03	459.22	6.32E-03	397.44		
6.42E-03	486.75	6.42E-03	401.68		
6.52E-03	468.82	6.52E-03	418.67		
6.62E-03	471.22	6.62E-03	392.27		
6.72E-03	471.22	6.72E-03	391.60		
6.82E-03	475.27	6.82E-03	426.94		
6.93E-03	476.25	6.93E-03	392.88		
7.04E-03	474.61	7.04E-03	393.28		
7.15E-03	467.27	7.15E-03	410.15		
7.26E-03	481.43	7.26E-03	391.20		
7.37E-03	503.38	7.37E-03	392.27		
7.49E-03	476.25	7.49E-03	397.44		
7.61E-03	489.37	7.61E-03	401.68		
7.73E-03	492.06	7.73E-03	401.68		
7.86E-03	495.80	7.86E-03	413.37		
7.98E-03	498.43	7.98E-03	392.27		
8.12E-03	495.80	8.12E-03	392.88		
8.40E-03	484.86	8.40E-03	404.13		
8.54E-03	487.79	8.54E-03	426.02		
8.70E-03	489.37	8.70E-03	426.02		
			8.81E-03	328.01	
				9.18E-03	417.20

Table D1d Heat transfer coefficient data from tests 16-19 (cont.)

Test 16	Test 17	Test 18	Test 19
x [m]	h [W/mK]	x [m]	h [W/mK]
8.86E-03	467.00	8.86E-03	412.80
9.03E-03	518.45	9.03E-03	409.91
9.21E-03	496.53	9.21E-03	410.47
9.40E-03	535.85	9.40E-03	415.10
9.60E-03	496.53	9.60E-03	411.67
9.83E-03	492.06	9.83E-03	413.37
1.01E-02	503.38	1.01E-02	417.49
1.04E-02	546.14	1.07E-02	408.25
1.07E-02	547.67	1.12E-02	408.25
1.12E-02	549.44	1.17E-02	426.02
1.17E-02	555.79	1.22E-02	424.21
1.22E-02	570.82	1.27E-02	422.31
1.27E-02	578.72	1.32E-02	419.94
1.32E-02	580.33	1.37E-02	441.58
1.37E-02	578.72	1.42E-02	425.30
1.42E-02	592.65	1.47E-02	454.16
1.47E-02	595.41	1.52E-02	441.58
1.52E-02	626.66	1.57E-02	466.00
1.57E-02	577.15	1.62E-02	497.27
1.62E-02	565.77	1.67E-02	469.90
1.67E-02	533.58	1.72E-02	516.39
1.72E-02	578.72	1.77E-02	481.90
1.77E-02	509.32	1.82E-02	502.70
1.82E-02	507.87	1.87E-02	476.05
1.87E-02	503.38	1.92E-02	496.22
1.92E-02	457.86	1.97E-02	491.99
1.97E-02	439.21	2.02E-02	491.99
2.02E-02	440.70	2.07E-02	497.27
2.07E-02	447.85	2.12E-02	491.99
2.12E-02	427.00	2.17E-02	497.27
2.17E-02	397.81	2.22E-02	489.44
2.22E-02	404.65	2.27E-02	489.44
2.27E-02	376.12	2.37E-02	450.47
2.32E-02	377.63	2.42E-02	469.15
2.37E-02	376.70	2.47E-02	460.00
2.42E-02	376.12	2.52E-02	419.06
2.47E-02	359.78	2.57E-02	418.67
2.52E-02	359.78	2.62E-02	406.01
2.57E-02	347.47	2.67E-02	406.01
2.62E-02	350.63	2.72E-02	350.41
2.67E-02	342.82	2.77E-02	368.76
2.72E-02	345.13	2.82E-02	380.07
2.77E-02	345.13	2.87E-02	380.07
2.82E-02	328.28	2.92E-02	355.43
2.87E-02	327.88	2.97E-02	334.77
2.92E-02	326.85	3.02E-02	333.43
2.97E-02	310.87	3.07E-02	331.74
3.02E-02	312.64	3.12E-02	329.95
3.07E-02	313.70	3.17E-02	331.74
3.12E-02	279.67	3.22E-02	318.04
3.17E-02	295.54	3.27E-02	303.03
3.22E-02	283.86	3.32E-02	303.03
3.27E-02	282.44	3.37E-02	303.51
3.32E-02	272.72	3.42E-02	300.33
3.37E-02	272.72	3.47E-02	299.09
3.42E-02	254.32	3.52E-02	278.76
3.47E-02	254.64	3.57E-02	280.04
3.52E-02	254.64	3.62E-02	267.19
3.57E-02	250.93	3.67E-02	274.38
3.62E-02	242.03	3.72E-02	261.52
3.67E-02	238.34	3.77E-02	254.59
3.72E-02	238.34	3.82E-02	254.08
3.77E-02	246.38	3.87E-02	261.30

Table D1d Heat transfer coefficient data from tests 16-19 (cont.)

Test 16 x [m]	h [W/mK] x [m]	Test 17 h [W/mK] x [m]	Test 18 h [W/mK] x [m]	Test 19 h [W/mK] x [m]	h [W/mK]
3.82E-02	237.45	3.92E-02	257.00	3.16E-02	332.46
3.87E-02	238.04	3.97E-02	248.10	3.18E-02	324.51
3.92E-02	230.05	4.02E-02	241.36	3.19E-02	323.36
3.97E-02	220.41	4.07E-02	241.54	3.21E-02	320.78
4.02E-02	223.92	4.12E-02	241.23	3.22E-02	315.40
4.07E-02	220.64	4.17E-02	235.96	3.24E-02	314.40
4.12E-02	224.80	4.22E-02	236.08	3.25E-02	312.35
4.17E-02	224.29	4.27E-02	235.82	3.27E-02	309.86
4.22E-02	223.39	4.32E-02	228.72	3.28E-02	307.86
4.27E-02	219.51	4.37E-02	228.96	3.30E-02	306.65
		4.42E-02	228.47	3.32E-02	301.98
				3.33E-02	301.74
				3.35E-02	300.55
				3.36E-02	299.92
				3.38E-02	298.15
				3.39E-02	296.83
				3.41E-02	295.50
				3.42E-02	293.80
				3.44E-02	290.66
				3.45E-02	288.64
				3.47E-02	287.84
				3.49E-02	286.54
				3.50E-02	284.43
				3.63E-02	271.33
				3.68E-02	270.74
				3.73E-02	257.40
				3.78E-02	256.87
				3.83E-02	248.20
				3.88E-02	248.48
				3.93E-02	243.17
				3.98E-02	243.24
				4.03E-02	230.59
				4.08E-02	228.40
				4.13E-02	219.43
				4.18E-02	215.04
				4.23E-02	251.16
				4.28E-02	216.15
				4.33E-02	214.16
				4.38E-02	214.82
				4.43E-02	211.08
				4.48E-02	210.96
				4.53E-02	211.27
				4.58E-02	194.63
				4.63E-02	192.99
				4.68E-02	192.89
				4.73E-02	194.25
				4.79E-02	189.15
				4.84E-02	196.06
				4.89E-02	182.79
				4.94E-02	187.06
				4.99E-02	178.76
				5.04E-02	191.28
				5.09E-02	180.39
				5.14E-02	178.42
				5.19E-02	170.31
				5.24E-02	178.47
				5.29E-02	167.31
					2.04E-02
					291.78
					2.06E-02
					287.58
					2.07E-02
					288.95
					2.09E-02
					288.55
					2.10E-02
					279.44
					2.12E-02
					276.87
					2.14E-02
					284.89
					2.15E-02
					283.93
					2.17E-02
					283.93
					2.18E-02
					282.38
					2.20E-02
					290.12
					2.21E-02
					280.85
					2.23E-02
					290.89
					2.24E-02
					283.23
					2.26E-02
					281.87
					2.28E-02
					276.50
					2.29E-02
					279.14
					2.31E-02
					285.15
					2.32E-02
					283.38
					2.34E-02
					268.66
					2.35E-02
					284.79
					2.37E-02
					282.22
					2.38E-02
					280.32
					2.40E-02
					278.21
					2.42E-02
					282.52
					2.43E-02
					275.12
					2.45E-02
					264.10
					2.46E-02
					278.92
					2.48E-02
					278.27
					2.49E-02
					276.80
					2.51E-02
					274.29
					2.52E-02
					275.06
					2.54E-02
					276.46
					2.55E-02
					281.90
					2.57E-02
					277.98
					2.59E-02
					286.36
					2.60E-02
					286.33
					2.62E-02
					286.38
					2.63E-02
					286.28
					2.65E-02
					286.17
					2.66E-02
					286.16
					2.68E-02
					286.24
					2.69E-02
					286.21
					2.71E-02
					286.27
					2.73E-02
					286.30
					2.74E-02
					286.30
					2.76E-02
					286.28
					2.77E-02
					286.18
					2.80E-02
					286.24
					2.82E-02
					286.42
					2.83E-02
					286.64
					2.85E-02
					286.42
					2.87E-02
					286.26
					2.88E-02
					286.25
					2.90E-02
					286.19
					2.91E-02
					286.11
					2.93E-02
					286.19
					2.94E-02
					286.24
					2.96E-02
					286.15
					2.97E-02
					294.60
					2.99E-02
					287.49
					3.00E-02
					288.89

Table D1d Heat transfer coefficient data from tests 16-19 (cont.)

Test 16 x [m]	Test 17 h [W/mK] x [m]	Test 18 h [W/mK] x [m]	Test 19 h [W/mK] x [m]	h [W/mK]
0.00E+00	2.1066	0.00E+00	1.6869	3.02E-02 293.98
8.47E-05	2.1642	8.47E-05	1.8233	3.04E-02 294.29
1.70E-04	2.0966	1.70E-04	1.7992	3.05E-02 286.15
2.54E-04	1.9854	2.54E-04	1.7316	3.07E-02 294.47
3.39E-04	2.0002	3.39E-04	1.6711	3.08E-02 294.60
4.24E-04	1.9603	4.24E-04	1.6657	3.10E-02 287.49
5.09E-04	1.9210	5.09E-04	1.6426	3.11E-02 286.95
5.94E-04	1.8637	5.94E-04	1.6085	3.13E-02 294.29
6.79E-04	1.8436	6.79E-04	1.5907	3.14E-02 307.33
7.64E-04	1.8162	7.64E-04	1.5674	3.16E-02 307.45
8.49E-04	1.7985	8.49E-04	1.5716	3.18E-02 307.88
9.35E-04	1.7720	9.35E-04	1.5293	3.19E-02 308.02
1.02E-03	1.7261	1.02E-03	1.5187	3.21E-02 320.80
1.11E-03	1.6787	1.11E-03	1.5059	3.22E-02 312.26
1.19E-03	1.6561	1.19E-03	1.4782	3.24E-02 314.80
1.28E-03	1.6121	1.28E-03	1.4439	3.25E-02 310.25
1.36E-03	1.6021	1.36E-03	1.4228	3.27E-02 288.46
1.45E-03	1.5864	1.45E-03	1.3831	3.28E-02 288.60
1.54E-03	1.5312	1.54E-03	1.3654	3.30E-02 292.46
1.62E-03	1.4796	1.62E-03	1.3445	3.32E-02 292.27
1.71E-03	1.4264	1.71E-03	1.3430	3.33E-02 288.60
1.80E-03	1.3781	1.80E-03	1.3119	
1.88E-03	1.3715	1.88E-03	1.3280	
1.97E-03	1.3604	1.97E-03	1.3405	
2.06E-03	1.3520	2.06E-03	1.3645	
2.15E-03	1.3604	2.15E-03	1.3299	
2.24E-03	1.3528	2.24E-03	1.3063	
2.32E-03	1.3669	2.32E-03	1.2770	
2.41E-03	1.3653	2.41E-03	1.2753	
2.50E-03	1.3965	2.50E-03	1.2839	
2.59E-03	1.4401	2.59E-03	1.2939	
2.68E-03	1.4399	2.68E-03	1.2692	
2.77E-03	1.4239	2.77E-03	1.2534	
2.86E-03	1.4306	2.86E-03	1.1833	
2.95E-03	1.3907	2.95E-03	1.1977	
3.05E-03	1.3952	3.05E-03	1.2077	

Table D1e Recovery temperature difference data from tests 1-5.

Test 1 x [m]	Test 2 Tr [K]	Test 3 x [m]	Test 4 Tr [K]	Test 5 x [m]	Tr [K]
0.00E+00	2.1066	0.00E+00	1.6869	0.00E+00	1.9376
8.47E-05	2.1642	8.47E-05	1.8233	8.47E-05	1.9067
1.70E-04	2.0966	1.70E-04	1.7992	1.70E-04	2.2459
2.54E-04	1.9854	2.54E-04	1.7316	2.54E-04	2.0644
3.39E-04	2.0002	3.39E-04	1.6711	3.39E-04	2.1087
4.24E-04	1.9603	4.24E-04	1.6657	4.24E-04	2.0082
5.09E-04	1.9210	5.09E-04	1.6426	5.09E-04	2.0532
5.94E-04	1.8637	5.94E-04	1.6085	5.94E-04	2.4633
6.79E-04	1.8436	6.79E-04	1.5907	6.79E-04	2.4356
7.64E-04	1.8162	7.64E-04	1.5674	7.64E-04	2.4071
8.49E-04	1.7985	8.49E-04	1.5716	8.49E-04	2.3888
9.35E-04	1.7720	9.35E-04	1.5293	9.35E-04	2.3668
1.02E-03	1.7261	1.02E-03	1.5187	1.02E-03	2.3361
1.11E-03	1.6787	1.11E-03	1.5059	1.11E-03	2.2865
1.19E-03	1.6561	1.19E-03	1.4782	1.19E-03	2.2376
1.28E-03	1.6121	1.28E-03	1.4439	1.28E-03	2.2024
1.36E-03	1.6021	1.36E-03	1.4228	1.36E-03	2.1551
1.45E-03	1.5864	1.45E-03	1.3831	1.45E-03	2.1241
1.54E-03	1.5312	1.54E-03	1.3654	1.54E-03	2.0939
1.62E-03	1.4796	1.62E-03	1.3445	1.62E-03	2.0756
1.71E-03	1.4264	1.71E-03	1.3430	1.71E-03	2.0456
1.80E-03	1.3781	1.80E-03	1.3119	1.80E-03	2.0336
1.88E-03	1.3715	1.88E-03	1.3280	1.88E-03	2.0449
1.97E-03	1.3604	1.97E-03	1.3405	1.97E-03	2.0245
2.06E-03	1.3520	2.06E-03	1.3645	2.06E-03	2.0038
2.15E-03	1.3604	2.15E-03	1.3299	2.15E-03	1.9795
2.24E-03	1.3528	2.24E-03	1.3063	2.24E-03	1.9743
2.32E-03	1.3669	2.32E-03	1.2770	2.32E-03	1.9633
2.41E-03	1.3653	2.41E-03	1.2753	2.41E-03	1.9551
2.50E-03	1.3965	2.50E-03	1.2839	2.50E-03	1.9357
2.59E-03	1.4401	2.59E-03	1.2939	2.59E-03	1.9058
2.68E-03	1.4399	2.68E-03	1.2692	2.68E-03	1.8705
2.77E-03	1.4239	2.77E-03	1.2534	2.77E-03	1.8612
2.86E-03	1.4306	2.86E-03	1.1833	2.86E-03	1.8425
2.95E-03	1.3907	2.95E-03	1.1977	2.95E-03	1.8380
3.05E-03	1.3952	3.05E-03	1.2077	3.05E-03	1.7911

Table D1e Recovery temperature difference data from tests 1-5. (cont.)

Test 1	Tr [K]	Test 2	Tr [K]	Test 3	Tr [K]	Test 4	Tr [K]	Test 5	Tr [K]
3.14E-03	1.3866	3.14E-03	1.1919	3.14E-03	1.7998	3.14E-03	1.6703	2.81E-03	1.4188
3.23E-03	1.4152	3.23E-03	1.1765	3.23E-03	1.7577	3.23E-03	1.7403	2.89E-03	1.3547
3.32E-03	1.3749	3.32E-03	1.1701	3.32E-03	1.7366	3.32E-03	1.5756	2.98E-03	1.2818
3.42E-03	1.3368	3.42E-03	1.1669	3.42E-03	1.7311	3.42E-03	1.6740	3.06E-03	1.3063
3.51E-03	1.3225	3.51E-03	1.1728	3.51E-03	1.7342	3.51E-03	1.9204	3.14E-03	1.3052
3.61E-03	1.2801	3.61E-03	1.2070	3.61E-03	1.7421	3.61E-03	1.5451	3.23E-03	1.3053
3.70E-03	1.3007	3.70E-03	1.2421	3.70E-03	1.6972	3.70E-03	1.6454	3.31E-03	1.3173
3.80E-03	1.3421	3.80E-03	1.2583	3.80E-03	1.6501	3.80E-03	1.3684	3.39E-03	1.3179
3.90E-03	1.3414	3.90E-03	1.3506	3.90E-03	1.6403	3.90E-03	1.3647	3.48E-03	1.3523
3.95E-03	1.8013	3.99E-03	1.3755	3.99E-03	1.5908	3.99E-03	1.3434	3.56E-03	1.4023
4.27E-03	1.3843	4.09E-03	1.4095	4.09E-03	1.5918	4.09E-03	1.3555	3.65E-03	1.4417
4.58E-03	1.5337	4.19E-03	1.4696	4.19E-03	1.5895	4.19E-03	1.4330	3.74E-03	1.4794
4.86E-03	1.5905	4.29E-03	1.4083	4.29E-03	1.5742	4.29E-03	1.5609	3.82E-03	1.4234
5.14E-03	1.6968	4.39E-03	1.3933	4.39E-03	1.5672	4.39E-03	1.4912	3.91E-03	1.3707
5.40E-03	1.6886	4.49E-03	1.3450	4.49E-03	1.5564	4.49E-03	1.5235	4.00E-03	1.3666
5.65E-03	1.7424	4.60E-03	1.4043	4.60E-03	1.6202	4.60E-03	1.8315	4.09E-03	1.3087
5.89E-03	1.5070	4.70E-03	1.4674	4.70E-03	1.6003	4.70E-03	1.3522	4.18E-03	1.3158
6.13E-03	1.4598	4.80E-03	1.3979	4.80E-03	1.5896	4.80E-03	1.7192	4.27E-03	1.3012
6.36E-03	1.5138	4.91E-03	1.4273	4.91E-03	1.5804	4.91E-03	1.1667	4.36E-03	1.2888
6.58E-03	1.4255	5.02E-03	1.3900	5.02E-03	1.5483	5.21E-03	1.6000	4.45E-03	1.2241
6.79E-03	1.4592	5.12E-03	1.3259	5.12E-03	1.5078	5.43E-03	1.4510	4.54E-03	1.1281
7.01E-03	1.4483	5.23E-03	1.4093	5.23E-03	1.4633	5.65E-03	1.3731	4.63E-03	1.1539
7.21E-03	1.3106	5.34E-03	1.4317	5.34E-03	1.4515	5.86E-03	1.5284	4.72E-03	1.1364
7.42E-03	1.2744	5.45E-03	1.4918	5.45E-03	1.4314	6.06E-03	1.1639	4.82E-03	1.1447
7.62E-03	1.2496	5.57E-03	1.4889	5.57E-03	1.3993	6.26E-03	0.9746	4.91E-03	1.1859
7.81E-03	1.3306	5.68E-03	1.4646	5.65E-03	1.5615	6.45E-03	1.2702	5.01E-03	1.1797
8.01E-03	1.4204	5.80E-03	1.4681	5.89E-03	1.4720	6.64E-03	1.1960	5.11E-03	1.2179
8.20E-03	1.4826	5.92E-03	1.4844	6.13E-03	1.3667	6.82E-03	1.2013	5.20E-03	1.2393
8.39E-03	1.4054	6.04E-03	1.5263	6.36E-03	1.4045	7.01E-03	1.0989	5.30E-03	1.2370
8.57E-03	1.3069	6.16E-03	1.5636	6.58E-03	1.4000	7.18E-03	1.1811	5.40E-03	1.2588
8.76E-03	1.2283	6.28E-03	1.5511	6.79E-03	1.4330	7.36E-03	1.1601	5.50E-03	1.2168
8.94E-03	1.1801	6.41E-03	1.5402	7.01E-03	1.3855	7.53E-03	1.1594	5.65E-03	1.1651
9.12E-03	1.1218	6.53E-03	1.5583	7.21E-03	1.3709	7.70E-03	1.0979	5.89E-03	1.2888
9.29E-03	1.1077	6.67E-03	1.5835	7.42E-03	1.3821	7.87E-03	1.0883	6.13E-03	1.3021
9.47E-03	1.1152	6.80E-03	1.6316	7.62E-03	1.3490	8.03E-03	1.1197	6.36E-03	1.3663
9.65E-03	1.0862	6.94E-03	1.7106	7.81E-03	1.3692	8.20E-03	1.0966	6.58E-03	1.2038
9.82E-03	1.0888	7.01E-03	1.7562	8.01E-03	1.3378	8.36E-03	1.1010	6.79E-03	1.1456
9.99E-03	1.0453	7.21E-03	1.8038	8.20E-03	1.3042	8.52E-03	1.0848	7.01E-03	1.1440
1.02E-02	1.0242	7.42E-03	1.8446	8.39E-03	1.2572	8.68E-03	1.0877	7.21E-03	1.1111
1.03E-02	1.0767	7.62E-03	1.9051	8.57E-03	1.3301	8.83E-03	1.0568	7.42E-03	1.0853
1.05E-02	1.0785	7.81E-03	1.9565	8.76E-03	1.3654	8.99E-03	1.0175	7.62E-03	1.0752
1.07E-02	1.1456	8.01E-03	1.9531	8.94E-03	1.1616	9.14E-03	0.8591	7.81E-03	1.1726
1.08E-02	1.1798	8.20E-03	1.9446	9.12E-03	1.0922	9.29E-03	0.8725	8.01E-03	1.1872
1.10E-02	1.0791	8.39E-03	1.9115	9.29E-03	1.0709	9.45E-03	0.7076	8.20E-03	1.0557
1.12E-02	1.1729	8.57E-03	1.8717	9.47E-03	1.0925	9.60E-03	0.6441	8.39E-03	1.1135
1.14E-02	1.1704	8.76E-03	1.8334	9.65E-03	1.0756	9.75E-03	0.7542	8.57E-03	1.0401
1.15E-02	1.2943	8.94E-03	1.7938	9.82E-03	1.0527	9.90E-03	0.8269	8.76E-03	0.9114
1.17E-02	1.3166	9.12E-03	1.7471	9.99E-03	1.0622	1.00E-02	0.8135	8.94E-03	0.9035
1.19E-02	1.2761	9.29E-03	1.6964	1.02E-02	1.0783	1.02E-02	0.6355	9.12E-03	0.8586
1.20E-02	1.1808	9.47E-03	1.6671	1.03E-02	1.1369	1.03E-02	1.0612	9.29E-03	0.8272
1.22E-02	1.0242	9.65E-03	1.6348	1.05E-02	1.1862	1.05E-02	1.0544	9.47E-03	0.8164
1.24E-02	0.9758	9.82E-03	1.5882	1.07E-02	1.1638	1.06E-02	0.5840	9.65E-03	0.8037
1.25E-02	1.1547	9.99E-03	1.5880	1.08E-02	1.2272	1.08E-02	0.5968	9.82E-03	0.8078
1.27E-02	1.3109	1.02E-02	1.5803	1.10E-02	1.0695	1.09E-02	1.1178	9.99E-03	0.8334
1.29E-02	1.2997	1.03E-02	1.5914	1.12E-02	1.1070	1.11E-02	0.5758	1.02E-02	0.8485
1.30E-02	1.3200	1.05E-02	1.5963	1.14E-02	1.1003	1.12E-02	1.3052	1.03E-02	0.8510
1.32E-02	1.2603	1.07E-02	1.6209	1.15E-02	1.2653	1.14E-02	0.6045	1.05E-02	0.8579
1.34E-02	1.3201	1.08E-02	1.6649	1.17E-02	1.2942	1.15E-02	1.1488	1.07E-02	0.9043
1.35E-02	1.0891	1.10E-02	1.6731	1.19E-02	1.1723	1.16E-02	0.9218	1.08E-02	0.8514
1.37E-02	1.1972	1.12E-02	1.6771	1.20E-02	1.2095	1.18E-02	0.8801	1.10E-02	0.7845
1.39E-02	1.0631	1.14E-02	1.7016	1.22E-02	1.0624	1.19E-02	1.0243	1.12E-02	0.8317
1.40E-02	1.3351	1.15E-02	1.6993	1.24E-02	1.0574	1.21E-02	0.8817	1.14E-02	0.8564
1.42E-02	1.3805	1.17E-02	1.7260	1.25E-02	1.1592	1.22E-02	0.8750	1.15E-02	0.9575

Table D1e Recovery temperature difference data from tests 1-5. (cont.)

Test 1	x [m]	Tr [K]	Test 2	x [m]	Tr [K]	Test 3	x [m]	Tr [K]	Test 4	x [m]	Tr [K]	Test 5	x [m]	Tr [K]
1.44E-02	1.2024	1.19E-02	1.7315	1.27E-02	1.2650	1.24E-02	0.7863	1.17E-02	0.9251					
1.45E-02	1.1301	1.20E-02	1.7562	1.29E-02	1.2565	1.25E-02	0.7956	1.19E-02	0.8106					
1.47E-02	1.4121	1.22E-02	1.7422	1.30E-02	1.2763	1.26E-02	0.9049	1.20E-02	0.9384					
1.49E-02	1.4519	1.24E-02	1.7465	1.32E-02	1.1453	1.28E-02	0.8518	1.22E-02	0.7880					
1.50E-02	1.2904	1.25E-02	1.7518	1.34E-02	1.1365	1.29E-02	0.8598	1.24E-02	0.9131					
1.52E-02	1.1166	1.27E-02	1.7699	1.35E-02	1.1567	1.31E-02	0.8752	1.25E-02	0.8582					
1.54E-02	1.0883	1.29E-02	1.7922	1.37E-02	1.2164	1.32E-02	0.9411	1.27E-02	0.8697					
1.56E-02	1.0669	1.30E-02	1.8171	1.39E-02	1.1231	1.34E-02	0.9563	1.29E-02	0.8895					
1.57E-02	1.0864	1.32E-02	1.7949	1.40E-02	1.1600	1.35E-02	0.8585	1.30E-02	0.9550					
1.59E-02	1.1216	1.34E-02	1.7928	1.42E-02	1.2081	1.37E-02	0.8107	1.32E-02	0.9407					
1.61E-02	1.1996	1.35E-02	1.7836	1.44E-02	1.0567	1.38E-02	0.8094	1.34E-02	0.9537					
1.62E-02	1.1420	1.37E-02	1.7955	1.45E-02	1.2487	1.39E-02	0.8739	1.35E-02	0.9069					
1.64E-02	1.1593	1.39E-02	1.7669	1.47E-02	1.2375	1.41E-02	0.8475	1.37E-02	0.9479					
1.66E-02	1.2152	1.40E-02	1.7641	1.49E-02	1.1813	1.42E-02	0.9147	1.39E-02	0.9695					
1.67E-02	1.1863	1.42E-02	1.7584	1.50E-02	1.0564	1.44E-02	0.9776	1.40E-02	1.0129					
1.69E-02	1.1728	1.44E-02	1.7249	1.52E-02	1.0943	1.45E-02	0.8489	1.42E-02	0.9118					
1.71E-02	1.1309	1.45E-02	1.6841	1.54E-02	0.9989	1.47E-02	0.7461	1.44E-02	0.7804					
1.72E-02	1.0585	1.47E-02	1.6800	1.56E-02	0.9596	1.48E-02	0.8001	1.45E-02	0.8576					
1.74E-02	1.1015	1.49E-02	1.6648	1.57E-02	1.0018	1.50E-02	0.8542	1.47E-02	0.9424					
1.76E-02	0.9087	1.50E-02	1.6377	1.59E-02	1.1141	1.51E-02	0.7756	1.49E-02	1.0086					
1.77E-02	0.9454	1.52E-02	1.6146	1.61E-02	1.0774	1.52E-02	0.8190	1.50E-02	0.7712					
1.79E-02	1.0091	1.54E-02	1.6127	1.62E-02	1.0373	1.54E-02	0.7339	1.52E-02	0.8499					
1.81E-02	1.0852	1.56E-02	1.6156	1.64E-02	1.0106	1.55E-02	0.7130	1.54E-02	0.6268					
1.82E-02	1.0602	1.57E-02	1.5937	1.66E-02	1.0140	1.57E-02	0.7646	1.56E-02	0.7714					
1.84E-02	0.8784	1.59E-02	1.5866	1.67E-02	1.0421	1.58E-02	0.6840	1.57E-02	0.8018					
1.86E-02	0.9013	1.61E-02	1.5994	1.69E-02	1.0708	1.60E-02	0.7823	1.59E-02	0.8801					
1.87E-02	1.1616	1.62E-02	1.6049	1.71E-02	1.0418	1.61E-02	0.6863	1.61E-02	0.7549					
1.89E-02	1.1534	1.64E-02	1.6058	1.72E-02	1.0761	1.62E-02	0.6871	1.62E-02	0.7799					
1.91E-02	1.1747	1.66E-02	1.6075	1.74E-02	0.9440	1.64E-02	0.8569	1.64E-02	0.7486					
1.93E-02	1.0889	1.67E-02	1.6024	1.76E-02	0.9856	1.65E-02	0.6908	1.66E-02	0.7595					
1.94E-02	1.0689	1.69E-02	1.5756	1.77E-02	0.9493	1.67E-02	0.6820	1.67E-02	0.7606					
1.96E-02	1.1661	1.71E-02	1.5413	1.79E-02	0.8624	1.68E-02	0.7253	1.69E-02	0.7259					
1.98E-02	1.1655	1.72E-02	1.5200	1.81E-02	0.7923	1.70E-02	0.8117	1.71E-02	0.7806					
1.99E-02	1.0731	1.74E-02	1.5044	1.82E-02	0.7911	1.71E-02	0.6806	1.72E-02	0.7275					
2.01E-02	1.1601	1.76E-02	1.4775	1.84E-02	0.7880	1.73E-02	0.6900	1.74E-02	0.7991					
2.03E-02	0.9641	1.77E-02	1.4713	1.86E-02	0.8645	1.74E-02	0.7762	1.76E-02	0.5724					
2.04E-02	0.8021	1.79E-02	1.4582	1.87E-02	0.8821	1.75E-02	0.7569	1.77E-02	0.5695					
2.06E-02	0.7603	1.81E-02	1.4487	1.89E-02	0.9873	1.77E-02	0.5577	1.79E-02	0.6972					
2.08E-02	0.7325	1.82E-02	1.4517	1.91E-02	0.9426	1.78E-02	0.6055	1.81E-02	0.5164					
2.09E-02	0.7600	1.84E-02	1.4659	1.93E-02	0.9361	1.80E-02	0.6107	1.82E-02	0.6558					
2.11E-02	0.8525	1.86E-02	1.4794	1.94E-02	0.9931	1.81E-02	0.6112	1.84E-02	0.6142					
2.13E-02	0.9321	1.87E-02	1.4759	1.96E-02	1.0140	1.83E-02	0.6822	1.86E-02	0.6576					
2.14E-02	0.9419	1.89E-02	1.4781	1.98E-02	1.0824	1.84E-02	0.6585	1.87E-02	0.6352					
2.16E-02	0.9021	1.91E-02	1.4852	1.99E-02	0.9230	1.86E-02	0.5206	1.89E-02	0.6772					
2.18E-02	0.9577	1.93E-02	1.4782	2.01E-02	0.8884	1.87E-02	0.4725	1.91E-02	0.6246					
2.19E-02	0.8949	1.94E-02	1.4850	2.03E-02	0.8959	1.88E-02	0.5145	1.93E-02	0.6684					
2.21E-02	0.7370	1.96E-02	1.4674	2.04E-02	0.8760	1.90E-02	0.5588	1.94E-02	0.5325					
2.23E-02	0.9503	1.98E-02	1.4565	2.06E-02	0.8844	1.91E-02	0.6470	1.96E-02	0.6569					
2.24E-02	1.1042	1.99E-02	1.4363	2.08E-02	0.6847	1.93E-02	0.6685	1.98E-02	0.6982					
2.26E-02	0.8322	2.01E-02	1.4188	2.09E-02	0.8832	1.94E-02	0.6458	1.99E-02	0.7199					
2.28E-02	0.7753	2.03E-02	1.4192	2.11E-02	0.8326	1.96E-02	0.6925	2.01E-02	0.7027					
2.29E-02	0.8077	2.04E-02	1.4176	2.13E-02	0.8046	1.97E-02	0.6588	2.03E-02	0.5575					
2.31E-02	1.1619	2.06E-02	1.3995	2.14E-02	0.8827	1.99E-02	0.6155	2.04E-02	0.5752					
2.33E-02	0.7321	2.08E-02	1.3726	2.16E-02	0.8808	2.00E-02	0.6330	2.06E-02	0.6195					
2.35E-02	0.9476	2.09E-02	1.3425	2.18E-02	1.0046	2.01E-02	0.5414	2.08E-02	0.6939					
2.36E-02	0.9682	2.11E-02	1.3456	2.19E-02	0.7459	2.03E-02	0.5641	2.09E-02	0.6841					
2.38E-02	0.8175	2.13E-02	1.3400	2.21E-02	0.7937	2.04E-02	0.7182	2.11E-02	0.5637					
2.40E-02	0.8933	2.14E-02	1.3214	2.23E-02	0.8449	2.06E-02	0.7094	2.13E-02	0.6004					
2.41E-02	0.8933	2.16E-02	1.3283	2.24E-02	0.9498	2.07E-02	0.6839	2.14E-02	0.4350					
2.43E-02	1.0073	2.18E-02	1.3329	2.26E-02	0.7926	2.09E-02	0.6315	2.16E-02	0.7219					
2.45E-02	0.8030	2.19E-02	1.3152	2.28E-02	0.7995	2.10E-02	0.6913	2.18E-02	0.6376					
2.46E-02	0.6710	2.21E-02	1.2998	2.29E-02	0.8114	2.11E-02	0.5810	2.19E-02	0.4296					
2.48E-02	0.5926	2.23E-02	1.2885	2.31E-02	0.8808	2.13E-02	0.5919	2.21E-02	0.4588					

Table D1e Recovery temperature difference data from tests 1-5. (cont.)

Test 1 x [m]	Tr [K]	Test 2 x [m]	Tr [K]	Test 3 x [m]	Tr [K]	Test 4 x [m]	Tr [K]	Test 5 x [m]	Tr [K]
2.50E-02	0.8564	2.24E-02	1.3019	2.33E-02	0.5972	2.14E-02	0.6073	2.23E-02	0.4789
2.51E-02	0.7561	2.26E-02	1.2874	2.35E-02	0.6792	2.16E-02	0.7331	2.24E-02	0.4818
2.53E-02	0.6794	2.28E-02	1.2757	2.36E-02	0.7836	2.17E-02	0.6061	2.26E-02	0.5550
2.55E-02	0.8314	2.29E-02	1.2845	2.38E-02	0.8429	2.19E-02	0.6473	2.28E-02	0.5145
2.56E-02	0.7165	2.31E-02	1.2662	2.40E-02	0.6319	2.20E-02	0.6179	2.29E-02	0.5557
2.58E-02	0.8091	2.33E-02	1.2587	2.41E-02	0.6942	2.22E-02	0.6043	2.31E-02	0.5142
2.60E-02	0.8550	2.35E-02	1.2494	2.43E-02	0.6452	2.23E-02	0.6213	2.33E-02	0.4636
2.61E-02	0.7381	2.36E-02	1.2445	2.45E-02	0.6450	2.24E-02	0.6261	2.35E-02	0.4720
2.63E-02	0.7095	2.38E-02	1.2491	2.46E-02	0.6556	2.26E-02	0.6478	2.36E-02	0.5084
2.65E-02	0.8139	2.40E-02	1.2283	2.48E-02	0.6370	2.27E-02	0.6942	2.38E-02	0.4852
2.66E-02	0.7654	2.41E-02	1.2160	2.50E-02	0.7166			2.40E-02	0.4235
2.68E-02	0.8760	2.43E-02	1.2060	2.51E-02	0.6879			2.41E-02	0.5946
2.70E-02	0.7666	2.45E-02	1.2055	2.53E-02	0.6389			2.43E-02	0.4408
2.72E-02	0.5970	2.46E-02	1.1974	2.55E-02	0.6884			2.45E-02	0.3817
2.73E-02	1.0012	2.48E-02	1.1796	2.56E-02	0.6678			2.46E-02	0.4286
2.75E-02	1.1350	2.50E-02	1.1922	2.58E-02	0.6935			2.48E-02	0.4368
2.77E-02	0.7698	2.51E-02	1.1781	2.60E-02	0.6154			2.50E-02	0.4422
2.78E-02	0.6254	2.53E-02	1.1659	2.61E-02	0.6400			2.51E-02	0.4560
2.80E-02	0.5901	2.55E-02	1.1717	2.63E-02	0.5088			2.53E-02	0.4789
2.82E-02	0.6467	2.56E-02	1.1691	2.65E-02	0.5608				
2.83E-02	0.6244	2.58E-02	1.1543	2.66E-02	0.7410				
2.85E-02	0.6725	2.60E-02	1.1330	2.68E-02	0.5433				
2.87E-02	0.7533	2.61E-02	1.1286	2.70E-02	0.5998				
2.88E-02	0.8162	2.63E-02	1.1255	2.72E-02	0.6383				
2.90E-02	0.7448	2.65E-02	1.0971	2.73E-02	0.6811				
2.92E-02	0.8379	2.66E-02	1.1271	2.75E-02	0.4594				
2.93E-02	0.9222	2.68E-02	1.1310	2.77E-02	0.5201				
2.95E-02	0.7276	2.70E-02	1.1332	2.78E-02	0.4319				
2.97E-02	0.7843	2.72E-02	1.1198	2.80E-02	0.4878				
2.98E-02	0.7353	2.73E-02	1.1140	2.82E-02	0.6204				
3.00E-02	0.7757	2.75E-02	1.1128	2.83E-02	0.6411				
3.02E-02	0.7268	2.77E-02	1.1178	2.85E-02	0.5238				
3.03E-02	0.7478	2.78E-02	1.1498	2.87E-02	0.6342				
3.05E-02	0.8220	2.80E-02	1.1732	2.88E-02	0.5806				
3.07E-02	0.8386	2.82E-02	1.1614	2.90E-02	0.6526				
3.09E-02	0.7208	2.83E-02	1.1569	2.92E-02	0.7038				
3.10E-02	0.6852	2.85E-02	1.1431	2.93E-02	0.7655				
3.12E-02	0.6462	2.87E-02	1.1814	2.95E-02	0.4867				
3.14E-02	0.7167	2.88E-02	1.2190	2.97E-02	0.5690				
3.15E-02	0.7323	2.90E-02	1.2269						
3.17E-02	0.7270	2.92E-02	1.1989						
		2.93E-02	1.1469						
		2.95E-02	1.1311						
		2.97E-02	1.1235						
		2.98E-02	1.1085						
		3.00E-02	1.0982						
		3.02E-02	1.0613						
		3.03E-02	1.0241						
		3.05E-02	1.0132						
		3.07E-02	1.0371						
		3.09E-02	1.0642						
		3.10E-02	1.0770						
		3.12E-02	1.0671						
		3.14E-02	1.0760						
		3.15E-02	1.0775						
		3.17E-02	1.0995						
		3.19E-02	1.0918						
		3.20E-02	1.0886						

Table D1f Recovery temperature difference data from tests 6-11.

Test 6	Test 7	Test 8	Test 9	Test 10			
x [m]	Tr [K]	x [m]	Tr [K]	x [m]	Tr [K]	x [m]	Tr [K]
0.00E+00	2.1733	0.00E+00	2.3912	0.00E+00	0.3858	0.00E+00	1.6751
7.63E-05	2.1063	7.41E-05	2.3664	7.69E-05	1.7366	7.69E-05	1.6211
1.53E-04	2.0135	1.48E-04	2.4204	1.54E-04	1.9368	1.54E-04	1.7405
2.29E-04	2.0673	2.22E-04	2.5109	2.31E-04	1.9027	2.31E-04	2.1757
3.05E-04	2.0399	2.96E-04	2.3995	3.08E-04	1.4439	3.08E-04	2.9903
3.82E-04	2.0305	3.71E-04	2.4762	3.85E-04	1.5329	3.85E-04	2.9097
4.58E-04	2.1608	4.45E-04	2.5280	4.62E-04	1.4262	4.62E-04	2.5172
5.35E-04	2.6248	5.19E-04	2.5775	5.39E-04	1.2384	5.39E-04	1.3030
6.11E-04	2.3028	5.93E-04	2.5045	6.16E-04	1.1539	6.16E-04	2.2563
6.88E-04	2.3095	6.68E-04	2.4783	6.93E-04	1.1942	6.93E-04	3.0932
7.65E-04	2.3882	7.42E-04	2.5953	7.71E-04	1.2487	7.71E-04	2.5736
8.41E-04	2.3931	8.16E-04	2.4997	8.48E-04	1.1927	8.48E-04	2.9064
9.18E-04	2.5197	8.91E-04	2.6902	9.25E-04	1.1447	9.25E-04	2.2979
9.95E-04	2.4264	9.66E-04	2.6556	1.00E-03	0.8825	1.00E-03	1.9441
1.07E-03	2.7001	1.04E-03	2.4324	1.08E-03	0.7634	1.08E-03	1.6452
1.15E-03	2.4030	1.12E-03	2.3036	1.16E-03	0.6908	1.16E-03	1.8429
1.23E-03	2.4277	1.19E-03	2.3105	1.24E-03	0.7734	1.24E-03	3.4356
1.30E-03	2.4962	1.27E-03	2.3439	1.31E-03	0.7769	1.31E-03	0.7004
1.38E-03	2.4655	1.34E-03	2.1127	1.39E-03	0.6589	1.39E-03	2.1769
1.46E-03	1.8036	1.42E-03	2.2449	1.47E-03	0.5539	1.47E-03	2.2938
1.54E-03	1.9665	1.49E-03	2.2755	1.55E-03	0.6589	1.55E-03	2.9588
1.62E-03	1.9796	1.57E-03	2.2917	1.63E-03	0.5591	1.63E-03	2.0216
1.69E-03	1.9244	1.64E-03	2.2286	1.71E-03	0.5810	1.71E-03	1.8830
1.77E-03	1.9729	1.72E-03	2.2573	1.79E-03	0.5510	1.79E-03	2.2319
1.85E-03	1.9332	1.79E-03	2.2706	1.86E-03	0.5571	1.86E-03	2.6045
1.93E-03	1.8665	1.87E-03	2.3009	1.94E-03	0.4748	1.94E-03	1.6336
2.01E-03	1.9151	1.95E-03	2.3131	2.02E-03	0.4177	2.02E-03	0.9522
2.09E-03	1.7715	2.02E-03	2.2300	2.10E-03	0.3555	2.10E-03	2.3027
2.17E-03	1.7667	2.10E-03	2.1666	2.18E-03	0.4287	2.18E-03	1.4511
2.25E-03	1.7420	2.18E-03	2.2131	2.26E-03	0.3328	2.26E-03	1.5762
2.33E-03	1.8762	2.26E-03	2.2545	2.34E-03	0.3903	2.34E-03	1.4726
2.41E-03	1.8814	2.33E-03	2.3248	2.43E-03	0.4722	2.43E-03	0.9221
2.49E-03	1.8697	2.41E-03	2.3023	2.78E-03	0.1759	2.51E-03	1.2094
2.57E-03	1.6892	2.49E-03	2.2867	3.21E-03	1.3630	2.59E-03	1.2939
2.65E-03	1.6840	2.57E-03	2.1516	3.60E-03	-0.5822	2.67E-03	1.1912
2.73E-03	1.5874	2.65E-03	2.3124	3.95E-03	-0.2819	2.75E-03	0.3357
2.81E-03	1.8808	2.72E-03	2.3541	4.27E-03	-0.3052	2.83E-03	0.5289
2.89E-03	1.6171	2.80E-03	2.1231	4.58E-03	0.2823	2.92E-03	0.4369
3.21E-03	1.4274	2.88E-03	2.1961	4.86E-03	0.1506	3.00E-03	1.1558
3.60E-03	1.3444	2.96E-03	2.2351	5.14E-03	0.0403	3.08E-03	0.5543
3.95E-03	1.4047	3.04E-03	2.1803	5.40E-03	-0.1585	3.17E-03	0.2926
4.27E-03	1.5135	3.12E-03	2.1235	5.65E-03	-0.0297	3.25E-03	0.4840
4.58E-03	1.9269	3.20E-03	2.0576	5.89E-03	0.0014	3.34E-03	0.5587
4.86E-03	1.8865	3.29E-03	2.0192	6.13E-03	-0.3205	3.42E-03	-0.0502
5.14E-03	1.8240	3.37E-03	2.1317	6.36E-03	-0.0292	3.60E-03	1.0192
5.40E-03	1.7109	3.45E-03	1.9814	6.58E-03	0.0364	3.95E-03	0.5466
5.65E-03	1.7521	3.53E-03	1.8189	6.79E-03	-0.2328	4.27E-03	0.7714
5.89E-03	1.6200	3.62E-03	2.1203	7.01E-03	-0.1223	4.58E-03	0.2869
6.13E-03	1.7455	3.70E-03	1.7213	7.21E-03	-0.2327	4.86E-03	0.6179
6.36E-03	1.4144	3.78E-03	1.7461	7.42E-03	-0.2556	5.14E-03	0.3933
6.58E-03	1.3621	3.87E-03	1.7790	7.62E-03	-0.3755	5.40E-03	0.3760
6.79E-03	1.4569	3.95E-03	1.7801	7.81E-03	-0.2593	5.65E-03	0.5978
7.01E-03	1.5342	4.04E-03	1.6817	8.01E-03	-0.2555	5.89E-03	0.1987
7.21E-03	1.5457	4.12E-03	2.0531	8.20E-03	-0.3184	6.13E-03	0.1016
7.42E-03	1.5359	4.21E-03	2.0530	8.39E-03	-0.4491	6.36E-03	0.0368
7.62E-03	1.5248	4.30E-03	1.8475	8.57E-03	-0.5984	6.58E-03	0.1527
7.81E-03	1.5500	4.39E-03	2.2084	8.76E-03	-0.4906	6.79E-03	0.2665
8.01E-03	1.4865	4.48E-03	1.9062	8.94E-03	-0.4171	7.01E-03	-0.0216
8.20E-03	1.5328	4.56E-03	1.9241	9.12E-03	-0.4586	7.21E-03	-0.1453
8.39E-03	1.4985	4.65E-03	1.5445	9.29E-03	-0.4675	7.42E-03	-0.1964
8.57E-03	1.4733	4.75E-03	1.5055	9.47E-03	-0.4837	7.62E-03	-0.2312
8.76E-03	1.3516	4.84E-03	1.7171	9.65E-03	-0.6184	7.81E-03	0.0497
8.94E-03	1.2865	4.93E-03	1.4168	9.82E-03	-0.6630	8.01E-03	0.0829
						7.01E-03	0.9813

Table D1f Recovery temperature difference data from tests 6-11. (cont.)

Test 6	x [m]	Tr [K]	Test 7	x [m]	Tr [K]	Test 8	x [m]	Tr [K]	Test 9	x [m]	Tr [K]	Test 10	x [m]	Tr [K]
9.12E-03	1.2531	5.02E-03	2.1713	9.99E-03	-0.6757	8.20E-03	-0.0143	7.21E-03	1.3237					
9.29E-03	1.2460	5.21E-03	1.2751	1.02E-02	-0.5533	8.39E-03	-0.2049	7.42E-03	1.4591					
9.47E-03	1.1993	5.43E-03	1.2096	1.03E-02	-0.5542	8.57E-03	-0.3558	7.62E-03	1.4220					
9.65E-03	1.2391	5.65E-03	1.1179	1.05E-02	-0.7070	8.76E-03	-0.4433	7.81E-03	0.9555					
9.82E-03	1.2172	5.86E-03	1.3719	1.07E-02	-0.4495	8.94E-03	-0.4706	8.01E-03	0.7737					
9.99E-03	1.1610	6.06E-03	1.2615	1.08E-02	-0.5563	9.12E-03	-0.3880	8.20E-03	1.1640					
1.02E-02	1.1321	6.26E-03	1.0436	1.10E-02	-0.4176	9.29E-03	-0.4308	8.39E-03	1.3591					
1.03E-02	1.0941	6.45E-03	1.1495	1.12E-02	-0.2475	9.47E-03	-0.5521	8.57E-03	1.0349					
1.05E-02	1.0760	6.64E-03	1.0996	1.14E-02	-0.1283	9.65E-03	-0.5339	8.76E-03	0.7110					
1.07E-02	0.9999	6.82E-03	1.0278	1.15E-02	-0.2451	9.82E-03	-0.6061	8.94E-03	1.0717					
1.08E-02	1.1999	7.01E-03	0.9021	1.17E-02	-0.2501	9.99E-03	-0.6164	9.12E-03	1.3534					
1.10E-02	1.1831	7.18E-03	0.9151	1.19E-02	-0.2238	1.02E-02	-0.6130	9.29E-03	1.1483					
1.12E-02	1.1946	7.36E-03	0.9192	1.20E-02	-0.3955	1.03E-02	-0.8786	9.47E-03	0.9019					
1.14E-02	1.0478	7.53E-03	0.8987	1.22E-02	-0.2206	1.05E-02	-0.8737	9.65E-03	0.8688					
1.15E-02	1.0774	7.70E-03	0.8771	1.24E-02	-0.1864	1.07E-02	-0.5830	9.82E-03	0.7998					
1.17E-02	1.1019	7.87E-03	0.8635	1.25E-02	-0.2569	1.08E-02	-0.3909	9.99E-03	0.7709					
1.19E-02	1.5310	8.03E-03	0.8564	1.27E-02	-0.2737	1.10E-02	-0.0826	1.02E-02	0.8343					
1.20E-02	1.3559	8.20E-03	0.8589	1.29E-02	-0.1926	1.12E-02	-0.3018	1.03E-02	0.9043					
1.22E-02	1.3706	8.36E-03	0.8255	1.30E-02	-0.0145	1.14E-02	-0.4180	1.05E-02	0.8387					
1.24E-02	1.0687	8.52E-03	0.7626	1.32E-02	-0.4405	1.15E-02	-0.1254	1.07E-02	0.8671					
1.25E-02	1.3482	8.68E-03	0.7522	1.34E-02	-0.0554	1.17E-02	-0.1656	1.08E-02	0.8131					
1.27E-02	1.3599	8.83E-03	0.7478	1.35E-02	-0.2896	1.19E-02	-0.7108	1.10E-02	0.7511					
1.29E-02	1.1510	8.99E-03	0.7834	1.37E-02	-0.3044	1.20E-02	-0.1641	1.12E-02	1.0843					
1.30E-02	1.3212	9.14E-03	0.7076	1.39E-02	-0.1046	1.22E-02	0.7356	1.14E-02	1.2249					
1.32E-02	1.2024	9.29E-03	0.7040	1.40E-02	-0.1134	1.24E-02	0.5456	1.15E-02	1.5313					
1.34E-02	1.1498	9.45E-03	0.6058	1.42E-02	0.0611	1.25E-02	0.1226	1.17E-02	1.3069					
1.35E-02	1.2708	9.60E-03	0.6442	1.44E-02	-0.0172	1.27E-02	-0.4123	1.19E-02	1.7644					
1.37E-02	1.3568	9.75E-03	0.5962	1.45E-02	0.0845	1.29E-02	-0.1137	1.20E-02	1.2820					
1.39E-02	1.2409	9.90E-03	0.6396	1.47E-02	0.1866	1.30E-02	0.1209	1.22E-02	1.4581					
1.40E-02	1.5301	1.00E-02	0.6596	1.49E-02	0.1827	1.32E-02	-0.6111	1.24E-02	1.5016					
1.42E-02	1.0809	1.02E-02	0.6482	1.50E-02	0.1789	1.34E-02	-0.0388	1.25E-02	1.2620					
1.44E-02	1.0722	1.03E-02	0.5642	1.52E-02	0.1453	1.35E-02	0.2446	1.27E-02	1.0905					
1.45E-02	1.0235	1.05E-02	0.5975	1.54E-02	-0.1500	1.37E-02	-0.2631	1.29E-02	1.2914					
1.47E-02	0.9543	1.06E-02	0.5598	1.56E-02	0.1099	1.39E-02	-0.1188	1.30E-02	1.2638					
1.49E-02	0.9772	1.08E-02	0.5731	1.57E-02	0.2851	1.40E-02	-0.1483	1.32E-02	1.0929					
1.50E-02	0.9240	1.09E-02	0.5320	1.59E-02	-0.0137	1.42E-02	-0.3706	1.34E-02	1.1402					
1.52E-02	0.8451	1.11E-02	0.5316	1.61E-02	-0.1208	1.44E-02	-0.2142	1.35E-02	1.4331					
1.54E-02	1.0190	1.12E-02	0.5365	1.62E-02	-0.1996	1.45E-02	-0.3288	1.37E-02	1.5888					
1.56E-02	0.8751	1.14E-02	0.6099	1.64E-02	0.0531	1.47E-02	-0.3671	1.39E-02	1.5734					
1.57E-02	0.9453	1.15E-02	0.6348	1.66E-02	-0.0754	1.49E-02	-0.3433	1.40E-02	1.6684					
1.59E-02	0.8953	1.16E-02	0.6601	1.67E-02	-0.0795	1.50E-02	0.0184	1.42E-02	1.5863					
1.61E-02	0.5126	1.18E-02	0.8222	1.69E-02	-0.1543	1.52E-02	0.0665	1.44E-02	1.4127					
1.62E-02	0.5703	1.19E-02	0.5208	1.71E-02	-0.2059	1.54E-02	-0.2850	1.45E-02	1.3440					
1.64E-02	0.3461	1.21E-02	0.5052	1.72E-02	0.0797	1.56E-02	-0.1559	1.47E-02	1.2955					
1.66E-02	0.4356	1.22E-02	0.4975	1.74E-02	0.0287	1.57E-02	-0.1910	1.49E-02	1.2420					
1.67E-02	0.3914	1.24E-02	0.4891	1.76E-02	-0.1467	1.59E-02	-0.2121	1.50E-02	1.2666					
1.69E-02	0.3650	1.25E-02	0.4627	1.77E-02	-0.2692	1.61E-02	-0.3528	1.52E-02	1.6206					
1.71E-02	0.3009	1.26E-02	0.5308	1.79E-02	-0.1786	1.62E-02	-0.3999	1.54E-02	1.4377					
1.72E-02	0.3381	1.28E-02	0.5197	1.81E-02	-0.1341	1.64E-02	-0.4164	1.56E-02	1.2665					
1.74E-02	0.2757	1.29E-02	0.5303	1.82E-02	-0.4397	1.66E-02	-0.4045	1.57E-02	1.2483					
1.76E-02	0.4241	1.31E-02	0.5349	1.84E-02	-0.6687	1.67E-02	-0.4913	1.59E-02	1.2774					
1.77E-02	0.4682	1.32E-02	0.4967	1.86E-02	-0.5375	1.69E-02	-0.3818	1.61E-02	1.3130					
1.79E-02	0.4782	1.34E-02	0.5094	1.87E-02	-0.4091	1.71E-02	-0.2912	1.62E-02	1.2504					
1.81E-02	0.1879	1.35E-02	0.3984	1.89E-02	-0.2128	1.72E-02	-0.3675	1.64E-02	1.2889					
1.82E-02	0.1765	1.37E-02	0.4830	1.91E-02	-0.2279	1.74E-02	-0.3973	1.66E-02	1.4105					
1.84E-02	0.4427	1.38E-02	0.2703	1.93E-02	-0.5531	1.76E-02	-0.4999	1.67E-02	1.5612					
1.86E-02	0.7148	1.39E-02	0.2707	1.94E-02	-0.3717	1.77E-02	-0.7394	1.69E-02	1.4999					
1.87E-02	0.5809	1.41E-02	0.4768	1.96E-02	-0.2367	1.79E-02	-0.5005	1.71E-02	1.4300					
1.89E-02	0.5726	1.42E-02	0.3463	1.98E-02	-0.2173	1.81E-02	-0.5351	1.72E-02	1.4420					
1.91E-02	0.1459	1.44E-02	0.3552	1.99E-02	-0.3565	1.82E-02	-0.4183	1.74E-02	1.4085					
1.93E-02	0.3617	1.45E-02	0.3753	2.01E-02	-0.2359	1.84E-02	-0.1776	1.76E-02	1.2507					
1.94E-02	0.4148	1.47E-02	0.3934	2.03E-02	-0.0728	1.86E-02	-0.1585	1.77E-02	1.0888					
1.96E-02	0.1956	1.48E-02	0.3728	2.04E-02	-0.0899	1.87E-02	-0.5929	1.79E-02	1.2112					

Table D1f Recovery temperature difference data from tests 6-11. (cont.)

Test 6	Test 7	Test 8	Test 9	Test 10				
x [m]	Tr [K]	x [m]	Tr [K]	x [m]	Tr [K]	x [m]	Tr [K]	
1.98E-02	0.2285	1.50E-02	0.3915	2.06E-02	-0.2318	1.89E-02	-0.5772	
1.99E-02	0.4817	1.51E-02	0.5496	2.08E-02	-0.1197	1.91E-02	-0.3933	
2.01E-02	0.5064	1.52E-02	0.5297	2.09E-02	-0.0109	1.93E-02	-0.3484	
2.03E-02	0.4925	1.54E-02	0.4961	2.11E-02	-0.1623	1.94E-02	-0.5389	
2.04E-02	0.4438	1.55E-02	0.3477	2.13E-02	-0.2831	1.96E-02	-0.3127	
2.06E-02	0.5515	1.57E-02	0.3579	2.14E-02	-0.4137	1.98E-02	-0.4112	
2.08E-02	0.6136	1.58E-02	0.3877	2.16E-02	-0.4109	1.99E-02	-0.2966	
2.09E-02	0.5491	1.60E-02	0.3394	2.18E-02	-0.7340	2.01E-02	-0.4712	
2.11E-02	0.3902	1.61E-02	0.3986	2.19E-02	-0.2552	2.03E-02	-0.3204	
2.13E-02	0.4318	1.62E-02	0.3938	2.21E-02	-0.2436	2.04E-02	-0.3777	
2.14E-02	0.4182	1.64E-02	0.3664	2.23E-02	-0.2205	2.06E-02	-0.1108	
2.16E-02	0.4838	1.65E-02	0.4864	2.24E-02	-0.2776	2.08E-02	-0.5322	
2.18E-02	0.2287	1.67E-02	0.4875	2.26E-02	-0.2806	2.09E-02	0.0157	
2.19E-02	0.2858	1.68E-02	0.4422	2.28E-02	-0.5071	2.11E-02	-0.6709	
2.21E-02	0.3281	1.70E-02	0.3995	2.29E-02	-0.6107	2.13E-02	-0.4412	
2.23E-02	0.3418	1.71E-02	0.4420	2.31E-02	-0.7152	2.14E-02	-0.4740	
2.24E-02	0.4145	1.73E-02	0.4471	2.33E-02	-0.2046	2.16E-02	-0.7653	
2.26E-02	0.1987	1.74E-02	0.4506	2.35E-02	-0.6049	2.18E-02	-0.7093	
2.28E-02	0.2741	1.75E-02	0.4223	2.36E-02	-0.4345	2.19E-02	-0.9055	
2.29E-02	0.2926	1.77E-02	0.4383	2.38E-02	-0.4846	2.21E-02	-0.7151	
2.31E-02	0.3065	1.78E-02	0.4319	2.40E-02	-0.4575	2.23E-02	-0.5408	
2.33E-02	0.2600	1.80E-02	0.4493	2.41E-02	-0.0718	2.24E-02	-0.6467	
2.35E-02	0.0303	1.81E-02	0.4655	2.43E-02	-0.2967	2.26E-02	-0.7694	
2.36E-02	0.1688	1.83E-02	0.4614	2.45E-02	-0.4393	2.28E-02	-0.5896	
2.38E-02	-0.1075	1.84E-02	0.4566	2.46E-02	-0.6253	2.29E-02	-0.2935	
2.40E-02	0.0130	1.86E-02	0.5100	2.48E-02	-0.8094	2.31E-02	-0.4475	
2.41E-02	-0.2287	1.87E-02	0.3958	2.50E-02	-0.5336	2.33E-02	-0.3553	
2.43E-02	-0.0061	1.88E-02	0.3847	2.51E-02	-0.4839	2.35E-02	-0.0135	
2.45E-02	-0.0217	1.90E-02	0.2912	2.53E-02	-0.4576	2.36E-02	-0.5991	
2.46E-02	0.1140	1.91E-02	0.3253	2.55E-02	-0.3890	2.38E-02	-0.3895	
2.48E-02	-0.0708	1.93E-02	0.3682	2.56E-02	-0.5584	2.40E-02	-0.2377	
2.50E-02	-0.0101	1.94E-02	0.4431	2.58E-02	-0.3576	2.41E-02	-0.4700	
2.51E-02	-0.0100	1.96E-02	0.4421	2.60E-02	-0.3829	2.43E-02	-0.5975	
2.53E-02	-0.0139	1.97E-02	0.4593		2.45E-02	0.0073	2.36E-02	0.8668
2.55E-02	-0.0328	1.99E-02	0.4128		2.46E-02	-0.5170	2.38E-02	0.9430
2.56E-02	0.0089	2.00E-02	0.4257		2.48E-02	-0.3970	2.40E-02	0.9369
2.58E-02	0.0419	2.01E-02	0.4789		2.50E-02	-0.2139	2.41E-02	0.8026
2.60E-02	0.0801	2.03E-02	0.3734		2.51E-02	-0.2493	2.43E-02	0.7812
2.61E-02	0.1957	2.04E-02	0.4281		2.53E-02	-0.4198	2.45E-02	0.7699
2.63E-02	0.1438	2.06E-02	0.4078		2.55E-02	-0.2105	2.46E-02	0.5853
2.65E-02	-0.3867	2.07E-02	0.4093		2.56E-02	-0.3244	2.48E-02	0.4184
2.66E-02	-0.1003	2.09E-02	0.4348		2.58E-02	-0.7702	2.50E-02	0.6105
2.68E-02	-0.0662	2.10E-02	0.3890		2.60E-02	-0.6849	2.51E-02	0.7404
2.70E-02	0.0895	2.11E-02	0.3470		2.61E-02	-0.6235	2.53E-02	0.7940
2.72E-02	0.2054	2.13E-02	0.3497		2.63E-02	-0.5275	2.55E-02	0.7937
2.73E-02	-0.1224	2.14E-02	0.3703		2.65E-02	-0.5831	2.56E-02	0.8155
2.75E-02	-0.2083	2.16E-02	0.3681		2.66E-02	-0.8685	2.58E-02	0.8481
2.77E-02	-0.1298	2.17E-02	0.4454		2.68E-02	-0.6837	2.60E-02	0.6160
2.78E-02	0.1164	2.19E-02	0.2810		2.70E-02	-0.6113	2.61E-02	0.6814
2.80E-02	0.1160	2.20E-02	0.2997		2.72E-02	-0.5304	2.63E-02	0.9132
2.82E-02	-0.1514	2.22E-02	0.2800		2.73E-02	-0.5189	2.65E-02	0.9885
2.83E-02	-0.1189	2.23E-02	0.2809		2.75E-02	-1.4123	2.66E-02	0.8769
2.85E-02	-0.0226	2.24E-02	0.3001		2.77E-02	-0.6873	2.68E-02	1.0164
2.87E-02	0.0116	2.26E-02	0.3271		2.78E-02	-0.8427	2.70E-02	1.0373
2.88E-02	-0.4075	2.27E-02	0.3102		2.80E-02	-1.0481	2.72E-02	1.1237
2.90E-02	-0.3593	2.29E-02	0.1684		2.82E-02	-1.0937	2.73E-02	1.0702
2.92E-02	-0.2230	2.30E-02	0.2499		2.83E-02	-0.8754	2.75E-02	1.1488
2.93E-02	-0.1634	2.32E-02	0.2829		2.85E-02	-0.6146	2.77E-02	1.1881
2.95E-02	-0.2779	2.33E-02	0.1546		2.87E-02	-1.0194	2.78E-02	0.8287
2.97E-02	-0.1006	2.35E-02	0.1671		2.88E-02	-0.9613	2.80E-02	1.0341
2.98E-02	-0.0040	2.36E-02	0.2443		2.90E-02	-0.6050	2.82E-02	1.1004
3.00E-02	0.0478	2.37E-02	0.2721		2.92E-02	-0.4493	2.83E-02	0.9657
3.02E-02	-0.0339	2.39E-02	0.3199		2.93E-02	-0.2030	2.85E-02	0.6285

Table D1f Recovery temperature difference data from tests 6-11. (cont.)

Test 6		Test 7		Test 8		Test 9		Test 10	
x [m]	Tr [K]	x [m]	Tr [K]	x [m]	Tr [K]	x [m]	Tr [K]	x [m]	Tr [K]
3.03E-02	-0.0312	2.40E-02	0.1798					2.87E-02	0.7396
3.05E-02	-0.2006	2.42E-02	0.2336					2.88E-02	0.7457
3.07E-02	0.4017	2.43E-02	0.1771					2.90E-02	0.9317
3.09E-02	0.3552	2.45E-02	0.1181					2.92E-02	0.8871
3.10E-02	0.1186	2.46E-02	0.1210					2.93E-02	1.1266
3.12E-02	-0.0703	2.48E-02	0.0615					2.95E-02	1.0128
3.14E-02	-0.3542	2.49E-02	0.1639					2.97E-02	0.2982
3.15E-02	-0.3587	2.50E-02	0.1772					2.98E-02	0.7362
3.17E-02	-0.0175	2.52E-02	0.0996					3.00E-02	0.8730
3.19E-02	0.1210							3.02E-02	0.8281
3.20E-02	0.1917							3.03E-02	0.9782
3.22E-02	0.1562							3.05E-02	1.0306
3.24E-02	0.1996							3.07E-02	0.7797
3.25E-02	0.3335							3.09E-02	1.0108
3.27E-02	0.5593							3.10E-02	1.2878
3.29E-02	0.4957							3.12E-02	1.4050
								3.14E-02	1.2738
								3.15E-02	1.5275
								3.17E-02	1.2834
								3.19E-02	1.3670
								3.20E-02	1.8346
								3.22E-02	1.8510
								3.24E-02	1.4657
								3.25E-02	1.3615
								3.27E-02	1.0148
								3.29E-02	1.0195
								3.30E-02	1.1381
								3.32E-02	1.4257
								3.34E-02	1.2346
								3.35E-02	1.4061
								3.37E-02	1.0951
								3.39E-02	1.0544
								3.40E-02	1.2560
								3.42E-02	1.3411
								3.44E-02	1.3941
								3.45E-02	0.9929
								3.47E-02	0.8346
								3.49E-02	0.9648

Table D1g Recovery temperature difference data from tests 11-15.

Test 11		Test 12		Test 13		Test 14		Test 15	
x [m]	Tr [K]								
0.00E+00	1.5821	0.00E+00	2.3228	0.00E+00	2.0775	0.00E+00	1.1369	0.00E+00	0.8035
7.63E-05	1.4430	7.63E-05	2.3136	7.41E-05	2.1332	6.71E-05	1.1007	6.71E-05	0.7549
1.53E-04	1.5223	1.53E-04	2.2337	1.48E-04	2.1671	1.34E-04	1.0497	1.34E-04	0.7618
2.29E-04	1.8865	2.29E-04	2.1961	2.22E-04	2.2538	2.01E-04	1.1907	2.01E-04	0.9111
3.05E-04	1.6813	3.05E-04	2.2710	2.96E-04	2.1952	2.69E-04	1.0877	2.69E-04	0.8459
3.82E-04	1.6905	3.82E-04	2.2885	3.71E-04	2.1732	3.36E-04	1.1250	3.36E-04	0.8761
4.58E-04	1.7896	4.58E-04	2.3445	4.45E-04	2.1135	4.03E-04	1.1688	4.03E-04	0.8823
5.35E-04	1.8726	5.35E-04	2.3793	5.19E-04	2.0802	4.70E-04	1.2154	4.70E-04	0.8901
6.11E-04	1.8971	6.11E-04	2.4553	5.93E-04	2.0249	5.37E-04	1.2624	5.37E-04	0.8425
6.88E-04	1.9024	6.88E-04	2.4853	6.68E-04	2.0021	6.05E-04	1.2846	6.05E-04	0.8150
7.65E-04	1.9023	7.65E-04	2.5619	7.42E-04	1.9423	6.72E-04	1.3075	6.72E-04	0.8160
8.41E-04	1.9009	8.41E-04	2.6558	8.16E-04	1.8370	7.39E-04	1.2978	7.39E-04	0.8199
9.18E-04	1.9331	9.18E-04	2.6984	8.91E-04	1.7651	8.07E-04	1.2801	8.07E-04	0.7685
9.95E-04	2.0289	9.95E-04	2.7514	9.66E-04	1.7094	8.74E-04	1.2631	8.74E-04	0.7182
1.07E-03	2.0754	1.07E-03	2.7747	1.04E-03	1.6772	9.42E-04	1.2545	9.42E-04	0.6540
1.15E-03	2.0016	1.15E-03	2.7650	1.12E-03	1.6918	1.01E-03	1.2628	1.01E-03	0.6288
1.23E-03	1.8949	1.23E-03	2.7953	1.19E-03	1.6702	1.08E-03	1.2456	1.08E-03	0.6130

Table D1g Recovery temperature difference data from tests 11-15. (cont.)

Test 11	x [m]	Tr [K]	Test 12	x [m]	Tr [K]	Test 13	x [m]	Tr [K]	Test 14	x [m]	Tr [K]	Test 15	x [m]	Tr [K]
1.30E-03	1.8022	1.30E-03	2.8005	1.27E-03	1.6511	1.15E-03	1.2332	1.15E-03	0.6372					
1.38E-03	1.7528	1.38E-03	2.8514	1.34E-03	1.6120	1.21E-03	1.2343	1.21E-03	0.6446					
1.46E-03	1.7050	1.46E-03	2.8196	1.42E-03	1.5990	1.28E-03	1.2523	1.28E-03	0.6325					
1.54E-03	1.7462	1.54E-03	2.7252	1.49E-03	1.6442	1.35E-03	1.2731	1.35E-03	0.5882					
1.62E-03	1.7777	1.62E-03	2.6868	1.57E-03	1.6562	1.42E-03	1.2869	1.42E-03	0.5779					
1.69E-03	1.7121	1.69E-03	2.6572	1.64E-03	1.6145	1.49E-03	1.3046	1.49E-03	0.5664					
1.77E-03	1.6822	1.77E-03	2.5571	1.72E-03	1.6278	1.55E-03	1.3051	1.55E-03	0.5573					
1.85E-03	1.6547	1.85E-03	2.5469	1.79E-03	1.6287	1.62E-03	1.2642	1.62E-03	0.5313					
1.93E-03	1.6546	1.93E-03	2.5183	1.87E-03	1.6262	1.69E-03	1.2718	1.69E-03	0.4755					
2.01E-03	1.6592	2.01E-03	2.4124	1.95E-03	1.6488	1.76E-03	1.3094	1.76E-03	0.4168					
2.09E-03	1.6574	2.09E-03	2.2845	2.02E-03	1.6548	1.83E-03	1.3488	1.83E-03	0.3597					
2.17E-03	1.5959	2.17E-03	2.1926	2.10E-03	1.6439	1.90E-03	1.3265	1.90E-03	0.2906					
2.25E-03	1.4993	2.25E-03	2.1432	2.18E-03	1.6291	1.97E-03	1.2933	1.97E-03	0.2601					
2.33E-03	1.3499	2.33E-03	2.0901	2.26E-03	1.5645	2.04E-03	1.3687	2.04E-03	0.2086					
2.41E-03	1.2272	2.41E-03	2.0640	2.33E-03	1.6383	2.11E-03	1.4111	2.11E-03	0.1526					
2.49E-03	1.2376	2.49E-03	2.0794	2.41E-03	1.6428	2.18E-03	1.4309	2.18E-03	0.1134					
2.57E-03	1.2821	2.57E-03	2.0335	2.49E-03	1.6254	2.25E-03	1.4900	2.25E-03	0.0870					
2.65E-03	1.2947	2.65E-03	2.0013	2.57E-03	1.5948	2.32E-03	1.5329	2.32E-03	0.0987					
2.73E-03	1.3036	2.73E-03	2.0073	2.65E-03	1.5546	2.39E-03	1.5123	2.39E-03	0.0787					
2.81E-03	1.1319	2.81E-03	2.0661	2.72E-03	1.5252	2.46E-03	1.5351	2.46E-03	0.0678					
2.89E-03	1.3379	2.89E-03	2.1531	2.80E-03	1.4707	2.53E-03	1.5988	2.53E-03	0.0700					
2.98E-03	1.4284	2.98E-03	2.2761	2.88E-03	1.4568	2.60E-03	1.7153	2.60E-03	0.0744					
3.06E-03	1.5256	3.06E-03	2.3276	2.96E-03	1.5194	2.67E-03	1.6806	2.67E-03	0.0866					
3.14E-03	1.5934	3.14E-03	2.3464	3.04E-03	1.4329	2.74E-03	1.7342	2.74E-03	0.1237					
3.23E-03	1.5187	3.23E-03	2.3860	3.12E-03	1.4277	2.82E-03	1.8155	2.82E-03	0.1435					
3.31E-03	1.4980	3.31E-03	2.3726	3.20E-03	1.5178	2.89E-03	1.8379	2.89E-03	0.1354					
3.39E-03	1.5440	3.39E-03	2.3868	3.29E-03	1.5959	2.96E-03	1.8374	2.96E-03	0.1630					
3.48E-03	1.5568	3.48E-03	2.4650	3.37E-03	1.5541	3.03E-03	1.8740	3.03E-03	0.1745					
3.56E-03	2.0015	3.56E-03	2.4645	3.45E-03	1.5130	3.11E-03	1.8411	3.11E-03	0.2422					
3.65E-03	2.0019	3.65E-03	2.3927	3.53E-03	1.5647	3.18E-03	1.7818	3.18E-03	0.2889					
3.74E-03	1.9079	3.74E-03	2.3383	3.62E-03	1.5008	3.25E-03	1.7056	3.25E-03	0.2916					
3.82E-03	1.8211	3.82E-03	2.6118	3.70E-03	1.3981	3.33E-03	1.6600	3.33E-03	0.3405					
3.91E-03	1.8296	3.91E-03	2.9459	3.78E-03	1.3615	3.40E-03	1.5367	3.40E-03	0.3646					
4.00E-03	1.8980	4.00E-03	3.0769	3.87E-03	1.2056	3.47E-03	1.3984	3.47E-03	0.3380					
4.09E-03	2.4253	4.09E-03	3.1168	3.95E-03	1.1130	3.55E-03	1.3469	3.55E-03	0.3479					
4.18E-03	2.1344	4.18E-03	3.0570	4.04E-03	1.0741	3.63E-03	1.3812	3.63E-03	0.3089					
4.27E-03	2.0779	4.27E-03	3.1605	4.12E-03	1.2663	3.70E-03	1.5089	3.70E-03	0.2744					
4.36E-03	1.8179	4.36E-03	3.2767	4.21E-03	1.4283	3.78E-03	1.5908	3.78E-03	0.2084					
4.45E-03	1.4415	4.45E-03	3.4264	4.30E-03	1.3081	3.85E-03	1.6873	3.85E-03	0.1583					
4.54E-03	1.6143	4.54E-03	3.4498	4.39E-03	1.4804	3.93E-03	1.6793	3.93E-03	0.1307					
4.63E-03	1.4480	4.63E-03	3.2428	4.48E-03	1.6964	4.01E-03	1.6551	4.01E-03	0.0625					
4.72E-03	1.2846	4.72E-03	3.1609	4.56E-03	1.5052	4.09E-03	1.7829	4.09E-03	0.0120					
4.82E-03	1.1980	4.82E-03	3.1807	4.65E-03	1.5535	4.16E-03	1.8292	4.16E-03	0.0060					
4.91E-03	0.6557	4.91E-03	3.3003	4.75E-03	1.7296	4.24E-03	1.9768	4.24E-03	-0.0259					
5.01E-03	0.8524	5.01E-03	3.3448	4.84E-03	1.8363	4.32E-03	1.9971	4.32E-03	-0.0302					
5.11E-03	1.1270	5.11E-03	3.1875	4.93E-03	1.7107	4.40E-03	1.9522	4.40E-03	0.0087					
5.20E-03	1.1991	5.20E-03	3.1857	5.02E-03	1.6362	4.48E-03	1.8116	4.48E-03	-0.0103					
5.30E-03	1.4383	5.30E-03	3.0957	5.12E-03	1.7635	4.56E-03	1.7423	4.56E-03	-0.0313					
5.40E-03	1.2402	5.40E-03	3.1928	5.21E-03	1.7462	4.64E-03	1.6454	4.64E-03	-0.0343					
5.50E-03	1.3093	5.50E-03	3.2966	5.14E-03	1.8746	4.73E-03	1.7390	4.73E-03	-0.0288					
5.61E-03	1.3309	5.61E-03	3.1306	5.40E-03	1.7727	4.81E-03	1.5236	4.81E-03	0.0535					
5.71E-03	1.2790	5.71E-03	3.2202	5.65E-03	1.7216	4.89E-03	1.4731	4.89E-03	0.1389					
5.82E-03	1.2775	5.82E-03	3.1539	5.89E-03	1.0678	4.98E-03	1.3607	4.98E-03	0.1321					
5.92E-03	1.3091	5.92E-03	3.2297	6.13E-03	1.1391	5.06E-03	1.2712	5.06E-03	0.1914					
6.03E-03	1.0141	6.03E-03	3.2102	6.36E-03	1.2124	5.15E-03	1.0557	5.15E-03	0.1627					
6.14E-03	1.2236	6.14E-03	3.1444	6.58E-03	0.9090	5.23E-03	1.0473	5.23E-03	0.1787					
6.25E-03	0.9431	6.25E-03	3.1649	6.79E-03	0.9518	5.32E-03	1.1303	5.32E-03	0.2245					
6.36E-03	1.0321	6.36E-03	3.0360	7.01E-03	1.0232	5.41E-03	1.2237	5.41E-03	0.2587					
6.48E-03	1.2042	6.48E-03	2.9161	7.21E-03	1.2231	5.50E-03	1.2949	5.50E-03	0.2205					
6.59E-03	1.3189	6.59E-03	3.0044	7.42E-03	1.3665	5.59E-03	1.3401	5.59E-03	0.2056					
6.71E-03	1.3542	6.71E-03	2.6349	7.62E-03	1.2660	5.68E-03	1.4151	5.68E-03	0.1523					
6.83E-03	1.2731	6.83E-03	2.8470	7.81E-03	1.2545	5.77E-03	1.3805	5.77E-03	0.1890					
6.96E-03	1.2298	6.96E-03	2.7513	8.01E-03	1.3558	5.86E-03	1.3119	6.05E-03	0.1364					

Table D1g Recovery temperature difference data from tests 11-15. (cont.)

Test 11	x [m]	Tr [K]	Test 12	x [m]	Tr [K]	Test 13	x [m]	Tr [K]	Test 14	x [m]	Tr [K]	Test 15	x [m]	Tr [K]
7.08E-03	1.2399	7.08E-03	2.6881	8.20E-03	1.4612	5.96E-03	1.3606	6.15E-03	0.1698					
7.21E-03	1.1096	7.21E-03	2.7364	8.39E-03	1.3513	6.05E-03	1.2229	6.25E-03	0.2166					
7.35E-03	1.3531	7.35E-03	2.7284	8.57E-03	1.3187	6.15E-03	0.9124	6.45E-03	0.2834					
7.48E-03	1.5194	7.48E-03	2.9857	8.76E-03	1.1606	6.25E-03	0.9094	6.55E-03	0.2730					
7.62E-03	1.5269	7.76E-03	2.8546	8.94E-03	1.0595	6.35E-03	0.7488	6.71E-03	-0.0241					
7.76E-03	1.5807	7.91E-03	3.0692	9.12E-03	0.9733	6.45E-03	0.8694	6.91E-03	-0.0276					
7.91E-03	1.5751	8.06E-03	3.1556	9.29E-03	0.9899	6.55E-03	0.7117	7.10E-03	-0.0143					
8.06E-03	1.5801	8.22E-03	2.5375	9.47E-03	1.0684	6.65E-03	0.6170	7.29E-03	-0.2495					
8.39E-03	1.5622	8.39E-03	2.5313	9.65E-03	1.0105	6.76E-03	0.6430	7.48E-03	-0.2114					
8.56E-03	1.5925	8.56E-03	2.4157	9.82E-03	1.0394	6.86E-03	0.6879	7.66E-03	-0.3228					
8.74E-03	1.0608	8.74E-03	2.2288	9.99E-03	1.1191	6.97E-03	0.8805	7.84E-03	-0.2559					
8.93E-03	1.0599	8.93E-03	1.8899	1.02E-02	0.9962	7.09E-03	1.1283	8.02E-03	-0.1695					
9.12E-03	1.3094	9.14E-03	1.6790	1.03E-02	0.8951	7.20E-03	1.1760	8.20E-03	-0.0241					
9.29E-03	1.0324	9.35E-03	1.8321	1.05E-02	1.2747	7.31E-03	0.9871	8.37E-03	-0.1524					
9.47E-03	1.0589	9.59E-03	1.4313	1.07E-02	1.6557	7.48E-03	0.9968	8.54E-03	-0.0568					
9.65E-03	1.1478	9.85E-03	1.4099	1.08E-02	1.5137	7.66E-03	0.9291	8.71E-03	-0.0692					
9.82E-03	1.2428	9.99E-03	0.9776	1.10E-02	1.1264	7.84E-03	0.8268	8.88E-03	0.0414					
9.99E-03	1.2519	1.02E-02	0.7005	1.12E-02	1.2442	8.02E-03	0.8510	9.05E-03	-0.0808					
1.02E-02	1.1487	1.03E-02	0.8813	1.14E-02	1.6106	8.20E-03	0.8577	9.21E-03	-0.1041					
1.03E-02	1.2414	1.05E-02	1.0119	1.15E-02	1.7369	8.37E-03	0.8106	9.38E-03	-0.0014					
1.05E-02	1.3252	1.07E-02	1.3067	1.17E-02	1.6352	8.54E-03	0.6987	9.54E-03	-0.0080					
1.07E-02	1.4697	1.08E-02	1.4024	1.19E-02	1.5442	8.71E-03	0.5826	9.70E-03	-0.2186					
1.08E-02	1.0684	1.10E-02	1.0351	1.20E-02	0.9739	8.88E-03	0.6630	9.86E-03	-0.0631					
1.10E-02	1.1126	1.12E-02	0.9772	1.22E-02	1.0345	9.05E-03	0.5136	1.00E-02	-0.0528					
1.12E-02	1.6630	1.14E-02	0.8617	1.24E-02	1.4051	9.21E-03	0.3645	1.02E-02	0.0547					
1.14E-02	1.5182	1.15E-02	0.8947	1.25E-02	1.7116	9.38E-03	0.3521	1.03E-02	-0.4100					
1.15E-02	1.7834	1.17E-02	0.8928	1.27E-02	1.6938	9.54E-03	0.4121	1.05E-02	-0.1592					
1.17E-02	1.3154	1.19E-02	0.8437	1.29E-02	1.9931	9.70E-03	0.4808	1.07E-02	-0.1093					
1.19E-02	1.0505	1.20E-02	0.8990	1.30E-02	1.9238	9.86E-03	0.4540	1.08E-02	-0.0061					
1.20E-02	1.5006	1.22E-02	1.0607	1.32E-02	1.5344	1.00E-02	0.4299	1.10E-02	-0.3204					
1.22E-02	1.2130	1.24E-02	0.9908	1.34E-02	1.4386	1.02E-02	0.3576	1.11E-02	-0.2431					
1.24E-02	1.3823	1.25E-02	1.1003	1.35E-02	1.4517	1.03E-02	0.4470	1.13E-02	-0.2977					
1.25E-02	1.2053	1.27E-02	1.1577	1.37E-02	1.4602	1.05E-02	0.4710	1.14E-02	-0.1669					
1.27E-02	1.2962	1.29E-02	1.2678	1.39E-02	1.4749	1.07E-02	0.2566	1.16E-02	-0.2693					
1.29E-02	1.8922	1.30E-02	1.3831	1.40E-02	1.6345	1.08E-02	0.3784	1.17E-02	-0.3676					
1.30E-02	1.4058	1.32E-02	1.4239	1.42E-02	1.6703	1.10E-02	0.6138	1.19E-02	-0.3916					
1.32E-02	1.7104	1.34E-02	1.2939	1.44E-02	1.3457	1.11E-02	0.4326	1.20E-02	-0.3305					
1.34E-02	1.6192	1.35E-02	1.1037	1.45E-02	1.0733	1.13E-02	0.5623	1.22E-02	-0.3069					
1.35E-02	1.8710	1.37E-02	1.2854	1.47E-02	1.4307	1.14E-02	0.4601	1.24E-02	-0.2453					
1.37E-02	1.9670	1.39E-02	1.3340	1.49E-02	1.6223	1.16E-02	0.8529	1.25E-02	-0.1652					
1.39E-02	1.9173	1.40E-02	1.3482	1.50E-02	1.5630	1.17E-02	0.3125	1.27E-02	-0.2397					
1.40E-02	1.9161	1.42E-02	1.3368	1.52E-02	1.4702	1.19E-02	0.4005	1.28E-02	0.1913					
1.42E-02	1.8936	1.44E-02	0.9388	1.54E-02	1.6239	1.20E-02	0.7548	1.30E-02	0.2129					
1.44E-02	1.8395	1.45E-02	0.9134	1.56E-02	1.3933	1.22E-02	0.8066	1.31E-02	0.2534					
1.45E-02	2.1292	1.47E-02	1.0264	1.57E-02	1.3620	1.24E-02	0.7555	1.33E-02	0.0873					
1.47E-02	2.2109	1.49E-02	1.0469	1.59E-02	1.3837	1.25E-02	0.7100	1.34E-02	0.1934					
1.49E-02	2.0455	1.50E-02	1.0786	1.61E-02	1.2073	1.27E-02	0.5514	1.36E-02	-0.0369					
1.50E-02	1.8923	1.52E-02	1.5360	1.62E-02	1.1332	1.28E-02	0.5589	1.38E-02	-0.0139					
1.52E-02	1.5808	1.54E-02	1.1916	1.64E-02	1.0987	1.30E-02	0.5983	1.39E-02	0.0234					
1.54E-02	1.4719	1.56E-02	0.9940	1.66E-02	1.1136	1.31E-02	0.7214	1.41E-02	0.1463					
1.56E-02	1.4325	1.57E-02	1.0341	1.67E-02	1.0758	1.33E-02	0.8479	1.42E-02	-0.1129					
1.57E-02	1.6915	1.59E-02	1.0633	1.69E-02	1.0753	1.34E-02	0.8996	1.44E-02	-0.0286					
1.59E-02	1.8781	1.61E-02	1.3654	1.71E-02	0.9760	1.36E-02	0.9527	1.45E-02	0.0949					
1.61E-02	1.3871	1.62E-02	1.3321	1.72E-02	0.9206	1.38E-02	0.7372	1.47E-02	0.0473					
1.62E-02	1.3990	1.64E-02	1.3031	1.74E-02	0.9131	1.39E-02	0.8667	1.48E-02	0.1766					
1.64E-02	1.5226	1.66E-02	1.2101	1.76E-02	0.9459	1.41E-02	0.6724	1.50E-02	-0.1438					
1.66E-02	1.7411	1.67E-02	0.7488	1.77E-02	0.8519	1.42E-02	0.7358	1.52E-02	-0.2342					
1.67E-02	1.5126	1.69E-02	0.7275	1.79E-02	0.9110	1.44E-02	0.8597	1.53E-02	-0.1774					
1.69E-02	1.4527	1.71E-02	0.9584	1.81E-02	1.0666	1.45E-02	0.4104	1.55E-02	0.0161					
1.71E-02	1.3593	1.72E-02	0.8478	1.82E-02	0.9213	1.47E-02	0.8488	1.56E-02	-0.0292					
1.72E-02	1.1403	1.74E-02	1.2792	1.84E-02	0.8793	1.48E-02	0.9212	1.58E-02	0.3549					
1.74E-02	0.8637	1.76E-02	1.4370	1.86E-02	0.9113	1.50E-02	0.5950	1.59E-02	-0.0916					
1.76E-02	0.9837	1.77E-02	1.6547	1.87E-02	0.9337	1.52E-02	0.6640	1.61E-02	-0.1391					

Table D1g Recovery temperature difference data from tests 11-15. (cont.)

Test 11	x [m]	Tr [K]	Test 12	x [m]	Tr [K]	Test 13	x [m]	Tr [K]	Test 14	x [m]	Tr [K]	Test 15	x [m]	Tr [K]
1.77E-02	1.1292	1.79E-02	1.3256	1.89E-02	1.1767	1.53E-02	0.6827	1.62E-02	-0.1728					
1.79E-02	1.0835	1.81E-02	1.2034	1.91E-02	1.0868	1.55E-02	0.7357	1.64E-02	-0.0789					
1.81E-02	0.7142	1.82E-02	1.0894	1.93E-02	1.1313	1.56E-02	0.7853	1.65E-02	-0.0096					
1.82E-02	0.6703	1.84E-02	1.1741	1.94E-02	1.0262	1.58E-02	0.5788	1.67E-02	-0.3111					
1.84E-02	0.6739	1.86E-02	1.1534	1.96E-02	0.9081	1.59E-02	0.6075	1.69E-02	-0.8194					
1.86E-02	0.8565	1.87E-02	1.0732	1.98E-02	0.5984	1.61E-02	0.5401	1.70E-02	-0.6240					
1.87E-02	0.9371	1.89E-02	1.2115	1.99E-02	0.9093	1.62E-02	0.6060	1.72E-02	-0.6383					
1.89E-02	0.9282	1.91E-02	1.5190	2.01E-02	1.1297	1.64E-02	0.6480	1.73E-02	-0.5056					
1.91E-02	0.9140	1.93E-02	1.0583	2.03E-02	1.2546	1.65E-02	0.6613	1.75E-02	-1.0235					
1.93E-02	1.0982	1.94E-02	1.1424	2.04E-02	1.2637	1.67E-02	0.6560	1.76E-02	-0.9369					
1.94E-02	1.0233	1.96E-02	1.3356	2.06E-02	1.1173	1.69E-02	0.5130	1.78E-02	-0.4951					
1.96E-02	1.0819	1.98E-02	1.3463	2.08E-02	1.0148	1.70E-02	0.5444	1.79E-02	-0.7442					
1.98E-02	1.1182	1.99E-02	1.5617	2.09E-02	1.3888	1.72E-02	0.7409	1.81E-02	-0.5336					
1.99E-02	1.4215	2.01E-02	1.4846	2.11E-02	0.9234	1.73E-02	0.7886	1.83E-02	-0.7852					
2.01E-02	1.2554	2.03E-02	1.3581	2.13E-02	0.9851	1.75E-02	0.2726	1.84E-02	-0.7458					
2.03E-02	1.1734	2.04E-02	1.4186	2.14E-02	1.2448	1.76E-02	0.4469	1.86E-02	-0.4040					
2.04E-02	1.3702	2.06E-02	1.4159	2.16E-02	1.3139	1.78E-02	0.2930	1.87E-02	-0.8226					
2.06E-02	1.2339	2.08E-02	1.0453	2.18E-02	2.0549	1.79E-02	0.4274	1.89E-02	-0.7115					
2.08E-02	1.2553	2.09E-02	0.9086	2.19E-02	1.2952	1.81E-02	0.3960	1.90E-02	-0.7825					
2.09E-02	1.1126	2.11E-02	1.4021	2.21E-02	1.2148	1.83E-02	0.5521	1.92E-02	-0.5632					
2.11E-02	0.9795	2.13E-02	1.3262	2.23E-02	1.2342	1.84E-02	0.2453	1.93E-02	-0.3836					
2.13E-02	0.8930	2.14E-02	1.2689	2.24E-02	2.9472	1.86E-02	0.2220	1.95E-02	-0.7456					
2.14E-02	1.0991	2.16E-02	1.6383	2.26E-02	0.6052	1.87E-02	0.2497	1.97E-02	-0.2234					
2.16E-02	1.3173	2.18E-02	1.9084	2.28E-02	1.7440	1.89E-02	0.4463	1.98E-02	-0.7404					
2.18E-02	1.3894	2.19E-02	0.9110	2.29E-02	1.4090	1.90E-02	0.4390	2.00E-02	-0.7659					
2.19E-02	0.4683	2.21E-02	0.9757	2.31E-02	0.6415	1.92E-02	0.5555	2.01E-02	-0.4484					
2.21E-02	0.7509	2.23E-02	0.8968	2.33E-02	1.4440	1.93E-02	0.4433	2.03E-02	-0.5136					
2.23E-02	0.9676	2.24E-02	1.4538	2.35E-02	1.4560	1.95E-02	0.4568	2.04E-02	-0.4987					
2.24E-02	0.9949	2.26E-02	1.2361	2.36E-02	1.3205	1.97E-02	0.4902	2.06E-02	-0.4733					
2.26E-02	0.9827	2.28E-02	1.1511	2.38E-02	2.4792	1.98E-02	0.3990	2.07E-02	-0.6814					
2.28E-02	0.9565	2.29E-02	1.2212	2.40E-02	2.1355	2.00E-02	0.5502	2.09E-02	-0.5108					
2.29E-02	0.7526	2.31E-02	1.0340	2.41E-02	2.0487	2.01E-02	0.6103	2.10E-02	-0.3288					
2.31E-02	0.6635	2.33E-02	1.0727	2.43E-02	2.2458	2.03E-02	0.4814	2.12E-02	-0.0546					
2.33E-02	0.6472	2.35E-02	1.2047	2.45E-02	2.1054	2.04E-02	0.4247	2.14E-02	0.0090					
2.35E-02	0.7626	2.36E-02	1.6372	2.46E-02	2.2526	2.06E-02	0.3285	2.15E-02	-0.0740					
2.36E-02	0.8550	2.38E-02	1.4869	2.48E-02	2.4418	2.07E-02	0.3515							
2.38E-02	0.8550	2.40E-02	1.2165	2.50E-02	2.4309	2.09E-02	0.4951							
2.40E-02	0.7825	2.41E-02	1.0997	2.51E-02	2.2680	2.10E-02	0.6905							
2.41E-02	0.7965	2.43E-02	1.5053	2.53E-02	2.0710	2.12E-02	0.5491							
2.43E-02	0.6239	2.45E-02	1.8411	2.55E-02	2.5497	2.14E-02	0.5718							
2.45E-02	0.8088	2.46E-02	1.6429	2.56E-02	1.8070	2.15E-02	0.5518							
2.46E-02	0.8249	2.48E-02	1.4220	2.58E-02	1.8706	2.17E-02	0.4463							
2.48E-02	0.9364	2.50E-02	1.4641	2.60E-02	2.0412	2.18E-02	0.6625							
2.50E-02	1.0030	2.51E-02	1.4272	2.61E-02	1.6236	2.20E-02	0.3000							
2.51E-02	0.9066	2.53E-02	1.3252	2.63E-02	1.5689	2.21E-02	0.3095							
2.53E-02	1.1533	2.55E-02	1.1369	2.65E-02	1.8485	2.23E-02	0.4611							
2.55E-02	1.1381	2.56E-02	1.0879	2.66E-02	1.6981	2.24E-02	0.5707							
2.56E-02	0.8999	2.58E-02	1.3157	2.68E-02	1.2930	2.26E-02	0.4767							
2.58E-02	0.9995	2.60E-02	1.4692	2.70E-02	1.2759	2.28E-02	0.4481							
2.60E-02	1.0101	2.61E-02	1.8255	2.72E-02	1.6514	2.29E-02	0.2977							
2.61E-02	0.7260	2.63E-02	1.8500	2.73E-02	1.1120	2.31E-02	0.3820							
2.63E-02	0.5138	2.65E-02	1.4294	2.75E-02	1.6931	2.32E-02	0.3999							
2.65E-02	0.6960	2.66E-02	1.4071	2.77E-02	1.7699	2.34E-02	0.4316							
2.66E-02	0.9557	2.68E-02	1.3503	2.78E-02	1.5433	2.35E-02	0.3618							
2.68E-02	0.9381	2.70E-02	1.1894	2.80E-02	1.7319	2.37E-02	-0.0591							
2.70E-02	0.6152	2.72E-02	1.4668	2.82E-02	1.7078	2.38E-02	-0.0202							
2.72E-02	0.6085	2.73E-02	1.6700	2.83E-02	1.6244	2.40E-02	0.1801							
2.73E-02	0.8927	2.75E-02	0.9683	2.85E-02	1.0611	2.42E-02	0.2856							
2.75E-02	0.1989	2.77E-02	1.3806	2.87E-02	1.2859	2.43E-02	0.2737							
2.77E-02	0.0390	2.78E-02	1.0812	2.88E-02	1.4154	2.45E-02	0.2691							
2.78E-02	-0.0572	2.80E-02	1.0623	2.90E-02	1.4817	2.46E-02	0.2933							
2.80E-02	0.2107	2.82E-02	1.0557	2.92E-02	1.6085	2.48E-02	0.1861							
2.82E-02	0.3118	2.83E-02	1.0895	2.93E-02	1.5270	2.49E-02	0.2506							

Table D1g Recovery temperature difference data from tests 11-15. (cont.)

Test 11 x [m]	Tr [K]	Test 12 x [m]	Tr [K]	Test 13 x [m]	Tr [K]	Test 14 x [m]	Tr [K]	Test 15 x [m]	Tr [K]
2.83E-02	0.5040	2.85E-02	1.1184	2.95E-02	1.1223	2.51E-02	0.2449		
2.85E-02	-0.0537	2.87E-02	1.0284	2.97E-02	2.2110	2.52E-02	0.4409		
2.87E-02	-0.0722	2.88E-02	1.0462	2.98E-02	1.8975	2.54E-02	0.4744		
2.88E-02	-0.3124	2.90E-02	1.1578	3.00E-02	1.6675	2.55E-02	0.4822		
2.90E-02	-0.1348	2.92E-02	1.4895	3.02E-02	1.6147	2.57E-02	0.6212		
2.92E-02	0.0506	2.93E-02	0.9332	3.03E-02	2.0451	2.59E-02	0.0969		
2.93E-02	-0.2854	2.95E-02	1.0855	3.05E-02	2.0386	2.60E-02	0.1175		
2.95E-02	-0.1220	2.97E-02	1.2265	3.07E-02	1.7461	2.62E-02	0.1475		
2.97E-02	-0.3411	2.98E-02	1.1932	3.09E-02	2.1804	2.63E-02	0.3230		
2.98E-02	-0.0865	3.00E-02	1.3061	3.10E-02	1.9888	2.65E-02	0.0954		
3.00E-02	-0.0017	3.02E-02	1.3183	3.12E-02	1.9841	2.66E-02	-0.0206		
3.02E-02	0.1587	3.03E-02	1.3830	3.14E-02	2.1351	2.68E-02	0.1785		
3.03E-02	0.3710	3.05E-02	1.1904	3.15E-02	2.0578	2.69E-02	0.1963		
3.05E-02	0.5602	3.07E-02	1.1164	3.17E-02	1.7686	2.71E-02	0.2871		
3.07E-02	0.3362	3.09E-02	1.1687	3.19E-02	1.8563	2.73E-02	0.3427		
3.09E-02	0.3821	3.10E-02	1.2087	3.20E-02	1.7850	2.74E-02	0.4147		
3.10E-02	0.4059	3.12E-02	1.2169	3.22E-02	1.9949	2.76E-02	0.5580		
3.12E-02	0.4697	3.14E-02	1.1404	3.24E-02	1.9884	2.77E-02	0.4006		
3.14E-02	0.3254	3.15E-02	1.4549	3.25E-02	1.5788	2.79E-02	0.6140		
3.15E-02	0.1540	3.17E-02	1.1551	3.27E-02	1.3494	2.80E-02	0.3677		
3.17E-02	0.1547	3.19E-02	1.3548	3.29E-02	1.3176	2.82E-02	0.3783		
		3.20E-02	1.6338	3.30E-02	1.4201	2.83E-02	0.3836		
		3.22E-02	1.4821	3.32E-02	1.0705	2.85E-02	0.2676		
		3.24E-02	1.5152	3.34E-02	1.0485	2.87E-02	0.2582		
		3.25E-02	1.2636	3.35E-02	1.1551				
		3.27E-02	1.5070	3.37E-02	1.7649				
		3.29E-02	1.6758	3.39E-02	1.3329				
		3.30E-02	1.6578	3.40E-02	1.3865				
		3.32E-02	1.4497	3.42E-02	1.2090				
		3.34E-02	2.4321	3.44E-02	0.7972				
		3.35E-02	1.9898	3.45E-02	0.8811				
		3.37E-02	1.8392	3.47E-02	1.1657				
		3.39E-02	1.3225	3.49E-02	1.0610				
		3.40E-02	1.2167	3.51E-02	1.1045				
		3.42E-02	0.9573	3.52E-02	1.1322				
		3.44E-02	1.0695	3.54E-02	0.8485				
		3.45E-02	1.6058	3.56E-02	0.8079				
		3.47E-02	1.6392	3.57E-02	2.1078				
		3.49E-02	1.6990	3.59E-02	2.1762				
		3.51E-02	1.8935	3.61E-02	2.2932				
		3.52E-02	1.9328	3.62E-02	1.7108				
		3.54E-02	1.7214	3.64E-02	1.3007				
		3.56E-02	1.9620	3.66E-02	1.4475				
		3.57E-02	1.7584	3.67E-02	1.5783				
		3.59E-02	1.6978	3.69E-02	1.3058				
		3.61E-02	1.7522	3.71E-02	1.0035				
		3.62E-02	1.4505	3.72E-02	1.0325				
		3.64E-02	2.0483	3.74E-02	0.6931				
		3.66E-02	1.2135	3.76E-02	0.5795				
		3.67E-02	1.2131						
		3.69E-02	1.2457						
		3.71E-02	1.4707						
		3.72E-02	1.5929						
		3.74E-02	1.5972						
		3.76E-02	1.6830						

Table D1h Recovery temperature difference data from tests 16-19.

Test 16	Test 17	Test 18	Test 19						
x [m]	Tr [K]	x [m]	Tr [K]	x [m]	Tr [K]	x [m]	Tr [K]	x [m]	Tr [K]
0.00E+00	-0.0314	0.00E+00	1.4716	0.00E+00	-0.1630	0.00E+00	0.6527		
6.54E-05	0.1257	6.54E-05	1.3052	6.58E-05	0.0242	6.71E-05	0.6569		
1.31E-04	0.1371	1.31E-04	1.3736	1.32E-04	0.0544	1.34E-04	0.9053		
1.96E-04	0.0802	1.96E-04	1.4041	1.97E-04	0.0635	2.01E-04	0.7176		
2.61E-04	0.0341	2.61E-04	1.2096	2.63E-04	-0.1447	2.69E-04	0.8694		
3.27E-04	0.0158	3.27E-04	1.1619	3.29E-04	-0.0971	3.36E-04	0.9159		
3.92E-04	-0.0004	3.92E-04	1.3432	3.95E-04	-0.0616	4.03E-04	0.9571		
4.58E-04	-0.0254	4.58E-04	1.4277	4.61E-04	-0.1040	4.70E-04	0.9766		
5.23E-04	-0.0439	5.23E-04	1.4580	5.27E-04	-0.0424	5.37E-04	1.0141		
5.89E-04	-0.0498	5.89E-04	1.4412	5.93E-04	-0.1155	6.05E-04	1.0325		
6.54E-04	-0.0418	6.54E-04	1.6257	6.59E-04	-0.0919	6.72E-04	1.0127		
7.20E-04	-0.0160	7.20E-04	1.1506	7.25E-04	-0.0824	7.39E-04	0.9848		
7.86E-04	0.0015	7.86E-04	1.1478	7.91E-04	-0.1199	8.07E-04	0.9571		
8.51E-04	-0.0108	8.51E-04	0.9757	8.57E-04	-0.0408	8.74E-04	0.9367		
9.17E-04	0.0020	9.17E-04	0.8532	9.23E-04	-0.1952	9.42E-04	0.9124		
9.83E-04	0.0021	9.83E-04	0.6864	9.90E-04	-0.4734	1.01E-03	0.8928		
1.05E-03	0.0122	1.05E-03	1.1993	1.06E-03	-0.3041	1.08E-03	0.8613		
1.12E-03	0.0229	1.12E-03	1.3493	1.12E-03	-0.2456	1.15E-03	0.8338		
1.18E-03	0.0100	1.18E-03	0.7108	1.19E-03	-0.2036	1.21E-03	0.8572		
1.25E-03	-0.0079	1.25E-03	0.7239	1.26E-03	-0.1625	1.28E-03	0.8544		
1.31E-03	-0.0287	1.31E-03	0.6126	1.32E-03	-0.1731	1.35E-03	0.8495		
1.38E-03	-0.0434	1.38E-03	0.7605	1.39E-03	-0.3889	1.42E-03	0.8325		
1.45E-03	-0.0751	1.45E-03	0.6132	1.46E-03	-0.4354	1.49E-03	0.8473		
1.51E-03	-0.0723	1.51E-03	0.7783	1.52E-03	-0.3877	1.55E-03	0.8268		
1.58E-03	-0.0715	1.58E-03	0.7995	1.59E-03	-0.4013	1.62E-03	0.8213		
1.65E-03	-0.0863	1.65E-03	0.9557	1.66E-03	-0.3623	1.69E-03	0.8198		
1.71E-03	-0.1257	1.71E-03	0.6881	1.73E-03	-0.2610	1.76E-03	0.8231		
1.78E-03	-0.1432	1.78E-03	0.9534	1.79E-03	-0.2769	1.83E-03	0.8027		
1.85E-03	-0.1672	1.85E-03	0.9440	1.86E-03	-0.3466	1.90E-03	0.8049		
1.92E-03	-0.1832	1.92E-03	1.2532	1.93E-03	-0.1122	1.97E-03	0.8045		
1.98E-03	-0.2154	1.98E-03	0.9748	2.00E-03	-0.1248	2.04E-03	0.8073		
2.05E-03	-0.1811	2.05E-03	1.0659	2.06E-03	-0.1038	2.11E-03	0.7859		
2.12E-03	-0.1851	2.12E-03	1.2851	2.13E-03	-0.1302	2.18E-03	0.8170		
2.19E-03	-0.2061	2.19E-03	0.9435	2.20E-03	-0.2568	2.25E-03	0.8365		
2.26E-03	-0.2217	2.26E-03	0.9198	2.27E-03	-0.1534	2.32E-03	0.8370		
2.32E-03	-0.2105	2.32E-03	1.1755	2.34E-03	0.0641	2.39E-03	0.8317		
2.39E-03	-0.2182	2.39E-03	0.9269	2.41E-03	-0.1559	2.46E-03	0.8087		
2.46E-03	-0.2415	2.46E-03	0.5550	2.48E-03	-0.3722	2.53E-03	0.8349		
2.53E-03	-0.2688	2.53E-03	0.4743	2.55E-03	-0.0405	2.60E-03	0.8660		
2.60E-03	-0.2871	2.60E-03	1.8445	2.62E-03	-0.3171	2.67E-03	0.8995		
2.67E-03	-0.3383	2.67E-03	0.5068	2.69E-03	-0.3127	2.74E-03	0.9133		
2.74E-03	-0.3273	2.74E-03	1.5631	2.76E-03	-0.2982	2.82E-03	0.9088		
2.81E-03	-0.3825	2.81E-03	1.2699	2.83E-03	-0.2982	2.89E-03	0.9239		
2.88E-03	-0.4396	2.88E-03	0.5644	2.90E-03	-0.0168	2.96E-03	0.9499		
2.95E-03	-0.5081	2.95E-03	0.2496	2.97E-03	-0.2769	3.03E-03	1.0016		
3.02E-03	-0.5709	3.02E-03	1.1096	3.04E-03	-0.2915	3.11E-03	1.0402		
3.09E-03	-0.5925	3.09E-03	1.0006	3.11E-03	-0.1633	3.18E-03	1.0457		
3.16E-03	-0.5917	3.16E-03	0.8018	3.18E-03	-0.4033	3.25E-03	1.0517		
3.23E-03	-0.6016	3.23E-03	1.0144	3.26E-03	-0.4530	3.33E-03	1.0439		
3.31E-03	-0.5984	3.31E-03	0.4818	3.33E-03	-0.4304	3.40E-03	1.0299		
3.38E-03	-0.6773	3.38E-03	1.0587	3.40E-03	-0.0852	3.47E-03	1.0472		
3.45E-03	-0.5849	3.45E-03	0.2488	3.47E-03	-0.3167	3.55E-03	1.0202		
3.52E-03	-0.5291	3.52E-03	0.9968	3.55E-03	-0.0712	3.63E-03	0.9975		
3.60E-03	-0.4970	3.60E-03	0.7742	3.62E-03	-0.4408	3.70E-03	0.9607		
3.67E-03	-0.5014	3.67E-03	1.7933	3.70E-03	-0.2965	3.78E-03	0.9609		
3.74E-03	-0.5014	3.74E-03	1.1607	3.77E-03	-0.3002	3.85E-03	0.9596		
3.82E-03	-0.4802	3.82E-03	0.8416	3.85E-03	-0.2764	3.93E-03	0.9098		
3.89E-03	-0.4126	3.89E-03	1.0144	3.92E-03	-0.1853	4.01E-03	0.8803		
3.97E-03	-0.3813	3.97E-03	0.9723	4.00E-03	0.1766	4.09E-03	0.8926		
4.04E-03	-0.3148	4.04E-03	0.5157	4.07E-03	-0.5164	4.16E-03	0.8823		
4.12E-03	-0.2958	4.39E-03	0.8741	4.15E-03	-0.4363	4.24E-03	0.8959		
4.20E-03	-0.2873	4.67E-03	1.0513	4.23E-03	-0.4451	4.32E-03	0.9758		
4.27E-03	-0.1425	4.93E-03	0.9273	4.30E-03	-0.2788	4.40E-03	1.0463		

Table D1h Recovery temperature difference data from tests 16-19. (cont.)

Test 16	Test 17	Test 18	Test 19				
x [m]	Tr [K]						
4.35E-03	-0.0658	5.18E-03	0.8186	4.38E-03	-0.3179	4.48E-03	1.0600
4.43E-03	-0.0233	5.42E-03	1.0495	4.46E-03	0.0331	4.56E-03	1.0977
4.51E-03	-0.0954	5.65E-03	1.0073	4.54E-03	0.1263	4.64E-03	1.1593
4.59E-03	-0.1160	5.87E-03	0.8662	4.62E-03	0.0216	4.73E-03	1.2065
4.67E-03	-0.0845	6.09E-03	0.6677	4.70E-03	-0.5120	4.81E-03	1.1732
4.75E-03	-0.0656	6.30E-03	0.3463	4.78E-03	-0.1353	4.89E-03	1.0821
4.83E-03	-0.1774	6.51E-03	0.7539	4.86E-03	-0.2674	4.98E-03	1.1150
4.91E-03	-0.2469	6.71E-03	0.8812	4.95E-03	-0.6691	5.06E-03	1.0166
4.99E-03	-0.4128	6.91E-03	0.7871	5.03E-03	-0.1149	5.15E-03	0.9332
5.07E-03	-0.3749	7.10E-03	0.6913	5.11E-03	-0.6016	5.23E-03	0.9204
5.16E-03	-0.3356	7.29E-03	0.6835	5.20E-03	-0.0788	5.32E-03	0.7707
5.24E-03	-0.2966	7.48E-03	0.6906	5.28E-03	0.1123	5.41E-03	0.7440
5.32E-03	-0.3036	7.66E-03	0.6984	5.37E-03	-0.1254	5.50E-03	0.6770
5.41E-03	-0.3908	7.84E-03	0.6259	5.45E-03	0.1557	5.59E-03	0.5758
5.50E-03	-0.4314	8.02E-03	0.6120	5.54E-03	0.2019	5.68E-03	0.5919
5.58E-03	-0.4177	8.20E-03	0.5536	5.63E-03	-0.2346	5.77E-03	0.4829
5.67E-03	-0.3476	8.37E-03	0.5426	5.72E-03	-0.7961	5.86E-03	0.5069
5.76E-03	-0.1189	8.54E-03	0.4845	5.81E-03	0.2540	5.96E-03	0.6535
5.85E-03	-0.0810	8.71E-03	0.3863	5.90E-03	-0.6628	6.05E-03	0.5951
5.94E-03	-0.0869	8.88E-03	0.5160	5.99E-03	-0.3051	6.15E-03	0.6100
6.04E-03	-0.1372	9.05E-03	0.5693	6.09E-03	0.0893	6.30E-03	0.8483
6.13E-03	-0.1240	9.21E-03	0.2527	6.18E-03	-0.0115	6.51E-03	1.4980
6.23E-03	-0.1328	9.38E-03	0.3560	6.28E-03	-0.1354	6.71E-03	1.1738
6.32E-03	0.0099	9.54E-03	0.3172	6.38E-03	-0.4513	6.91E-03	0.6649
6.42E-03	0.0392	9.70E-03	0.3100	6.48E-03	-0.4175	7.10E-03	0.7377
6.52E-03	0.0224	9.86E-03	0.3885	6.71E-03	0.0298	7.29E-03	0.7161
6.62E-03	-0.1404	1.00E-02	0.3268	6.91E-03	0.0092	7.48E-03	0.7083
6.72E-03	-0.2077	1.02E-02	0.1746	7.10E-03	0.0048	7.66E-03	0.6035
6.82E-03	-0.3445	1.03E-02	0.4025	7.29E-03	0.0561	7.84E-03	0.5660
6.93E-03	-0.3510	1.05E-02	0.3793	7.48E-03	0.1027	8.02E-03	0.5380
7.04E-03	-0.3455	1.07E-02	0.2759	7.66E-03	0.0494	8.20E-03	0.4632
7.15E-03	-0.3481	1.08E-02	0.4959	7.84E-03	0.0634	8.37E-03	0.4120
7.26E-03	-0.5365	1.10E-02	0.5679	8.02E-03	0.0215	8.54E-03	0.6412
7.37E-03	-0.5835	1.11E-02	0.3778	8.20E-03	-0.0155	8.71E-03	0.4554
7.49E-03	-0.5890	1.13E-02	0.2962	8.37E-03	-0.0024	8.88E-03	0.4423
7.61E-03	-0.6581	1.14E-02	0.2184	8.54E-03	0.0839	9.05E-03	0.2979
7.73E-03	-0.6591	1.16E-02	0.1174	8.71E-03	0.0474	9.21E-03	0.2281
7.86E-03	-0.4873	1.17E-02	0.2606	8.88E-03	0.0585	9.38E-03	0.2464
7.98E-03	-0.2639	1.19E-02	0.2945	9.05E-03	-0.1110	9.54E-03	-0.0729
8.12E-03	-0.1182	1.20E-02	0.3195	9.21E-03	-0.1920	9.70E-03	-0.0550
8.25E-03	0.2672	1.22E-02	0.3067	9.38E-03	0.0171	9.86E-03	-0.0610
8.40E-03	0.3604	1.24E-02	0.2784	9.54E-03	-0.0656	1.00E-02	-0.2162
8.54E-03	0.4325	1.25E-02	0.2138	9.70E-03	-0.2562	1.02E-02	-0.1047
8.70E-03	0.3210	1.27E-02	0.3131	9.86E-03	-0.1539	1.03E-02	-0.0664
8.86E-03	0.3625	1.28E-02	0.3896	1.00E-02	-0.2103	1.05E-02	-0.1310
9.03E-03	0.4596	1.30E-02	0.4491	1.02E-02	-0.2258	1.07E-02	0.1236
9.21E-03	0.4636	1.31E-02	0.4192	1.03E-02	0.0180	1.08E-02	-0.1125
9.40E-03	0.2057	1.33E-02	0.4870	1.05E-02	0.0258	1.10E-02	0.1098
9.60E-03	0.0154	1.34E-02	0.2251	1.07E-02	-0.0254	1.11E-02	0.2142
9.83E-03	-0.2576	1.36E-02	0.0801	1.08E-02	0.0169	1.13E-02	0.7836
1.01E-02	-0.2625	1.38E-02	0.1857	1.10E-02	-0.0117	1.14E-02	0.0593
1.04E-02	-0.1446	1.39E-02	0.3619	1.11E-02	-0.1186	1.16E-02	0.5680
1.07E-02	0.0636	1.41E-02	0.2689	1.13E-02	-0.1178	1.17E-02	0.3646
1.12E-02	0.1342	1.42E-02	0.1309	1.14E-02	-0.1355	1.19E-02	0.6171
1.17E-02	0.1002	1.44E-02	0.1398	1.16E-02	-0.2998	1.20E-02	0.4768
1.22E-02	0.1404	1.45E-02	0.1710	1.17E-02	-0.1885	1.22E-02	0.6848
1.27E-02	0.3301	1.47E-02	0.1800	1.19E-02	-0.2860	1.24E-02	0.4250
1.32E-02	0.2550	1.48E-02	0.1930	1.20E-02	-0.4858	1.25E-02	0.1875
1.37E-02	0.2632	1.50E-02	0.1864	1.22E-02	-0.1042	1.27E-02	0.3100
1.42E-02	0.3754	1.52E-02	0.2459	1.24E-02	-0.0678	1.28E-02	0.3100
1.47E-02	0.3720	1.53E-02	0.2143	1.25E-02	-0.0718	1.30E-02	0.2209
1.48E-02	0.3531	1.55E-02	0.1021	1.27E-02	-0.2210	1.31E-02	0.5465
1.50E-02	0.3923	1.56E-02	0.2028	1.28E-02	0.0502	1.33E-02	0.4854

Table D1h Recovery temperature difference data from tests 16-19. (cont.)

Test 16	Test 17	Test 18	Test 19				
x [m]	Tr [K]	x [m]	Tr [K]	x [m]	Tr [K]	x [m]	Tr [K]
1.52E-02	0.3515	1.58E-02	0.3022	1.30E-02	-0.0947	1.34E-02	0.5534
1.53E-02	-0.0703	1.59E-02	0.2060	1.31E-02	-0.0766	1.36E-02	0.6955
1.55E-02	0.1330	1.61E-02	0.2763	1.33E-02	0.0035	1.38E-02	0.6789
1.56E-02	0.2737	1.62E-02	0.1872	1.34E-02	-0.0082	1.39E-02	0.6913
1.58E-02	0.2984	1.64E-02	0.1670	1.36E-02	0.0127	1.41E-02	0.7237
1.59E-02	0.3471	1.65E-02	0.1783	1.38E-02	-0.0667	1.42E-02	1.0932
1.61E-02	0.3157	1.67E-02	0.1351	1.39E-02	-0.0374	1.44E-02	1.0141
1.62E-02	0.1423	1.69E-02	0.1622	1.41E-02	-0.1038	1.45E-02	0.7299
1.64E-02	-0.2035	1.70E-02	0.0905	1.42E-02	-0.1130	1.47E-02	0.7217
1.65E-02	-0.3259	1.72E-02	0.1153	1.44E-02	-0.3149	1.48E-02	1.2255
1.67E-02	-0.5086	1.73E-02	0.1933	1.45E-02	0.0526	1.50E-02	1.2451
1.69E-02	-0.2736	1.75E-02	0.2454	1.47E-02	-0.0680	1.52E-02	0.9043
1.70E-02	0.1358	1.76E-02	0.1966	1.48E-02	0.0799	1.53E-02	0.5801
1.72E-02	0.0116	1.78E-02	0.2293	1.50E-02	0.1367	1.55E-02	0.5591
1.73E-02	-0.2001	1.79E-02	0.2961	1.52E-02	0.1259	1.56E-02	0.6264
1.75E-02	-0.2005	1.81E-02	0.4165	1.53E-02	0.1963	1.58E-02	0.6659
1.76E-02	-0.2385	1.83E-02	0.4445	1.55E-02	0.0699	1.59E-02	0.9450
1.78E-02	-0.4345	1.84E-02	0.4517	1.56E-02	-0.0459	1.61E-02	1.0929
1.79E-02	-0.5877	1.86E-02	0.4234	1.58E-02	-0.0034	1.62E-02	1.0525
1.81E-02	-0.4847	1.87E-02	0.3951	1.59E-02	0.0657	1.64E-02	0.9447
1.83E-02	-0.2875	1.89E-02	0.3848	1.61E-02	-0.0910	1.65E-02	0.8443
1.84E-02	0.9788	1.90E-02	0.4046	1.62E-02	-0.2649	1.67E-02	0.9051
1.86E-02	0.1858	1.92E-02	0.4663	1.64E-02	-0.2611	1.69E-02	1.0282
1.87E-02	0.0288	1.93E-02	0.4248	1.65E-02	-0.2712	1.70E-02	0.9379
1.89E-02	-0.2803	1.95E-02	0.3686	1.67E-02	-0.2740	1.72E-02	0.7482
1.90E-02	-0.0915	1.97E-02	0.4377	1.69E-02	-0.3049	1.73E-02	0.8598
1.92E-02	-0.3457	1.98E-02	0.3847	1.70E-02	-0.2648	1.75E-02	1.0289
1.93E-02	-0.2853	2.00E-02	0.2774	1.72E-02	-0.2892	1.76E-02	0.8946
1.95E-02	-0.7000	2.01E-02	0.2845	1.73E-02	-0.3286	1.78E-02	0.7268
1.97E-02	-0.5873	2.03E-02	0.2404	1.75E-02	-0.3544	1.79E-02	0.6327
1.98E-02	-0.3513	2.04E-02	0.3193	1.76E-02	-0.4238	1.81E-02	0.7061
2.00E-02	-0.3189	2.06E-02	0.3776	1.78E-02	0.0705	1.83E-02	0.7329
2.01E-02	-0.4506	2.07E-02	0.2387	1.79E-02	0.0392	1.84E-02	0.9911
2.03E-02	-0.2478	2.09E-02	0.0975	1.81E-02	0.0274	1.86E-02	0.2877
2.04E-02	-0.1554	2.10E-02	0.3542	1.83E-02	0.1230	1.87E-02	0.4535
2.06E-02	-0.2785	2.12E-02	0.6046	1.84E-02	0.0714	1.89E-02	0.7137
2.07E-02	-0.2228	2.14E-02	0.4407	1.86E-02	0.0260	1.90E-02	0.6455
2.09E-02	-0.2375	2.15E-02	0.3294	1.87E-02	0.0245	1.92E-02	0.5464
2.10E-02	-0.3211	2.17E-02	0.4259	1.89E-02	-0.0715	1.93E-02	0.5968
2.12E-02	-0.1851	2.18E-02	0.3205	1.90E-02	-0.3849	1.95E-02	0.3849
2.14E-02	0.1286	2.20E-02	0.2359	1.92E-02	-0.2058	1.97E-02	0.5347
2.15E-02	-0.1062	2.21E-02	0.2219	1.93E-02	-0.0276	1.98E-02	0.6037
2.17E-02	-0.0933	2.23E-02	0.1664	1.95E-02	0.0186	2.00E-02	0.6406
2.18E-02	-0.0741	2.24E-02	0.2568	1.97E-02	-0.0130	2.01E-02	0.7496
2.20E-02	-0.0820	2.26E-02	0.0273	1.98E-02	-0.1074	2.03E-02	0.7103
2.21E-02	-0.2963	2.28E-02	-0.0939	2.00E-02	-0.1828	2.04E-02	0.4746
2.23E-02	-0.3178	2.29E-02	-0.2220	2.01E-02	-0.1580	2.06E-02	0.5690
2.24E-02	-0.3238	2.31E-02	-0.1619	2.03E-02	-0.2114	2.07E-02	0.5445
2.26E-02	-0.4064	2.32E-02	-0.1220	2.04E-02	-0.1242	2.09E-02	0.5610
2.28E-02	-0.3619	2.34E-02	-0.0881	2.06E-02	-0.2302	2.10E-02	0.7858
2.29E-02	-0.2042	2.35E-02	-0.0481	2.07E-02	-0.3027	2.12E-02	0.8104
2.31E-02	-0.3233	2.37E-02	-0.1176	2.09E-02	-0.1606	2.14E-02	0.5711
2.32E-02	-0.3023	2.38E-02	-0.2274	2.10E-02	-0.1782	2.15E-02	0.5887
2.34E-02	-0.1387	2.40E-02	0.4675	2.12E-02	-0.1455	2.17E-02	0.5887
2.35E-02	-0.1447	2.42E-02	0.3494	2.14E-02	-0.1593	2.18E-02	0.6297
2.37E-02	-0.3012	2.43E-02	0.2297	2.15E-02	-0.4638	2.20E-02	0.3921
2.38E-02	-0.4235	2.45E-02	0.2137	2.17E-02	-0.5236	2.21E-02	0.5578
2.40E-02	-0.3093	2.46E-02	0.2795	2.18E-02	-0.4544	2.23E-02	0.3359
2.42E-02	-0.4139	2.48E-02	0.4049	2.20E-02	-0.3749	2.24E-02	0.4762
2.43E-02	-0.4692	2.49E-02	0.5440	2.21E-02	-0.3263	2.26E-02	0.5084
2.45E-02	-0.4162	2.51E-02	0.3741	2.23E-02	-0.1717	2.28E-02	0.5306
2.46E-02	-0.4933	2.52E-02	0.3440	2.24E-02	-0.2137	2.29E-02	0.4593
2.48E-02	-0.5929	2.54E-02	0.2529	2.26E-02	-0.2408	2.31E-02	0.3056

Table D1h Recovery temperature difference data from tests 16-19. (cont.)

Test 16	Test 17	Test 18	Test 19				
x [m]	Tr [K]	x [m]	Tr [K]	x [m]	Tr [K]	x [m]	Tr [K]
2.49E-02	-0.6980	2.55E-02	0.1394	2.28E-02	-0.1940	2.32E-02	0.3320
2.51E-02	-0.4154	2.57E-02	0.2351	2.29E-02	-0.1556	2.34E-02	0.7084
2.52E-02	-0.7052	2.59E-02	0.2129	2.31E-02	-0.0786	2.35E-02	0.2864
2.54E-02	-0.5992	2.60E-02	0.1445	2.32E-02	-0.0928	2.37E-02	0.3526
2.55E-02	-0.5410	2.62E-02	0.1714	2.34E-02	-0.0119	2.38E-02	0.3878
2.57E-02	-0.5698	2.63E-02	0.2081	2.35E-02	-0.1231	2.40E-02	0.4234
2.59E-02	-0.6364	2.65E-02	0.8062	2.37E-02	-0.1567	2.42E-02	0.2912
2.60E-02	-0.5177	2.66E-02	0.7565	2.38E-02	-0.1036	2.43E-02	0.4211
2.62E-02	-0.5309	2.68E-02	0.5779	2.40E-02	-0.0185	2.45E-02	0.6282
2.63E-02	-0.6224	2.69E-02	0.1020	2.42E-02	-0.0382	2.46E-02	0.2084
2.65E-02	-0.5819	2.71E-02	0.0902	2.43E-02	0.0227	2.48E-02	0.2124
2.66E-02	-0.5204	2.73E-02	0.0863	2.45E-02	-0.0017	2.49E-02	0.2336
2.68E-02	-0.8090	2.74E-02	0.4266	2.46E-02	-0.0623	2.51E-02	0.2824
2.69E-02	-0.7164	2.76E-02	0.4583	2.48E-02	-0.0922	2.52E-02	0.2551
2.71E-02	-0.6026	2.77E-02	0.4962	2.49E-02	-0.1068	2.54E-02	0.2177
2.73E-02	-0.4798	2.79E-02	0.2034	2.51E-02	-0.2822	2.55E-02	0.0772
2.74E-02	-0.7486	2.80E-02	-0.0126	2.52E-02	-0.2720	2.57E-02	0.1455
2.76E-02	-0.5132	2.82E-02	0.0962	2.54E-02	-0.2513	2.59E-02	0.2117
2.77E-02	-0.3163	2.83E-02	0.0097	2.55E-02	-0.3164		
2.79E-02	-0.1741	2.85E-02	0.0995	2.57E-02	-0.3899		
2.80E-02	-0.6097	2.87E-02	0.0368	2.59E-02	-0.3890		
2.82E-02	-0.4495	2.88E-02	0.0274	2.60E-02	-0.3925		
2.83E-02	-0.5602	2.90E-02	0.1198	2.62E-02	-0.3645		
2.85E-02	-0.4622	2.91E-02	0.1059	2.63E-02	-0.1828		
2.87E-02	-0.2936	2.93E-02	-0.3029	2.65E-02	-0.2636		
2.88E-02	-0.5593	2.94E-02	-0.1486	2.66E-02	-0.2988		
2.90E-02	-0.5137	2.96E-02	0.0501	2.68E-02	-0.2679		
2.91E-02	-0.4632	2.97E-02	-0.0458	2.69E-02	-0.2661		
2.93E-02	-0.4285	2.99E-02	-0.0231	2.71E-02	-0.2369		
2.94E-02	-0.5047	3.00E-02	-0.2276	2.73E-02	-0.2111		
2.96E-02	-0.6556	3.02E-02	-0.0702	2.74E-02	-0.1007		
2.97E-02	-0.6114	3.04E-02	-0.0694	2.76E-02	-0.1828		
2.99E-02	-0.5719	3.05E-02	-0.0642	2.77E-02	-0.2199		
3.00E-02	-0.3783	3.07E-02	-0.0010	2.79E-02	-0.0395		
3.02E-02	-0.5162	3.08E-02	0.0305	2.80E-02	0.0391		
3.04E-02	-0.6641	3.10E-02	-0.0404	2.82E-02	0.1261		
3.05E-02	-0.5259	3.11E-02	-0.1037	2.83E-02	-0.1793		
3.07E-02	-0.4612	3.13E-02	-0.0817	2.85E-02	-0.1382		
3.08E-02	-0.4480	3.14E-02	-0.1118	2.87E-02	-0.0102		
3.10E-02	-0.6984	3.16E-02	-0.0032	2.88E-02	-0.5455		
3.11E-02	-0.5912	3.18E-02	0.1240	2.90E-02	-0.4872		
3.13E-02	-0.2800	3.19E-02	0.1300	2.91E-02	0.0567		
3.14E-02	-0.6902	3.21E-02	0.0932	2.93E-02	-0.1379		
3.16E-02	-0.6108	3.22E-02	0.0201	2.94E-02	-0.4793		
3.18E-02	-0.5836	3.24E-02	-0.0051	2.96E-02	-0.6061		
3.19E-02	-0.4225	3.25E-02	0.0145	2.97E-02	-0.5341		
3.21E-02	-0.4605	3.27E-02	0.2735	2.99E-02	-0.0919		
3.22E-02	-0.5904	3.28E-02	0.0573	3.00E-02	-0.6572		
3.24E-02	-0.5725	3.30E-02	0.1040	3.02E-02	-0.5821		
3.25E-02	-0.3725	3.32E-02	0.0261	3.04E-02	-0.5106		
3.27E-02	-0.4636	3.33E-02	-0.0159	3.05E-02	-0.3744		
3.28E-02	-0.4438	3.35E-02	0.0708	3.07E-02	-0.3538		
3.30E-02	-0.6111	3.36E-02	0.2017	3.08E-02	-0.3983		
3.32E-02	-0.3575	3.38E-02	0.2789	3.10E-02	-0.5255		
3.33E-02	-0.3735	3.39E-02	0.1657	3.11E-02	-0.2591		
3.35E-02	-0.6013	3.41E-02	-0.0112	3.13E-02	-0.5355		
3.36E-02	-0.4877	3.42E-02	-0.0251	3.14E-02	-0.4898		
3.38E-02	-0.4956	3.44E-02	0.0013	3.16E-02	-0.5313		
3.39E-02	-0.5178	3.45E-02	-0.0374	3.18E-02	-0.0294		
3.41E-02	-0.5899	3.47E-02	-0.1881	3.19E-02	-0.1775		
3.42E-02	-0.5785	3.49E-02	-0.2469	3.21E-02	-0.2522		
3.44E-02	-0.3745	3.50E-02	-0.2336	3.22E-02	-0.0634		
3.45E-02	-0.5118			3.24E-02	-0.0642		

Table D1h Recovery temperature difference data from tests 16-19. (cont.)

Test 16	Tr [K]	Test 17	Tr [K]	Test 18	Tr [K]	Test 19	Tr [K]
x [m]		x [m]		x [m]		x [m]	
3.47E-02	-0.2852			3.25E-02	0.0470		
3.49E-02	-0.2055			3.27E-02	-0.0085		
3.50E-02	0.0162			3.28E-02	-0.4444		
				3.30E-02	-0.3839		
				3.32E-02	-0.1668		
				3.33E-02	-0.1882		
				3.35E-02	-0.7786		
				3.36E-02	-0.3022		
				3.38E-02	-0.2230		
				3.39E-02	-0.4583		
				3.41E-02	-0.4184		
				3.42E-02	-0.6439		
				3.44E-02	-0.5833		
				3.45E-02	-0.5837		
				3.47E-02	-0.7458		
				3.49E-02	-0.6186		
				3.50E-02	-0.4898		

References

1. Glauert, M. B., "The wall jet," J. of Fluid Mechanics, v.1, Part 6, pp625-643 Dec. 1956.
2. Meyers, G. E., Schauer, J. J. and Eustis, R. H., "Heat transfer to plane turbulent wall jets," J. of Heat Transfer, pp209-214, Aug. 1963.
3. Miyazaki, H., and Silberman E., "Flow and heat transfer on a plate normal to a two-dimensional laminar jet issuing from a nozzle of finite height," Int. J. of Heat and Mass Transfer, v.15, pp2097-2107, 1972.
4. Sparrow, E. M. and Lee, L., "Analysis of flow field and impingement heat/mass transfer due to a nonuniform slot jet," J. of Heat Transfer, pp191-197, May 1975.
5. Scholtz, M. T. and Trass, O., "Mass transfer in a nonuniform impinging jet, Part I. Stagnation flow-velocity and pressure distribution," AIChE Journal, pp82-89, January 1970.
6. Scholtz, M. T. and Trass, O., "Mass transfer in a nonuniform impinging jet, Part II. Boundary layer flow-mass transfer," AIChE Journal, pp82-89, January 1970.
7. Kumada, M. and Mabuchi, I., "Studies on the heat transfer of impinging jet, (1st Report, mass transfer for two-dimensional jet of air impinging normally on a flat plate)," Bulletin of the JSME, v.13, n.55, pp77-85, 1970.

8. Miyazaki, H. and Silberman, E., "Flow and heat transfer on a flat plate normal to a two-dimensional laminar jet issuing from a nozzle of finite height," Int. J. of Heat and Mass Transfer, v.15, pp2097-2107, 1972.
9. Anderson, D. A., Tannehill, J. C. and Pletcher, R. H., Computational fluid mechanics and heat transfer, Hemisphere Publishing Corporation, 1984.
10. Wolfshtein, M., "Some solutions of the plane turbulent impinging jet," J. of Basic Engineering, pp915-922, Dec. 1970.
11. Amano, R. S. and Brandt, H., "Numerical study of turbulent axisymmetric jets impinging on a flat plate and flowing into an axisymmetric cavity," J. of Fluid Engineering, v.106, pp410-417, 1984.
12. Chaung, S. H., "Numerical simulation of an impinging jet on a flat plate," Int. J. for Numerical Methods in Fluids, v.9, pp1413-1426, 1989.
13. Hwang, C. J. and Liu, J. L., "Numerical study of two-dimensional impinging jet flow fields," AIAA Journal, v.27, n.7, pp841-842, 1989.
14. Agarwal, R. K. and Bower, W. W., "Navier Stokes computations of turbulent compressible two-dimensional impinging jet flow fields," AIAA Journal, v.20, n.5, pp577-584, 1982.
15. Malin, J., "Modeling the effects of lateral divergence on radially spreading turbulent jets," Computers and Fluids, v.17, n.3, pp453-465, 1989.

16. Chaung, S. H., "Numerical simulation of twin-jet impingement on a flat plate coupled with cross-flow," Int. J. for Numerical Methods in fluids, v.14, pp459-475, 1992.
17. Hwang, J. C. and Tsou, F. K., "Numerical solutions for flow and heat transfer of a plane turbulent oblique impinging jet," Numerical Properties and Methodologies in Heat Transfer, editor Shih, T. M., Hemisphere Publishing Co., 1981.
18. Looney, M. K. and Walsh, J. J., "Mean-flow and turbulent characteristics of free and impinging jet flows," Journal of Fluid Mechanics, v.147, pp397-429, 1984.
19. Polat, S., Mujumdar, A. S., van Heiningen, A. R. P. and Douglas, W. J. M., "Effects of near-wall modeling on prediction of impingement heat transfer," Drying Technology, v.8(4), pp705-730, 1990.
20. Yuan, T. D. and Liburdy, J. A., "Application of a surface renewal model to the prediction of heat transfer in an impinging jet," Int. J. of Heat and Mass Transfer, v.35, n.8 pp1905-1912, 1992.
21. Rodi, W. and Scheuerer, G., "Calculation of heat transfer to convection-cooled gas turbine blades," J. of Engineering for Gas Turbines and Power, v.107, pp620-627, July 1985.

22. Lam, C. K. G. and Bremhorst, K. A., "Modified form of the k - ϵ model for predicting wall turbulence," J. of Fluids Engineering, v.103, pp456-460, 1981.
23. Chang, B. H. and Mills, A. F., "Computation of heat transfer from impinging turbulent jets," 6th Int. Symposium on Transport Phenomena in Thermal Engineering, May 9-13, 1993.
24. Yap, C., "Turbulent heat transfer and momentum transfer in recirculating and impinging flows," Ph.D. Dissertation, Faculty of Technology, University of Manchester, United Kingdom, 1987.
25. Jones, W. P. and Launder, B. E., "The calculation of low-Reynolds number phenomena with a two-equation model of turbulence," Int. J. of Heat and Mass Transfer, v.16, pp1119-1130, 1972.
26. Bose, T. K., "Laminar jet Mach number and temperature effects on heat transfer," J. of Thermophysics and Heat Transfer, v.6, n.2, pp 308-313, April-June 1992.
27. Jambunathan, K., Lai, E., Moss, M. A., and Button, B. L., "A review of heat transfer data for single circular jet impingement," Int. J. of Heat and Fluid Flow, v.13, n.2, June 1992.
28. Martin, H., "Heat and mass transfer between impinging gas jets and solid surfaces," Advances in Heat Transfer, Academic Press, New York, pp1-60, 1970.

29. Obit, N. T., Mujumdar, A. S. and Douglas, W. J. M., "Design correlations for heat and mass transfer under various turbulent impinging jet configurations," *Developments in Drying*, pp388-402, 1979.
30. Metzger, D. E., Yamashita, T. and Jenkins, C. W. "Impingement cooling of concave surfaces with lines of circular air jets," *J. of Engineering for Power*, pp149-158, July 1969.
31. Tabakoff, W. and Clevenger, W., "Gas turbine blade heat transfer augmentation by impingement of air jets having various configurations," *J. of Engineering for Power*, pp51-60, Jan. 1972.
32. Hrycat, P., "Heat transfer from a row of impinging jets to concave cylindrical surfaces," *Int. J. of Heat and Mass Transfer*, v.24, pp407-419, 1981.
33. Livingood, J. N. B. and Gauntner, J. W., "Average heat-transfer characteristics of a row of circular air jets impinging on a concave surface," *NASA TM X-2657*, 1972.
34. Livingood, J. N. B. and Gauntner, J. W., "Local heat-transfer characteristics of a row of circular air jets impinging on a concave semicylindrical surface," *NASA TM D-7127*, 1972.
35. Livingood, J. N. B. and Gauntner, J. W., "Heat-transfer characteristics of a single circular jet impinging on a concave hemispherical shell," *NASA TM X-2895*, 1972.

36. Gau, C. and Chung, C. M., "Surface curvature effect on slot-air-jet impingement cooling flow and heat transfer process," Transactions of the ASME, v.113, Nov. 1991.
37. Chupp, R. E., Helms, H. E., McFadden, P. W. and Brown, T. R., "Evaluation of internal heat transfer coefficients for impingement-cooled turbine airfoils," J. Aircraft, v.6, pp203-208, 1969.
38. Jusionis, V. J., "Heat transfer from impinging gas jets on an enclosed concave surface," J. Aircraft, v.7, pp87-88, 1970.
39. Hollworth, B. R. and Gero, L. R., "Entrainment effects on impingement heat transfer: Part I-Measurements of heated jet velocity and temperature distributions and recovery temperature on target surfaces," J. Heat Transfer, v.106, pp797-803, 1984.
40. Hollworth, B. R. and Gero, L. R., "Entrainment effects on impingement heat transfer: Part II-Local heat transfer measurements," J. Heat Transfer, v.107, pp910-915, 1985.
41. Goldstein, R. J., Behbahani, A. I. and Heppelmann, K. K., "Streamwise distribution of the recovery factor and the local heat transfer coefficient to an impinging circular air jet," Int. J. of Heat and Mass Transfer, v.29, n.8, pp1227-1235, 1986.

42. Goldstein, R. J. and Seol, W. S., "Heat transfer to a row of impinging circular air jets including the effect of entrainment," *Int. J. of Heat and Mass Transfer*, v.34, n.8, pp2133-2147, 1991.
43. Baughn, J. W., Hechanova, A. E. and Yan, X., "An experimental study of entrainment effects on the heat transfer from a flat surface to a heated circular impinging jet," *J. Heat Transfer*, v.113, pp1023-1025, Nov. 1991.
44. Popiel, C. O. and Trass, O., "Visualization of a free impinging round jet," *Experimental Thermal and Fluid Sciences*, v.4, pp253-264, 1991.
45. Stevens, J., Pan, Y. and Webb, B. W., "Effect of nozzle configuration on transport in the stagnation zone of axisymmetric, impinging free-surface liquid jets: Part 1-Turbulent flow structure," *Transactions of the ASME*, v.114, pp874-879, Nov. 1992.
46. Brown, G. H. and Shaw, W. G., "The mesomorphic state: Liquid crystals," *Chemistry review*, v.57, pp1049-1157, 1957.
47. Fergason, J. L., "Liquid crystals," *Scientific American*, v.211, n.2, pp76-86, Aug. 1964.
48. Stephen, M. J. and Straley, J. P., "Physics of liquid crystals," *Review of Modern Physics*, v.46, n.4, pp617-704, Oct. 1974.
49. Castellano, J. A. and Brown, G. H., "Thermotropic liquid crystals: Part I. The underlying science," *Chemical Technology*, pp47-52, Jan. 1973.

50. Castellano, J. A. and Brown, G. H., "Thermotropic liquid crystals: Part II. Current uses and future ones," Chemical Technology, pp229-253, Apr. 1973.
51. Woodmansee, W. E., "Aerospace thermal mapping applications of liquid crystals," Applied Optics, v.7, n.9, pp1721-1729, Sept. 1968.
52. Klein, E. J., "Applications of liquid crystals to boundary layer flow visualization," AIAA 3rd Aerodynamic Testing Conference, AIAA paper 68-376, Apr. 1968.
53. Klein, E. J., "Liquid crystals in aerodynamic testing," Astronautics and Aeronautics, v.6, n.7, pp70-73, 1968.
54. Keilmann, F., "Infrared interferometry with a CO₂ laser source and liquid crystal detection," Applied Optics, v.9, n.6, pp1319-1322, June 1980.
55. Raad, T. and Myer, J. E., "Nucleation studies in pool boiling on thin plates using liquid crystals," AIChE J., v.5, pp1260-1261, 1971.
56. Ashforth-Frost, F. and Jambunathan, K., "Flow visualization using liquid crystals," SPIE J., v.2005, pp237-245, 1993.
57. Cooper, T. E., Field, R. J. and Meyer, J. F., "Liquid crystal thermography and its application to the study of convective heat transfer," Transactions of the ASME, pp442-449, Aug. 1975.

58. Hippensteele, S. A., Russell, L. M. and Torres, F. J., "Use of a liquid-crystal and heater-element composite for quantitative, high-resolution heat-transfer coefficients on a turbine airfoil including turbulence and surface-roughness effects," NASA Technical Memorandum 87355, 1987.
59. Byerley, A. R., Jones, T. V. and Ireland, P. T., "Internal cooling passage heat transfer near the entrance to a film cooling hole: Experimental and computational results," ASME Paper 92-GT-24, 1992.
60. Baughn, J. W. and Yan, X., "Local heat transfer measurements in square ducts with transverse ribs," J. Enhanced Heat Transfer, v.202, pp1-7, 1992.
61. Wang, Z., Ireland, P. T. and Jones, T. V., "An advanced method of processing liquid crystal video signals from transient heat transfer experiments," ASME Paper 93-GT-282, 1993.
62. Saabas, H. J., Arora, S. C. and Messeh, W. A., "Application of the transient test technique to measure local heat transfer coefficients associated with augmented airfoil cooling passages," ASME Paper 87-GT-212, 1987.
63. Camci, C., Kim, K, Hippensteele, S. A. and Poinsatte, P. E., "Evaluation of a hue capturing based transient liquid crystal method for high-resolution mapping of convective heat transfer on curved surfaces," J. of Heat Transfer, v.115, pp311-318, May 1993.

64. Dini, S., Saniei, N. and Wyse, D. W., "Heat transfer and pressure drop measurements in a pipe bend with annular ring flow disturbers," ASME Paper 93-WA/HT-41, 1993.
65. Abuaf, N. and Kercher, D. M., "Heat transfer and turbulence in a turbulated blade cooling circuit," ASME Paper 92-GT-187, 1992.
66. Goldstein R. J. and Franchett, M. E., "Heat transfer from a flat surface to an oblique impinging jet," Transactions of the ASME, v.110, pp84-90, Feb. 1989.
67. Lucas, M. G., Ireland, P. T., Wang, Z., Jones, T. V. and Pearce, W. J. "Fundamental studies of impingement cooling thermal boundary condition," AGARD Conference Proc., Heat Transfer and Cooling in Gas Turbines, Paper 14, Feb. 1993.
68. Metzger, D. E. and Kim, Y. K., "Local heat transfer measurement with liquid crystals on rotating surfaces including non-axisymmetric cases," AGARD Conference Proc., Heat Transfer and Cooling in Gas Turbines, Paper 17, Feb. 1993.
69. Lee, S. J., Lee, J. H. and Lee, D. H., "Local heat transfer measurements from an elliptic jet impinging on a flat plate using liquid crystal," Int. J. of Heat and Mass Transfer, v.37, n.6, pp967-976, 1994.
70. Huber A. M. and Viskanta, R., "Convective heat transfer to a confined impinging array of air jets with spent air exits," Transactions of the ASME, v.116, pp570-576, Aug. 1994.

71. Herold, W. and Wiegel, D., "Problems of the photographic documentation of liquid crystalline thermographs," *Advances in Liquid Crystal Research and Applications*, editor Bata, L., Pergamon Press, Oxford, pp1255-1259, 1980.
72. Akino, N., Kunugi, T., Ichimiya, K., Mitsushiro, K. and Ueda, M., "Improved liquid-crystal thermometry excluding human color sensation," *Transactions of the ASME*, v.111, pp558-565, May 1989.
73. Camci, C., Kim, K. and Hippensteele, S. A., "A new hue capturing technique for the quantitative interpretation of liquid crystal images used in convective heat transfer studies," *J. of Turbomachinery*, v.114, pp765-775, Oct. 1992.
74. Chan T. L., Jambunathan, K., Leung, T. P. and Ashforth-Frost, S., "A surface temperature calibration method for thermochromic liquid crystals using true-colour image processing," *Proc. of the 10th Int. Heat Transfer conference*, Brighton, UK, Editor Hewitt, G. F., pp201-205, 1994.
75. Farina, D. J., Hacker, J. M., Moffat, R. J. and Eaton, J. K., "Illuminant invariant calibration of thermochromatic liquid crystals," *Experimental Thermal and Fluid Sciences*, v.9, pp1-12, 1994.
76. Kimoto, H., Iizuka, H. and Hamabe, K., "Precise convenient measurement of the temperature profile appearing on a temperature-sensitive liquid-crystal film," *Trans. JSME*, 57, (533B), pp262-267, 1991.

77. von Wolfersdorf, J., Hoecker, R. and Sattelmayer, T., "A hybrid transient step-heating heat transfer measurement technique using heater foils and liquid-crystal thermography," *J. of Heat Transfer*, v.115, pp319-324, May 1993.
78. Pan Y., Stevens, J. and Webb, B. W., "Effect of nozzle configuration on transport in the stagnation zone of axisymmetric, impinging free-surface liquid jets: Part 2-Local heat transfer," *Trans. of the ASME*, v.114, pp880-886, Nov. 1992.
79. Lytle D. and Webb, B. W., "Air jet impingement heat transfer at low nozzle-plate spacing," *Int. J. of Heat and Mass Transfer*, v.37, n.12, pp1687-1697, 1994.
80. Metzger, D. E. and Larson, D. E., "Use of melting point surface coatings for local convection heat transfer measurements in rectangular channel flows with 90-deg turns," *Trans. of the ASME*, v.108, pp48-54, Feb. 1986.
81. Friestad, R. M., Berkel, T. R., Henson, M. C. and Rockoff, H., "Leading edge structural design criteria," McDonnell Douglas Report, N. C1064900, Mar. 20, 1992.
82. Gardon, R. and Akfirat, J. C., "Heat transfer characteristics of impinging two-dimensional air jets," *J. of Heat Transfer*, pp101-108, Feb. 1966.
83. Carslaw, H. S. And Jaeger, J. C., *Conduction of Heat in Solids*, Oxford University Press, pp70-72, 1959.

84. Tan, Benjamin, "Design and Testing of an Automated System Using Thermochromatic Liquid Crystals to Determine Local Heat Transfer Coefficients for an Impinging Jet," M.S. Thesis, School of Engineering and Applied Science, University of California Los Angeles, 1995.
85. Saad, N. R., Polat, S. and Douglas, W. J. M., "Confined multiple impinging slot jets without crossflow effects," Int. J. of Heat and Mass Transfer, v. 13, n. 1, March 1992.
86. Shoukri, M. and Calka, A., "On the heat transfer characteristics of constrained air jets impinging on a flat surface," Int. J. of Heat and Mass Transfer, v. 30, n. 1, pp203-205, 1987.
87. Gardon, R. and Cobonpue, J., "Heat transfer between a flat plate and jets of air impinging on it," International Developments in Heat Transfer, Proc. of the 2nd Int. Heat Transfer Conference, ASME, New York, pp454-460, 1962.
88. Stickney, T. M., "Recovery and time-response characteristics of six thermocouple probes in subsonic and supersonic flow," NACA TN-3455, July, 1955.
89. Simmons, F. S., "Recovery corrections for butt-welded, straight-wire thermocouples in high-velocity, high-temperature gas streams," NACA RM-E54G22a, Sept., 1954.